

Modeling and Analysis of Synchronous Machines

Power quality problems of synchronous machines can be of the following types due to abnormal operation:

- unbalanced load,
- torques during faults such as short-circuits (e.g., balanced three-phase short-circuit, line-to-line short-circuit), out-of-phase synchronization, unbalanced line voltages, reclosing,
- winding forces during abnormal operation and faults,
- excessive saturation of iron cores,
- excessive voltage and current harmonics,
- harmonic torques,
- mechanical vibrations and hunting,
- static and dynamic rotor eccentricities,
- bearing currents and shaft fluxes,
- insulation stress due to nonlinear sources (e.g., inverters) and loads (e.g., rectifiers),
- dynamic instability when connected to weak systems, and
- premature aging of insulation material caused by cyclic operating modes as experienced by machines, for example, in pumped-storage and wind-power plants.

The theory of synchronous machines under load was developed during the first half of the twentieth century by Blondel [1], Doherty and Nickle [2, 3], Park [4, 5], Kilgore [6], Concordia [7], and Lyon [8] – just to name a few of the hundreds of engineers and scientists who have published in this area of expertise. In these works mostly balanced steady-state, transient, and subtransient performances of synchronous machines are analyzed. Most power quality problems as listed above are neglected in these early publications because power quality was not an issue during the last century. However, the asymmetric properties of synchronous machines are well known, resulting in an infinite series of even-current harmonics in the rotor and an infinite series of odd-current harmonics in the stator. An extremely asymmetric machine is the single-phase synchronous machine. Such machines are still used today – albeit with a very strong damper winding (amortisseur) in order to attenuate the higher harmonics within the machine. This attenuation of

harmonics requires large amortisseurs and results in very large machines; that is, the volume per generated power is large. Examples are the 16 2/3 Hz generator of the German railroad system [9].

Application of power electronic devices, nonlinear loads, and distributed generation (DG) due to renewable energy sources in interconnected and islanding power systems causes concerns with respect to the impact of harmonics and poor power quality on the performance and stability of synchronous generators. Although standards generally accept small to medium-sized distorting loads, for large nonlinear loads a detailed harmonic flow study is desirable. For strong power systems, studies do not extend beyond the substation level, but for weak power systems the analysis may need to include generators of larger generating plants. For the analysis of such systems and for the optimal design of newly developed DG and isolated systems as well as synchronous motor drives, accurate harmonic models of synchronous machines are required. An example for the latter is the connection of wind-farm generators (without power electronic interface) to a weak power system.

The synchronous machine is an essential component of a power system; it allows conversion from mechanical to electrical energy. It is a device that works in synchronism with the rest of the electrical network. Several frames of reference have been used to model synchronous machine operation. The first and still the most widely used model is based on the concept of the $dq0$ -coordinate system [4, 5]. The synchronous machine has also been represented in $\alpha\beta0$ coordinates [10] to allow a natural transition between abc and $dq0$ coordinates. Detailed models of the synchronous machine have also been developed for harmonic analysis [11–13].

All these models, however, cannot accurately describe the transient and steady-state unbalanced operation of a synchronous machine unless transient and subtransient parameters are introduced. A machine model in the abc -coordinate system can naturally simulate these abnormal operating conditions, because it is based on a realistic representation that can take into account the explicit time-varying

nature of the stator inductances and that of the mutual stator–rotor inductances, as well as spatial harmonic effects. In one of the first models in the a,b,c time domain [14], the analysis illustrates the advantages of this abc -coordinate system (as applied to synchronous machine representation) compared with the models based on $dq0$ and $\alpha\beta0$ coordinates. For example, a model in abc coordinates is used for the dynamic analysis of a three-phase synchronous generator feeding a static converter for high-voltage DC (HVDC) transmission [15]: harmonic terms up to the fourth order are introduced in the stator-inductance matrix. In more recent contributions [16, 17], a,b,c time-domain models of a synchronous machine are proposed where saturation effects are incorporated.

This chapter reviews the electrical and mechanical equations related to synchronous machines, and their conventional model in $dq0$ coordinates – which is suitable for sinusoidal operating conditions – is presented. It investigates the behavior of synchronous machines under faults (e.g., balanced and unbalanced short-circuits, out-of-phase synchronization, reclosing) and the influence of harmonics superimposed with the fundamental quantities, and it introduces various harmonic models of synchronous machines.

4.1 SINUSOIDAL STATE-SPACE MODELING OF A SYNCHRONOUS MACHINE IN THE TIME DOMAIN

A synchronous machine is a complicated electromagnetic device, and it is very important for the operation of power systems. Detailed models are needed to analyze its behavior under different (e.g., steady-state, transient, subtransient, imbalance, under the influence of harmonics) operating conditions and to understand their impact on the power system. Before introducing the conventional $dq0$ model of synchronous machines for sinusoidal operating conditions, the associated electrical and mechanical equations and magnetic nonlinearities are presented.

4.1.1 Electrical Equations of a Synchronous Machine

Based on the stator and rotor equivalent circuits, voltage equations can be obtained in terms of flux linkages and winding resistances [17]. According to Faraday's and Kirchhoff's laws

$$v = Ri + \frac{d\Psi}{dt}. \quad (4-1)$$

Neglecting saturation the flux linkages are proportional to the currents; thus

$$\Psi = Li. \quad (4-2)$$

Substitution of Eq. 4-2 into Eq. 4-1 yields – after solving for $d\Psi/dt$ – the differential equation

$$\frac{d\Psi}{dt} = v - RL^{-1}\Psi. \quad (4-3)$$

However, it is required to take into account the interaction between self- and mutual inductances of the windings residing on the stator and rotor members. Thus, a set of differential equations can be written in matrix form for the stator and rotor circuits as

$$v_{abc} = R_S i_{abc} + p\Psi_{abc}, \quad (4-4)$$

$$v_{fdq} = R_R i_{fdq} + p\Psi_{fdq}, \quad (4-5)$$

where subscripts abc and fdq represent the stator (e.g., abc components) and rotor (e.g., field, d - and q -axes components), respectively, and p is the differential operator.

The matrix equation for the flux linkages is

$$\begin{bmatrix} \Psi_{abc} \\ \Psi_{fdq} \end{bmatrix} = [L] \begin{bmatrix} i_{abc} \\ i_{fdq} \end{bmatrix}. \quad (4-6)$$

In Eqs. 4-1 to 4-6:

$$p\Psi = p[\Psi_{abc} \quad \Psi_{fdq}]^T = p[\Psi_a \quad \Psi_b \quad \Psi_c \quad \Psi_f \quad \Psi_{kd1} \quad \dots \quad \Psi_{kdn} \quad \Psi_{kq1} \dots \quad \Psi_{kqn}]^T, \quad (4-7)$$

$$v = [v_{abc} \quad v_{fdq}]^T = [v_a \quad v_b \quad v_c \quad v_f \quad v_{kd1} \quad \dots \quad v_{kdn} \quad v_{kq1} \quad \dots \quad v_{kqn}]^T, \quad (4-8)$$

$$i = [i_{abc} \quad i_{fdq}]^T = [i_a \quad i_b \quad i_c \quad i_f \quad i_{kd1} \quad \dots \quad i_{kdn} \quad i_{kq1} \quad \dots \quad i_{kqn}]^T, \quad (4-9)$$

$$R = \text{diag}[R_a \quad R_b \quad R_c \quad R_f \quad R_{kd1} \quad \dots \quad R_{kdn} \quad R_{kq1} \quad \dots \quad R_{kqn}]^T, \quad (4-10)$$

where kdn and kqn are the number of damper windings of the d - and q -axes, respectively. The inductance matrix L has the form

$$[L] = \begin{bmatrix} L_{ss} & L_{sr} \\ L_{rs} & L_{rr} \end{bmatrix}. \quad (4-11)$$

L_{SS} are stator self-inductances, L_{SR} are stator–rotor mutual inductances, where $L_{SR} = [L_{RS}]^T$, and L_{RR} are rotor self-inductances. T indicates the transpose of a matrix. Note that L_{SS} , L_{SR} , and L_{RS} consist of time-varying inductances representing the interrelationships between the stator and rotor windings as a function of the rotor position angle θ .

Therefore, the inductance matrix is a function of time due to θ which itself is a function of time (e.g., $\theta = \omega t + \delta - \pi/2$, where ω and δ are rotor angular velocity and rotor angle, respectively):

$$L = \begin{bmatrix} L_{aa} & L_{ab} & L_{ac} & L_{af} & L_{akd} & L_{akq} & L_{akD} & L_{akQ} \\ L_{ba} & L_{bb} & L_{bc} & L_{bf} & L_{bkd} & L_{bkq} & L_{dkD} & L_{bkQ} \\ L_{ca} & L_{cb} & L_{cc} & L_{cf} & L_{ckd} & L_{ckq} & L_{ckD} & L_{ckQ} \\ L_{fa} & L_{fb} & L_{fc} & L_{ff} & L_{fkd} & 0 & L_{fkD} & 0 \\ L_{kda} & L_{kdb} & L_{kdc} & L_{kdf} & L_{kkd} & 0 & L_{kdkD} & 0 \\ L_{kqa} & L_{kqb} & L_{kqc} & 0 & 0 & L_{kkq} & 0 & L_{kakQ} \\ L_{kDa} & L_{kDb} & L_{kDc} & L_{kDf} & L_{kDkd} & 0 & L_{kkD} & 0 \\ L_{kQa} & L_{kQb} & L_{kQc} & 0 & 0 & L_{kQkq} & 0 & L_{kkQ} \end{bmatrix}. \quad (4-12a)$$

$$L_{SS} = \begin{bmatrix} L_{aa0} + \sum_{h=2}^n L_{aa_h} \cosh h\theta & -L_{ab_0} - \sum_{h=2}^n L_{ab_h} \cosh(h\theta + \pi/6) & -L_{ac_0} - \sum_{h=2}^n L_{ac_h} \cosh(h\theta + 5\pi/6) \\ -L_{ba_0} - \sum_{h=2}^n L_{ba_h} \cosh(h\theta + \pi/6) & L_{bb_0} + \sum_{h=2}^n L_{bb_h} \cosh(h\theta - 2\pi/3) & -L_{bc_0} - \sum_{h=2}^n L_{bc_h} \cosh(h\theta - \pi/2) \\ -L_{ac_0} - \sum_{h=2}^n L_{ac_h} \cosh(h\theta + 5\pi/6) & -L_{cb_0} - \sum_{h=2}^n L_{cb_h} \cosh(h\theta - \pi/2) & L_{cc_0} + \sum_{h=2}^n L_{cc_h} \cosh(h\theta + 2\pi/3) \end{bmatrix}. \quad (4-12c)$$

- Considering odd harmonics (h) up to the m th order, L_{SR} has the form

$$L_{SR} = \begin{bmatrix} \sum_{h=1}^m M_{i_a} \cos h\theta & \sum_{h=1}^m M_{kd_a} \cos h\theta & -\sum_{h=1}^m M_{kq_a} \cos h\theta & \sum_{h=1}^m M_{kD_a} \cos h\theta & -\sum_{h=1}^m M_{kQ_a} \cos h\theta \\ \sum_{h=1}^m M_{i_a} \cos h(\theta - 2\pi/3) & \sum_{h=1}^m M_{kd_a} \cos h(\theta - 2\pi/3) & -\sum_{h=1}^m M_{kq_a} \cos h(\theta - 2\pi/3) & \sum_{h=1}^m M_{kD_a} \cos h(\theta - 2\pi/3) & -\sum_{h=1}^m M_{kQ_a} \cos h(\theta - 2\pi/3) \\ \sum_{h=1}^m M_{i_a} \cos h(\theta + 2\pi/3) & \sum_{h=1}^m M_{kd_a} \cos h(\theta + 2\pi/3) & -\sum_{h=1}^m M_{kq_a} \cos h(\theta + 2\pi/3) & \sum_{h=1}^m M_{kD_a} \cos h(\theta + 2\pi/3) & -\sum_{h=1}^m M_{kQ_a} \cos h(\theta + 2\pi/3) \end{bmatrix}. \quad (4-12d)$$

Combining Eqs. 4-3 to 4-12 results in a unified representation for the electrical part of the synchronous machine having the form

$$p\Psi = v - RL^{-1}\Psi. \quad (4-13)$$

It is important to note that, for the computation of the state variables with Eq. 4-13, the inverse of the time-varying inductance matrix must be obtained at each step of integration.

The electric torque is expressed in terms of the stator currents and flux linkages as

In the above equations, only two damper windings along the d - and q -axes are assumed and [17]:

- The entries of L_{RR} represent – neglecting saturation – constant inductances, independent of the rotor position θ . L_{RR} has the form

$$L_{RR} = \begin{bmatrix} L_{ff} & L_{fkD} & 0 & L_{fkD} & 0 \\ L_{kdf} & L_{kkd} & 0 & L_{kdkD} & 0 \\ 0 & 0 & L_{kkq} & 0 & L_{kqkQ} \\ L_{kDf} & L_{kDkd} & 0 & L_{kkD} & 0 \\ 0 & 0 & L_{kQkq} & 0 & L_{kkQ} \end{bmatrix}. \quad (4-12b)$$

- Considering even harmonics (h) up to the n th order, L_{SS} has the form

$$T_e = p \frac{2}{3\sqrt{3}} [\Psi_a(i_b - i_c) + \Psi_b(i_c - i_a) + \Psi_c(i_a - i_b)], \quad (4-14)$$

where p is the number of poles.

4.1.2 Mechanical Equations of Synchronous Machine

The second-order mechanical equation of a synchronous machine can be decomposed into two first-order differential equations: one for the mechanical

angular velocity of the rotor ω_r and the other for the mechanical rotor angle δ . The constant k_D is usually incorporated into the angular velocity equation to add a damping component that is proportional to the difference of angular velocities ω_r and ω_B :

$$\frac{d\omega_r}{dt} = \frac{\omega_B}{2H}(T_m - T_e - k_D(\omega_r - \omega_B)). \quad (4-15)$$

$$\frac{d\delta}{dt} = \omega_r - \omega_B, \quad (4-16)$$

where

$$H = \frac{1}{2} \frac{J\omega_B^2}{VA_{\text{base}}} \text{ seconds.} \quad (4-17)$$

In the above equations ω_B is the rated angular velocity of the rotor, k_D is the damping factor (pu torque/pu angular velocity), H is the unit inertia constant (watt-s/VA at rated angular velocity), J is the axial combined (rotor and prime mover) moment of inertia (kg m^2), and VA_{base} is the apparent power base S_{base} .

4.1.3 Magnetic Saturation of Synchronous Machine

This section introduces a simple approach to approximately include magnetic saturation in the synchronous machine equations [17]. The nonlinear effect of saturation in a synchronous machine is modeled according to the following algorithm, which is based on modifying the stator currents in $dq0$ coordinates.

- For the input stator currents and fluxes (e.g., i_a , i_b , i_c , and Ψ_a , Ψ_b , Ψ_c) apply the $dq0$ transformation to obtain i_d , i_q , i_o , and Ψ_d , Ψ_q , Ψ_o :

$$\begin{bmatrix} i_d \\ i_q \\ i_o \end{bmatrix} = [T_{\text{PARK}}] \begin{bmatrix} i_a \\ i_b \\ i_c \end{bmatrix} \quad (4-18a)$$

$$\begin{bmatrix} \Psi_d \\ \Psi_q \\ \Psi_o \end{bmatrix} = [T_{\text{PARK}}] \begin{bmatrix} \Psi_a \\ \Psi_b \\ \Psi_c \end{bmatrix},$$

where the Park transformation is

$$[T_{\text{PARK}}] = \sqrt{\frac{2}{3}} \begin{bmatrix} \cos\theta & \cos(\theta - 120^\circ) & \cos(\theta + 120^\circ) \\ -\sin\theta & -\sin(\theta - 120^\circ) & -\sin(\theta + 120^\circ) \\ 1/\sqrt{2} & 1/\sqrt{2} & 1/\sqrt{2} \end{bmatrix}. \quad (4-18b)$$

- Calculate the dq -components of the total mmf in the machine as

$$I_d = i_d + i_f + \sum_{j=1}^{kdn} i_{kdj}, \quad I_q = i_q + \sum_{j=1}^{kqn} i_{kj}, \quad (4-19)$$

where kdn and kqn are the number of damper windings of d - and q -axes, respectively.

- For given saturation characteristics of the d - and q -axes, saturated mmfs (I'_d and I'_q) are calculated based on a polynomial approximation, for example,

$$I'_d = \alpha_d \Psi_d + \beta_d \Psi_d^n, \quad I'_q = \alpha_q \Psi_q + \beta_q \Psi_q^m. \quad (4-20)$$

- The relationship between the saturated mmfs of Eq. 4-20 and linear mmfs of Eq. 4-19 are

$$K_d = I'_d / I_d, \quad K_q = I'_q / I_q. \quad (4-21)$$

- Stator and rotor currents are now adjusted for saturation, as follows:

$$\begin{aligned} i'_a &= K_d i_a, & i'_b &= K_d i_b, & i'_c &= K_d i_c \\ i'_f &= K_d i_f \\ i'_{kd} &= K_d i_{kd}, & i'_{kD} &= K_d i_{kD} \\ i'_{kq} &= K_q i_{kq}, & i'_{kQ} &= K_q i_{kQ} \end{aligned} \quad . \quad (4-22)$$

4.1.4 Sinusoidal Model of a Synchronous Machine in $dq0$ Coordinates

Several reference frames can be employed to represent synchronous machine operation. The first and most widely used model is based on the concept of the ideal synchronous machine represented by fictitious $dq0$ coordinates attached to the rotating rotor reference frame [4, 5], as shown in Fig. 4.1. This model assumes balanced operating conditions at the input terminals and within the machine. Synchronous machines can be also represented in $\alpha\beta0$ coordinates [10] to allow for a natural transition between abc and $dq0$ coordinates.

4.2 STEADY-STATE, TRANSIENT, AND SUBTRANSIENT OPERATION

Numerical methods such as the finite-difference and finite-element methods [18] enable the engineer to

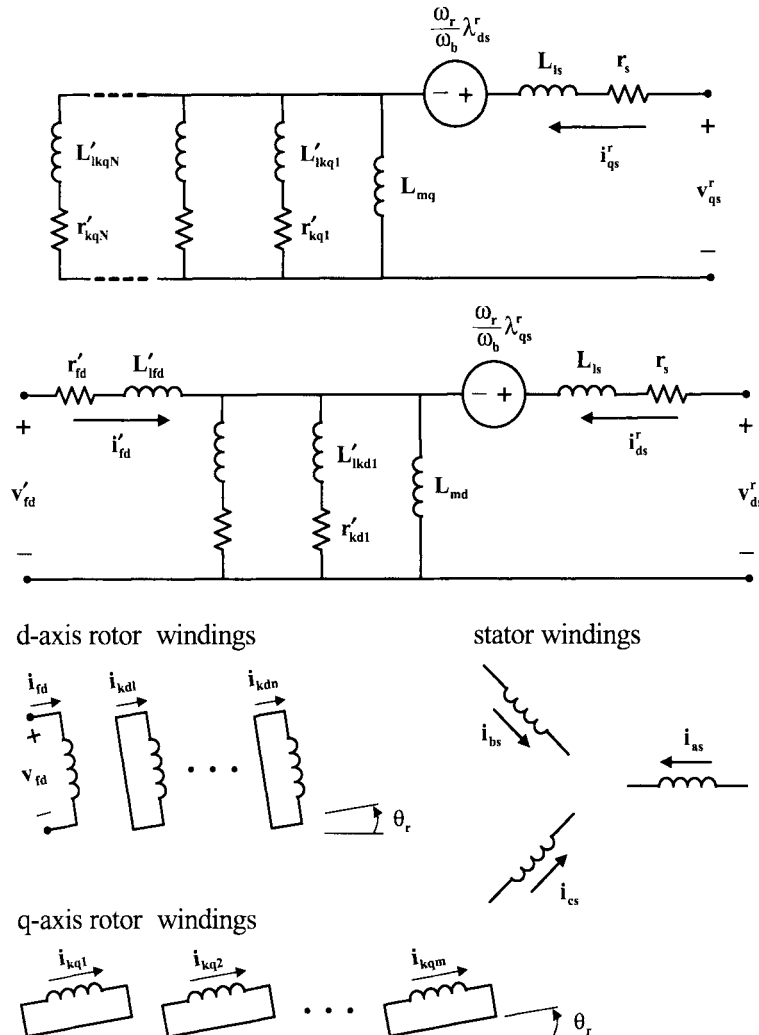


FIGURE 4.1 Synchronous machine model represented in dq0 coordinates for sinusoidal analysis [1, 2].

compute no-load and full-load magnetic fields and those associated with short-circuit and starting conditions, as well as fields for the calculation of leakage, synchronous, transient, and subtransient inductances or reactances. Figures 4.2, 4.3, and 4.4 represent the no-load, short-circuit, and full-load fields, respectively, of a four-pole generator [19, 20]. Figure 4.5 illustrates the winding forces during steady-state short-circuit conditions. These forces were computed based on the “Maxwell stress” discussed later in this chapter. Figure 4.2b [21] shows that at rated voltage only a small amount of flux (e.g., 1.4 mT) enters the space between the iron core (stator back iron) and the stator frame, and the eddy currents induced in the solid key bars are negligible. Figures 4.5 and 4.6 illustrate synchronous linear L_d , L_q inductances or synchronous X_d , X_q reactances [19, 20, 22] of a two-

pole generator. Figures 4.5 and 4.6 do not indicate any coupling between the d - and q -axes. Such a coupling is due to the saturation and is called cross-coupling [23], which will be neglected in subsequent sections. Figure 4.7 pertains to the calculation of the transient inductance L'_d or transient reactance X'_d [19, 22]. Figure 4.8 illustrates the field of a two-pole generator at full load.

In general, for synchronous machines with a field-current excitation in the d -axis the following inequalities are valid: $X_d \geq X_q$, $X'_d \leq X'_q$, and $X''_d \leq X''_q$. However, for inverter-fed synchronous machines with permanent-magnet excitation – also called brushless DC machines – as used in high-efficiency, variable-speed drives [24, 25], due to the lack of field and damper windings in such machines, the transient and subtransient reactances are not defined. Figures

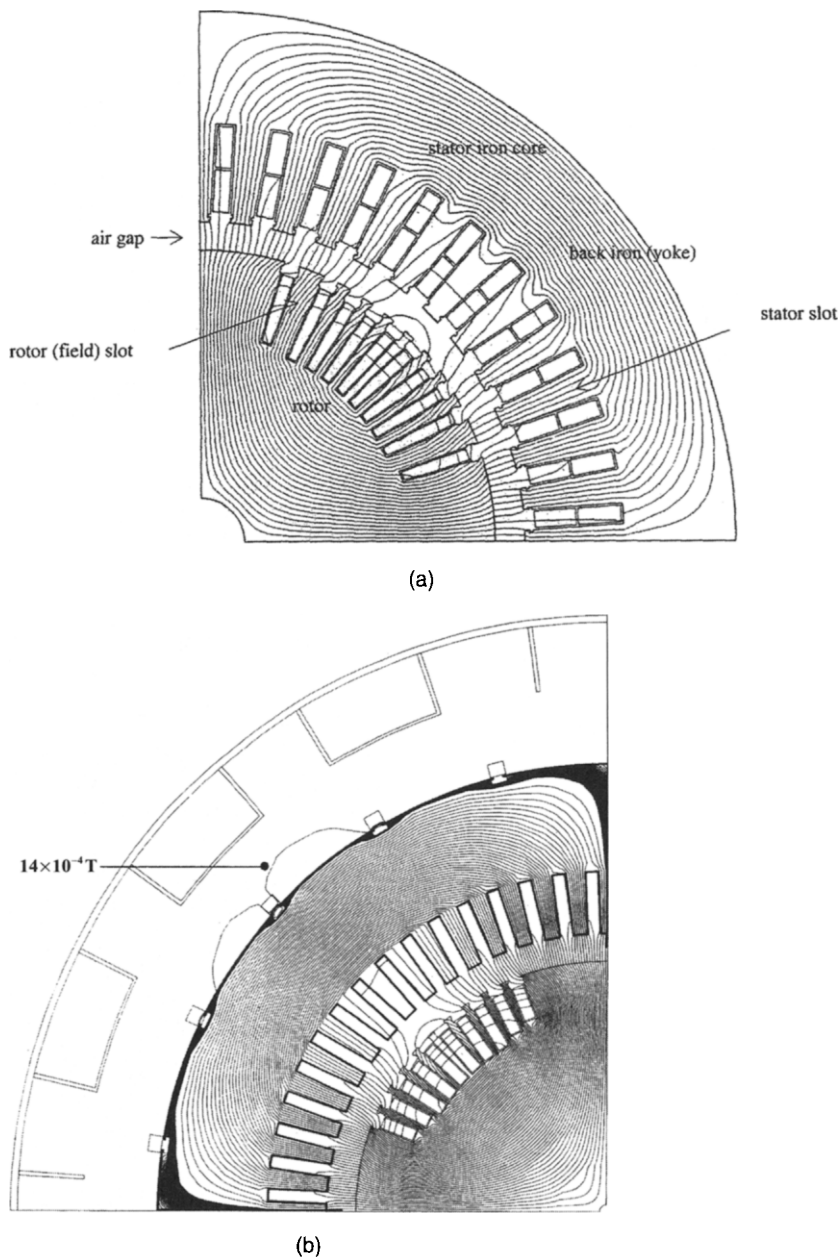


FIGURE 4.2 (a) No-load field of four-pole synchronous generator. (b) No-load field of four-pole synchronous generator including leakage fields outside the iron core [21].

4.9 and 4.10 depict no-load and full-load fields of a permanent-magnet machine, respectively, whereas Fig. 4.11 illustrates the field for the calculation of the stator self-inductance (e.g., L_q). In permanent-magnet machines the leakage is defined as the leakage flux between two stator winding phases and not the leakage flux between the stator and the rotor windings (which do not exist) as it is normally defined for other types of machines. In addition L_q is larger than L_d , and there is a significant amount of cogging [26].

4.2.1 Definition of Transient and Subtransient Reactances as a Function of Leakage and Mutual Reactances

The $dq0$ model requires the availability of values for the synchronous (X_d , X_q), transient (X'_d , X'_q), and subtransient (X''_d , X''_q) reactances of synchronous machines. Most turbogenerators have field windings in the d -axis only and none in the q -axis, therefore $X'_q \approx X_q$. The transient reactance X'_d can be defined in terms of leakage and mutual reactances, as depicted in Fig. 4.12:

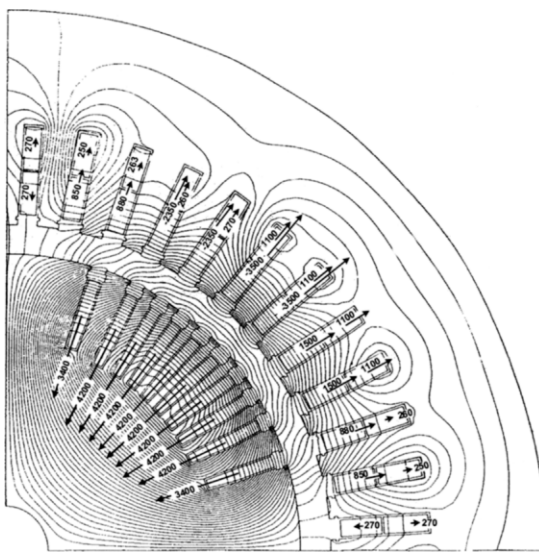


FIGURE 4.3 Short-circuit field and force (measured in N/m, see Section 4.2.14) distribution of four-pole synchronous generator. The arrows indicate the direction and value (length of arrow) of the winding forces developed due to balanced steady-state, three-phase short-circuit.

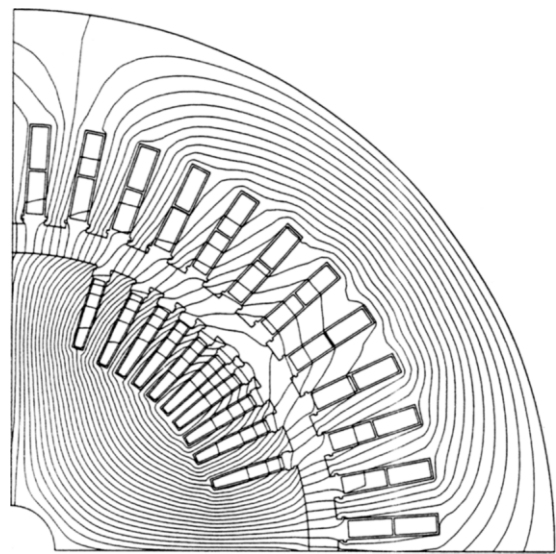


FIGURE 4.4 Full-load field of four-pole synchronous generator.

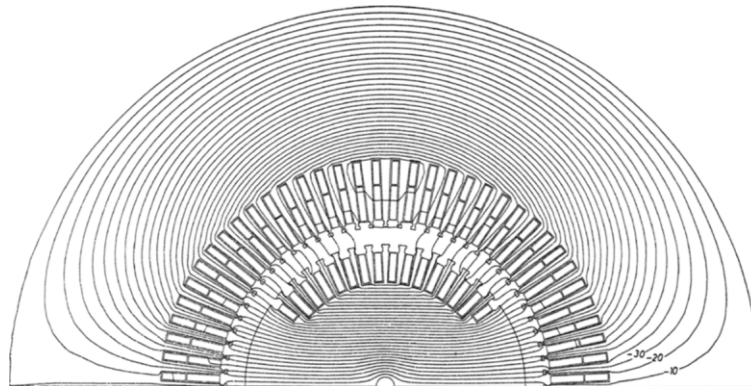


FIGURE 4.5 Field of two-pole synchronous generator for the calculation of either L_d or X_d .

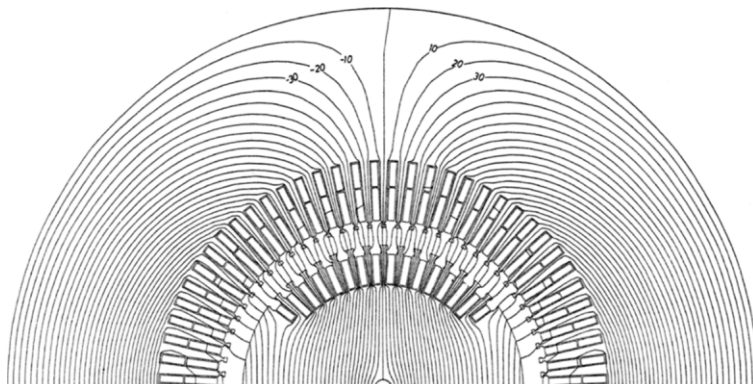


FIGURE 4.6 Field of two-pole synchronous generator for the calculation of either L_q or X_q .

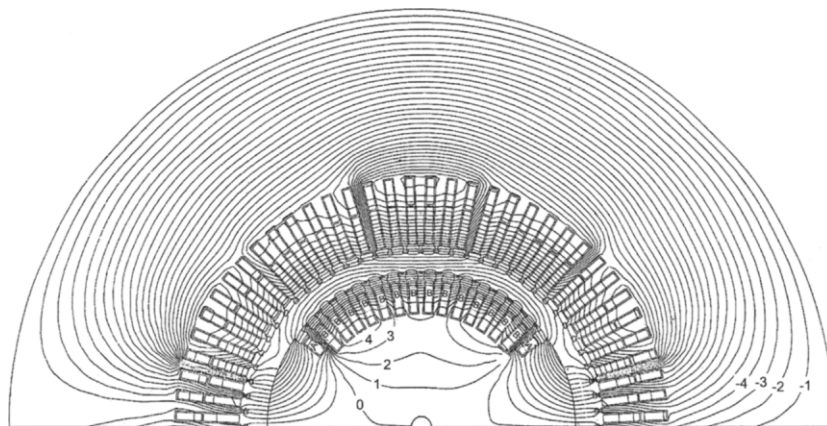


FIGURE 4.7 Field of two-pole synchronous generator for the calculation of either L'_d or X'_d .

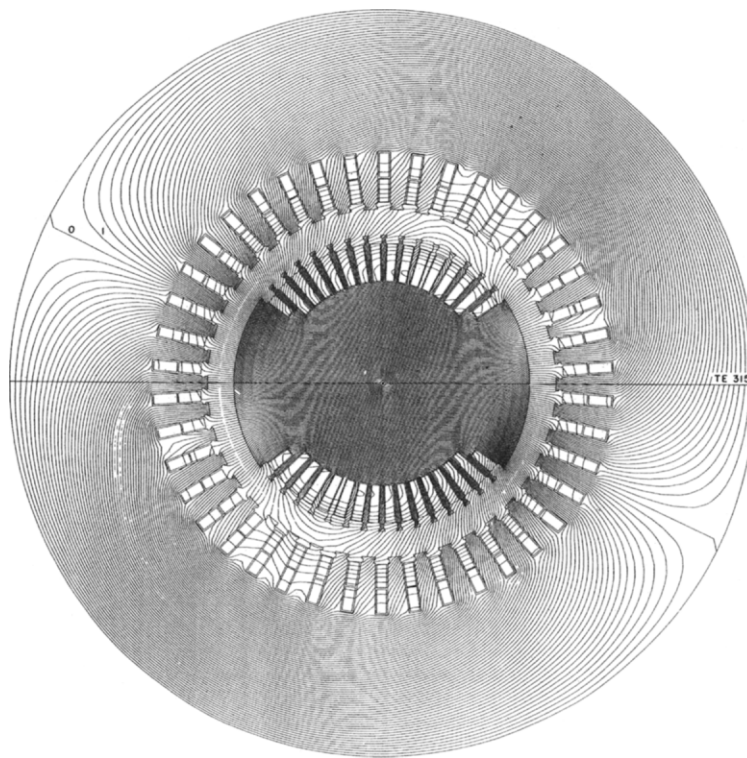


FIGURE 4.8 Magnetic field of a two-pole, three-phase synchronous machine under full load [27].

$$X'_d = X_{al} + \frac{X_{af}X_{fl}}{X_{af} + X_{fl}}, \quad (4-23)$$

$$X''_d = X_{al} + \frac{X_{af}X_{fl}X_{dl}}{X_{af}X_{fl} + X_{af}X_{dl} + X_{dl}X_{fl}}, \quad (4-24)$$

where X_{al} is the amature (stator) leakage reactance, X_{fl} is the field leakage reactance, and X_{af} is the mutual reactance between armature and field circuits.

Correspondingly, one obtains for the subtransient reactance X''_d (Fig. 4.13):

where X_{dl} is the d-axis damper winding leakage reactance.

Representative per-unit values for a typical turbo-generator are

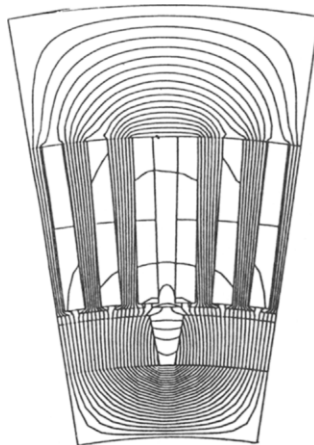


FIGURE 4.9 Flux distribution at no load of a permanent-magnet machine.

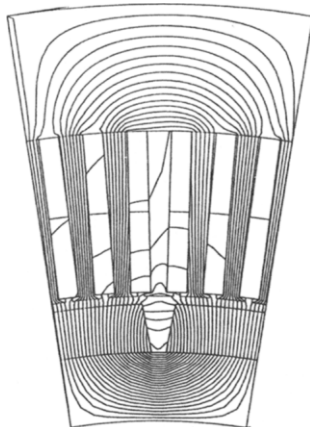


FIGURE 4.10 Flux distribution at full load of a permanent-magnet machine.

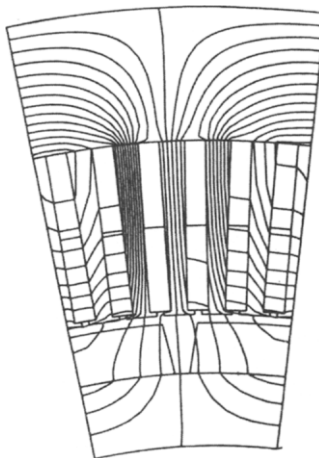


FIGURE 4.11 Flux distribution for self-inductance calculation (L_q) of a permanent-magnet machine. $\phi = Li$

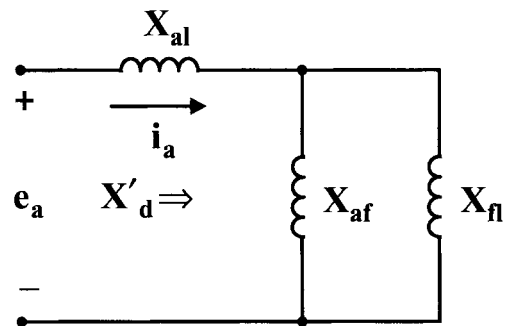


FIGURE 4.12 Equivalent circuit for the definition of the transient reactance X'_d .

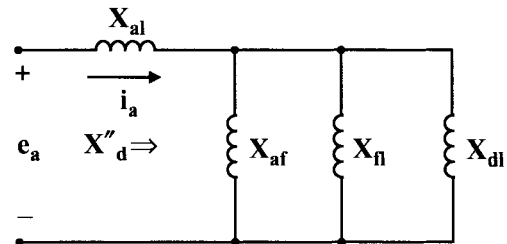


FIGURE 4.13 Equivalent circuit for the definition of the subtransient reactance X''_d .

$$X_d = 1.6, X_q = 1.4, X'_d = 0.2, X''_d = 0.15. \quad (4-25)$$

In general, $1 \text{ pu} \leq X_d \leq 2 \text{ pu}$, $1 \text{ pu} \leq X_q \leq 2 \text{ pu}$, $0.2 \text{ pu} \leq X'_d \leq 0.4 \text{ pu}$, $0.1 \text{ pu} \leq X''_d \leq 0.3 \text{ pu}$, and the values of X'_q and X''_q depend on the field and damper winding design within the q -axis, respectively. Note that the value of X''_q depends on the rotor construction and the damper winding associated with the q -axis: if there are no additional damper bars located on the rotor pole, then X''_q is relatively large and in the neighborhood of X_q . In the presence of damper windings in the q -axis X''_q is somewhat larger than X''_d because the damper winding (e.g., solid rotor or embedded damper bars on the rotor pole) of the q -axis is less effective than that of the d -axis. The rationale for selecting the above ranges for the various reactances lies in the stability requirements for generators when operating on the power system: machines with small reactances exhibit better stability than machines with large reactances; or in other words, machines with small reactances or inductances have smaller time constants than those with large reactances or inductances. Small reactances require a large air gap and a large field current for setting up the maximum flux density across the air gap of about $B_{\max} = 0.7 \text{ T}$. The large air gap makes

machines less efficient as compared to those with small air gaps. One has to weigh the benefits of a more stable but less efficient machine versus that with less stability but greater efficiency. In addition, machines with small reactances result in larger short-circuit currents and larger transient torques and winding forces than machines with larger reactances.

4.2.2 Phasor Diagrams for Round-Rotor Synchronous Machines

There are two ways of drawing equivalent circuits and phasor diagrams of synchronous machines. The first one is based on the so-called consumer system, where the terminal current flows into the equivalent circuit, and the second one is the generator system, where the terminal current flows out of the equivalent circuit. The first one is mostly employed by engineers concerned with drives, and the latter one is mostly used by power system engineers who are concerned with generation issues.

4.2.2.1 Consumer (Motor) Reference Frame

Figure 4.14a depicts the equivalent circuit of a round-rotor synchronous machine based on the consumer (motor) reference current system. Figure 4.14b illustrates the corresponding phasor diagram for overexcited operation, and Fig. 4.14c pertains to underexcited operation. Note that the polarity of the voltages is indicated by + and - signs as well as by arrows, where the head of the arrow coincides with the + sign and the tail of the arrow with the - sign. Such an arrow notation makes it easier to draw phasor diagrams. The phasor diagrams are not to scale because the ohmic voltage drop \tilde{V}_R is normally much smaller than the reactive voltage drop \tilde{V}_X .

4.2.2.2 Generator Reference Frame

Figure 4.15a depicts the equivalent circuit of a round-rotor synchronous machine based on the generator reference current system. Figure 4.15b,c illustrate the corresponding phasor diagram for overexcited and underexcited operation, respectively.

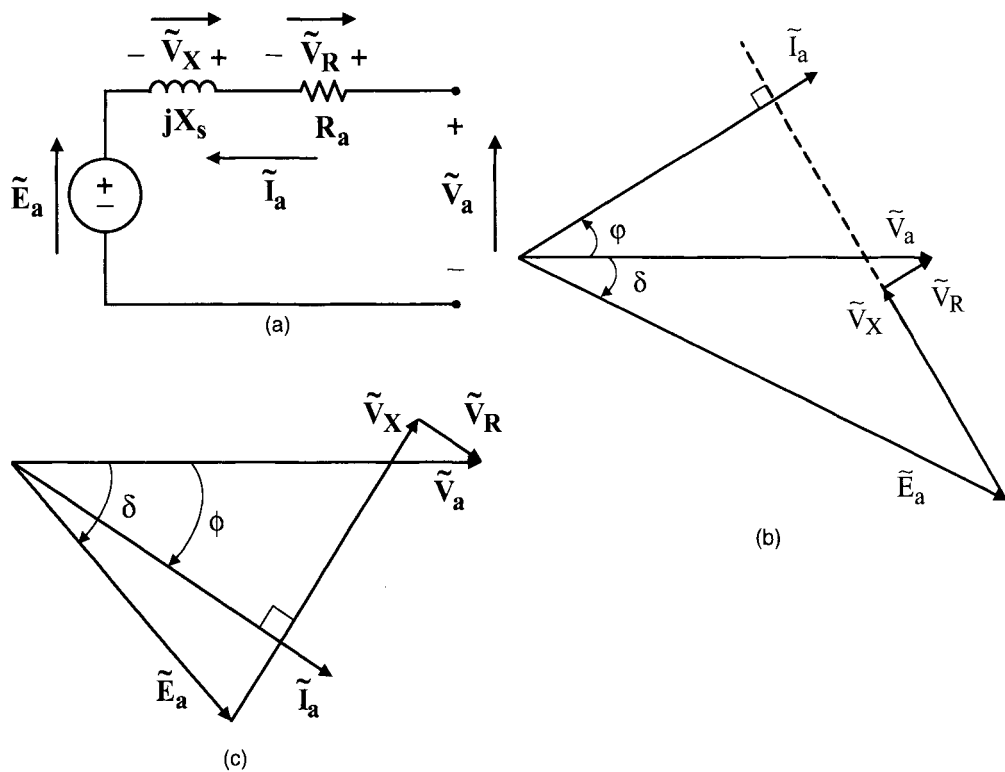


FIGURE 4.14 (a) Equivalent circuit based on consumer (motor) reference frame for the terminal current \tilde{I}_a . (b) Phasor diagram based on consumer (motor) reference frame for leading (overexcited) terminal current \tilde{I}_a . (c) Phasor diagram based on consumer (motor) reference frame for lagging (underexcited) terminal current \tilde{I}_a .

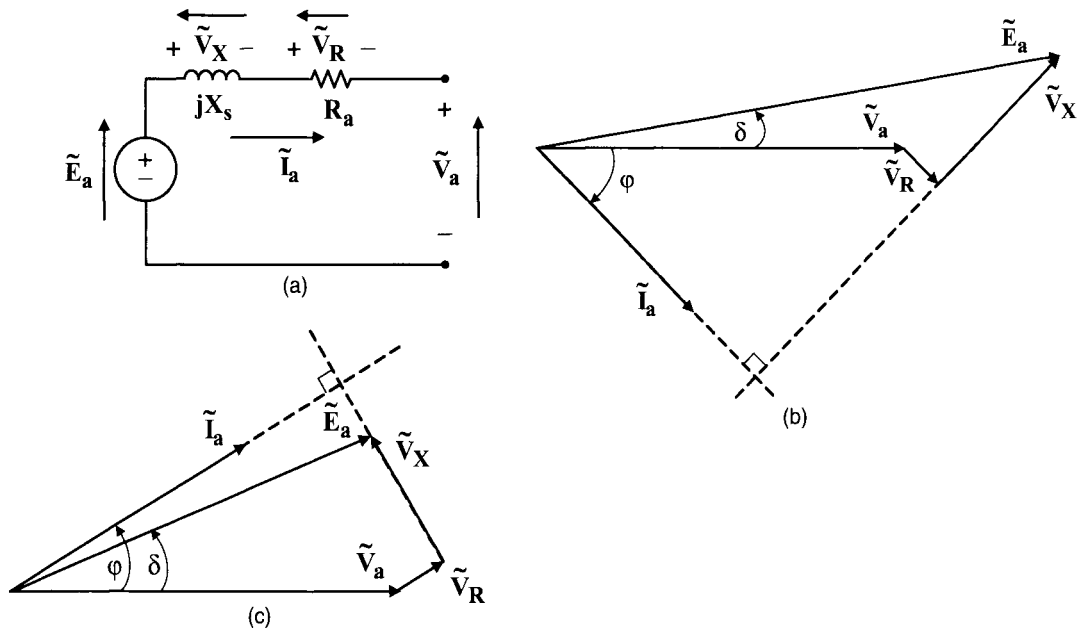


FIGURE 4.15 (a) Equivalent circuit based on generator reference frame for the terminal current \tilde{I}_a . (b) Phasor diagram based on generator reference frame for lagging (overexcited) terminal current \tilde{I}_a . (c) Phasor diagram based on generator reference frame for leading (underexcited) terminal current \tilde{I}_a .

4.2.2.3 Similarities between Synchronous Machines and Pulse-Width-Modulated (PWM) Current-Controlled, Voltage-Source Inverters

Inverters are electronic devices transforming voltages and currents from a DC source to an equivalent AC source. Figure 4.16a illustrates the actual circuit of an inverter, where the input voltage is a DC voltage V_d and the output voltage is an AC voltage \tilde{V}_{load} . It is assumed that the PWM switching is lossless. In Fig. 4.16b the DC voltage ($V_d/2$) is transformed to the AC side and represented by the phasor $(\tilde{V}_d/2)$, which makes the equivalent circuit of Fig. 4.16b similar to that of a round-rotor synchronous machine, as depicted in Fig. 4.15a. The relation between the (fundamental) output voltage $|\tilde{V}_{load}|$ of the inverter and the input voltage $\tilde{V}_d/2$ (transformed to the AC side) is given [28] by

$$|\tilde{V}_{load}| = m \cdot \frac{(V_d/2)}{\sqrt{2}}, \quad (4-26)$$

where $m \leq 1$ is the modulation index of the (sinusoidal) PWM. This relation appears to hold for operation around unity displacement (fundamental power) factor only [29, 30]. In these references it is shown that at lagging (overexcited, delivering reactive power to the grid) displacement power factor a much

higher input voltage V_d than specified by Eq. 4-26 is required, whereas for leading (underexcited, absorbing reactive power from the grid) displacement power factor a smaller input voltage V_d is sufficient. For example, although for unity displacement factor $V_{d_unity_pf} = 400$ V is acceptable, a much higher input voltage, e.g., $V_{d_lagging_pf} = 600$ V is required for displacement factors larger than $\cos \varphi = 0.8$ lagging (overexcited) [29, 30] at $\tilde{V}_{load} = 139$ V.

4.2.2.4 Phasor Diagram of a Salient-Pole Synchronous Machine

The d - and q -equivalent circuits and the associated phasor diagram of a (balanced) salient-pole synchronous machine are given in Fig. 4.17a,b,c. Note there is no zero-sequence equivalent circuit, which becomes important for unbalanced operation (e.g., asymmetrical short-circuits) of synchronous machines only. Figure 4.17c represents the phasor diagram without cross-coupling between the d - and q -axes due to saturation. The relation between voltages, currents, and reactances is given by the phasor diagram of Fig. 4.18 including cross-coupling of d - and q -axes parameters [20, 23]. This cross-coupling is due to saturation of the machine and will be neglected in subsequent sections.

According to [7] the following relations are valid:

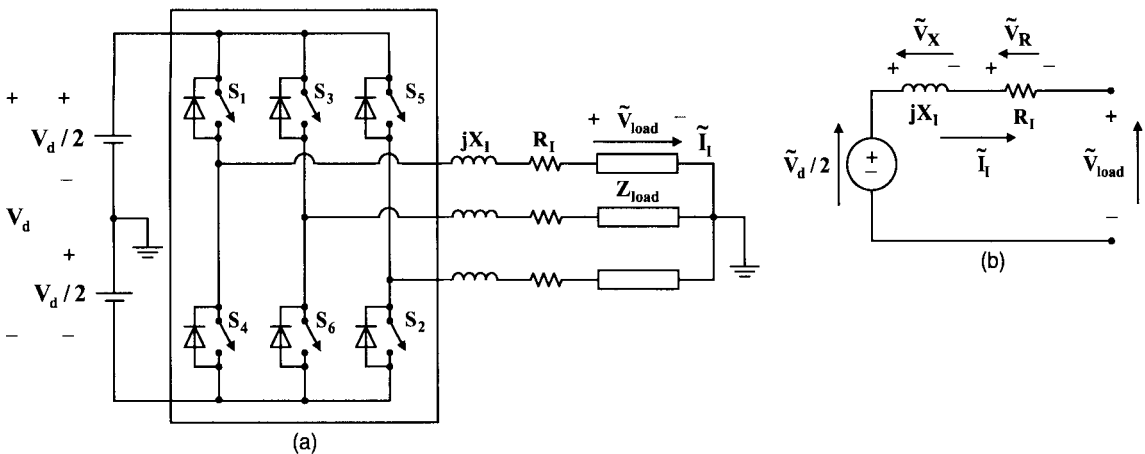


FIGURE 4.16 (a) Equivalent circuit for inverter (feeding a load) where input voltage V_d is referred to the primary side. (b) Equivalent circuit for inverter where input voltage $V_d/2$ is referred to the secondary side.

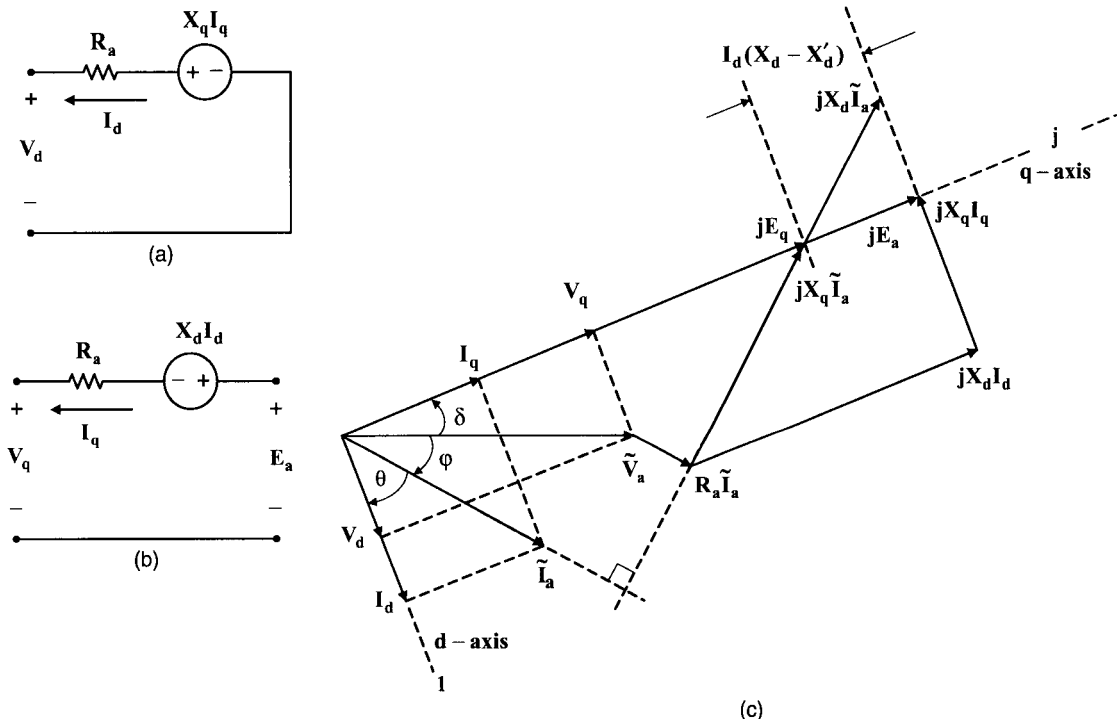


FIGURE 4.17 (a) The d-equivalent circuit of salient-pole synchronous machine without cross-coupling of d - and q -axes. (b) The q -equivalent circuits of salient-pole synchronous machine without cross-coupling of d - and q -axes. (c) Phasor diagram of salient-pole synchronous machine without cross-coupling of d - and q -axes.

Terminal voltage component in d -axis as a function of the fluxes and currents in d - and q -axes:

$$V_d = -\Psi_q - R_a I_d = X_q I_q - R_a I_d. \quad (4-27)$$

Terminal voltage component in q -axis:

$$V_q = \Psi_d - R_a I_q = E_a - X_d I_d - R_a I_q. \quad (4-28)$$

Eqs. 4-27 and 4-28 solved for I_d and I_q yield

$$I_d = \frac{-R_a V_d + X_q (E_a - V_q)}{X_d X_q + R_a^2}, \quad (4-29)$$

$$I_q = \frac{X_d V_d + R_a (E_a - V_q)}{X_d X_q + R_a^2}, \quad (4-30)$$

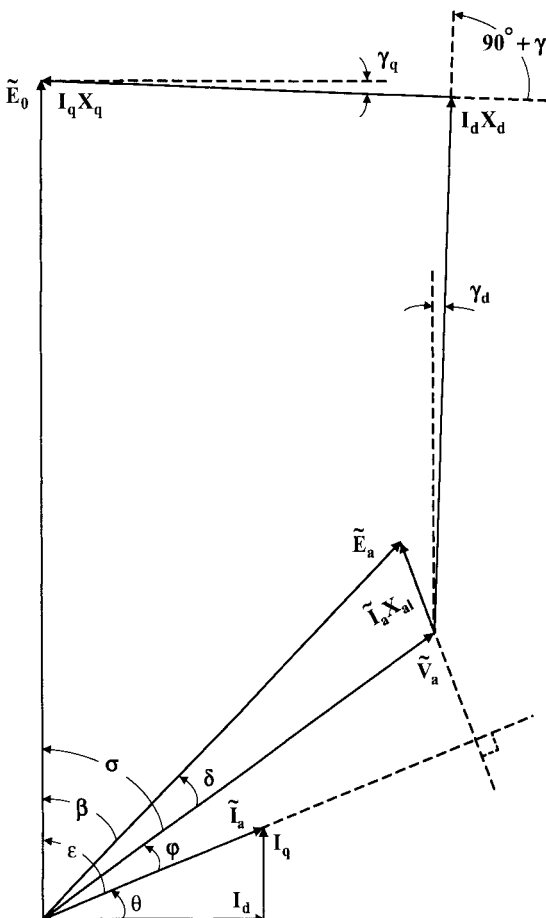


FIGURE 4.18 Phasor diagram of salient-pole synchronous machine with cross-coupling of d - and q -axes [19, 20].

which may be written in terms of the terminal voltage \tilde{V}_a :

$$I_d = \frac{-R_a |\tilde{V}_a| \sin \delta + X_q (E_a - |\tilde{V}_a| \cos \delta)}{X_d X_q + R_a^2}, \quad (4-31)$$

$$I_q = \frac{X_d |\tilde{V}_a| \sin \delta + R_a (E_a - |\tilde{V}_a| \cos \delta)}{X_d X_q + R_a^2}, \quad (4-32)$$

where

$$|\tilde{V}_a| = \sqrt{V_d^2 + V_q^2}, \quad (4-33)$$

$$|\tilde{I}_a| = \sqrt{I_d^2 + I_q^2}. \quad (4-34)$$

4.2.3 Application Example 4.1: Steady-State Analysis of a Nonsalient-Pole (Round-Rotor) Synchronous Machine

A three-phase ($m = 3$), four-pole ($p = 4$) nonsalient-pole (round-rotor) synchronous machine has the

parameters $X_s = 2$ pu and $R_a = 0.05$ pu. It is operated at (the phase voltage) $V_a = 1$ pu at an overexcited (lagging current based on the generator reference system, where the current flows out of the machine) displacement power factor of $\cos \varphi = 0.8$ lagging, and per-phase current $|\tilde{I}_a| = 1$ pu. The base (rated phase) values are $|\tilde{V}_{a\text{rated}}| = V_{\text{base}} = 24$ kV, $|\tilde{I}_{a\text{rated}}| = I_{\text{base}} = 1.4$ kA, and the base impedance is $Z_{\text{base}} = V_{\text{base}}/I_{\text{base}} = 17.14 \Omega$.

1. Draw the per-phase equivalent circuit of this machine.
2. What is the total rated apparent input power S (expressed in MVA)?
3. What is the total rated real input power P (expressed in MW)?
4. Draw a per-phase phasor diagram with the voltage scale of $1.0 \text{ pu} \equiv 3$ inches, and the current scale of $1.0 \text{ pu} \equiv 2.5$ inches.
5. From this phasor diagram determine the per-phase induced voltage $|\tilde{E}_a|$ and the torque angle δ .
6. Calculate the rated speed (in rpm) of this machine at $f = 60$ Hz.
7. Calculate the angular velocity ω_s (in rad/s).
8. Calculate the total (approximate) shaft power $P_{\text{shaft}} \approx 3(E_a \cdot V_a \cdot \sin \delta)/X_s$.
9. Find the shaft torque T_{shaft} (in Nm).
10. Determine the total ohmic loss of the motor $P_{\text{loss}} = 3 \cdot R_a |\tilde{I}_a|^2$.
11. Repeat the above analysis for $\cos \varphi = 0.8$ underexcited (leading current based on generator notation) displacement power factor and $|\tilde{I}_a| = 0.5$ pu.

4.2.4 Application Example 4.2: Calculation of the Synchronous Reactance X_s of a Cylindrical-Rotor (Round-Rotor, Nonsalient-Pole) Synchronous Machine

A $p = 2$ pole, $f = 60$ Hz synchronous machine (generator, alternator, motor) is rated $S_{\text{rat}} = 16$ MVA at a lagging (generating reference system) displacement power factor $\cos \varphi = 0.8$, a line-to-line terminal voltage of $V_{L-L} = 13,800$ V, and a (one-sided) air-gap length of $g = 0.0127$ m. The stator has 48 slots and has a three-phase double-layer, 60° phase-belt winding with 48 armature coils having a short pitch of $2/3$. Each coil consists of one turn $N_{\text{coil}} = 1$. Sixteen stator coils are connected in series, that is, the number of series turns per phase of the stator (st) are $N_{st\text{phase}} = 16$ (see Fig. E4.2.1). The maximum air-gap flux density at no load (stator current $I_{st\text{phase}} = 0$) is $B_{st\text{max}} = 1$ T.

There are eight field coils per pole (see Fig. E4.2.2) and they are pitched 44–60–76–92–124–140–156–172 degrees, respectively, as indicated in Fig. E4.2.2. Each field coil has 18 turns. The developed rotor (field) magnetomotive force (*mmf*) F , is depicted in Fig. E4.2.3. Note that the field *mmf* is approximately sinusoidal.

- Calculate the distribution (breadth) factor of the stator winding $k_{st,b}$ ($=k_{st,d}$).
- Calculate the fundamental pitch factor of the stator winding $k_{st,pl}$.

- Calculate the pitch factor of the rotor (r) winding k_{rp} .
- Determine the stator flux φ_{stmax} .
- Compute the area ($area_p$) of one pole.
- Compute the field (f) current I_{fo} required at no load.
- Determine the synchronous (s) reactance (per phase value) X_s of this synchronous machine in ohms.
- Find the base impedance Z_{base} expressed in ohms.
- Express the synchronous reactance X_s in per unit (pu).

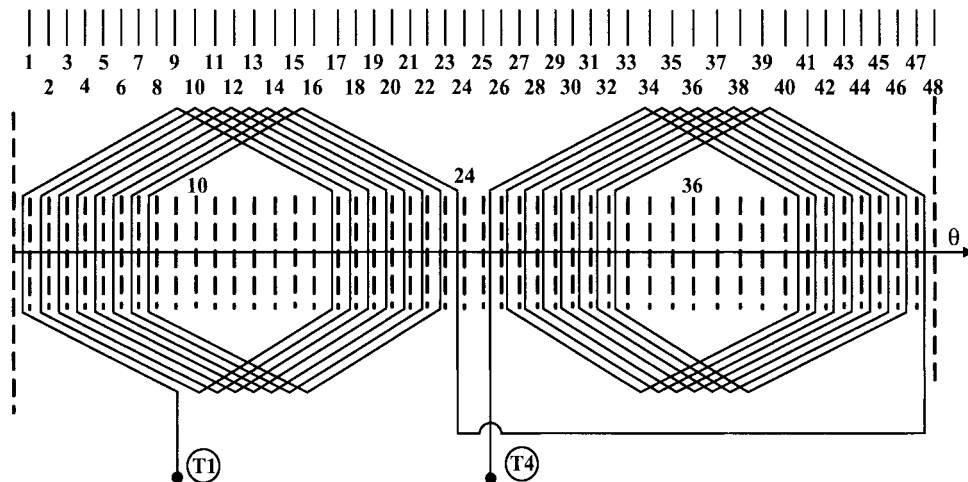


FIGURE E4.2.1 Stator winding of two-pole, three-phase synchronous machine.

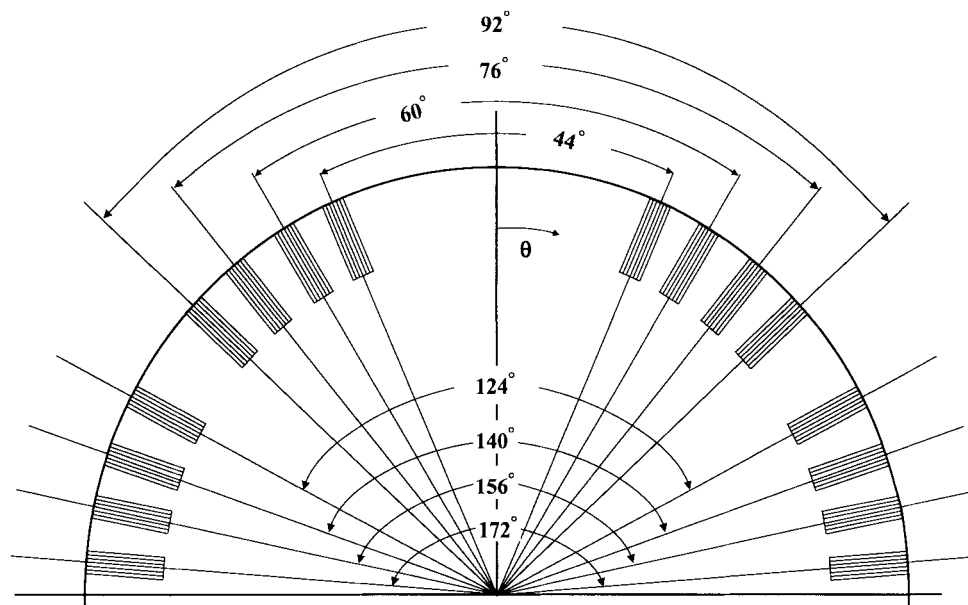


FIGURE E4.2.2 Rotor winding of two-pole, three-phase synchronous machine.

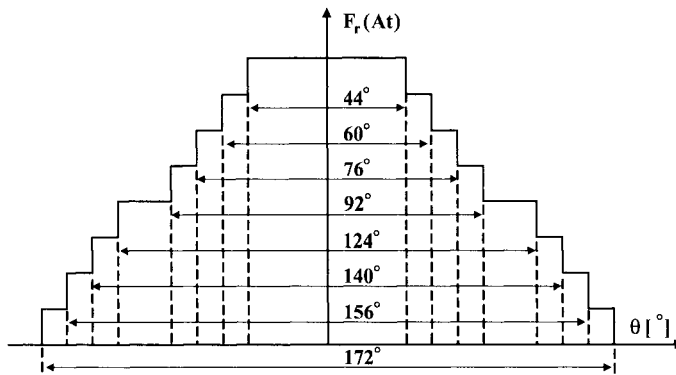


FIGURE E4.2.3 Rotor mmf F_r of two-pole, three-phase synchronous machine.

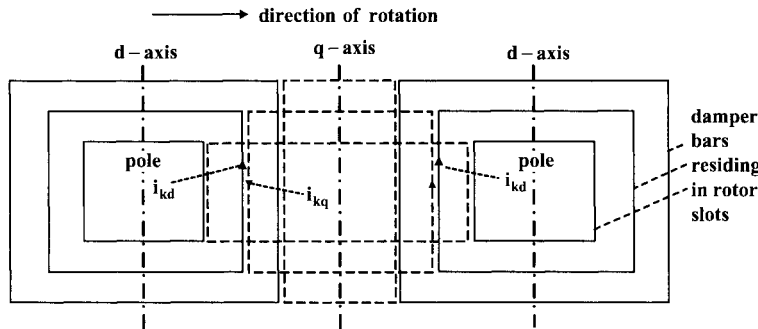


FIGURE E4.4.1 Decomposition of amortisseur winding of a two-pole generator [40]. In this graph only six damper windings are shown: three in the d -axis and three in the q -axis. Figures E4.4.2 to E4.4.4 and E4.4.11 to E4.4.13 provide details about the location of the 16 damper bars within the rotor slots.

4.2.5 Application Example 4.3: $dq0$ Modeling of a Salient-Pole Synchronous Machine

Engineers are most concerned about the torques generated by the machine under abnormal operating conditions such as

- balanced three-phase short-circuit,
- line-to-line short-circuit,
- line-to-neutral short-circuit,
- out-of-phase synchronization,
- synchronizing and damping torques,
- reclosing, and
- stability.

Linear (not saturation-dependent) reactances are assumed and amortisseur (damper) windings are neglected except for some out-of-phase synchronization results and for reclosing events. Most machines have very weak damper windings and, therefore, this assumption is justified.

4.2.6 Application Example 4.4: Calculation of the Amortisseur (Damper Winding) Bar Losses of a Synchronous Machine during Balanced Three-Phase Short-Circuit, Line-to-Line Short-Circuit, Out-of-Phase Synchronization, and Unbalanced Load Based on the Natural abc Reference System [40]

For the analysis of subtransient phenomena, a simulation of the damper-winding system of alternators is of utmost importance. Concordia [7] expanded the usual d - and q -axes decomposition by introducing more than two (e.g., d and q) damper winding systems. In this application example the amortisseur is approximated by 16 damper windings in the d - and q -axes as shown in Fig. E4.4.1, that is, 8 damper windings in the d -axis and 8 damper windings in the q -axis. Damper bars reside in the rotor slots and some bars are embedded in the solid rotor pole zone. To simplify this analysis it is assumed that the rotor

is laminated; that means no eddy currents are induced, saturation is neglected, and there are no damper bars embedded in the pole zone.

4.2.7 Application Example 4.5: Measured Voltage Ripple of a 30 kVA Permanent-Magnet Synchronous Machine, Designed for a Direct-Drive Wind-Power Plant

A permanent-magnet generator is to be designed [29, 30] for a variable-speed drive of a wind-power plant without any mechanical gear. The rated speed range is from 60 to 120 rpm. Line-to-neutral voltages V_{L-N} and line-to-line voltages V_{L-L} are recorded at no load and under rated load.

The voltage wave shapes are subjected to a Fourier analysis. Figures E4.5.1 and E4.5.2 depict the line-to-neutral voltages at no load and rated load, respectively, and Tables E4.5.1 and E4.5.2 represent their Fourier coefficients. Figures E4.5.3 and E4.5.4 represent the line-to-line voltages at no load and at rated load, and Tables E4.5.3 and E4.5.4 list their spectra. To minimize the size of this low-speed generator, the stator pitch k_p and distribution k_d winding factors are chosen relatively high ($k_p \cdot k_d = 0.8$) resulting in a somewhat nonsinusoidal voltage wave shape. The generator feeds a rectifier and for this

reason the nonsinusoidal voltage wave shape does not matter, except it increases the generator losses within acceptable limits.

4.2.8 Application Example 4.6: Calculation of Synchronous Reactances X_d and X_q from Measured Data Based on Phasor Diagram

Synchronous reactances are defined for fundamental frequency. Subjecting the voltage and current to a Fourier series yields the following data: line-to-neutral terminal voltage $V_{(l-n)}$, phase current $I_{(l-n)}$, instead of the induced voltage E the no-load voltage

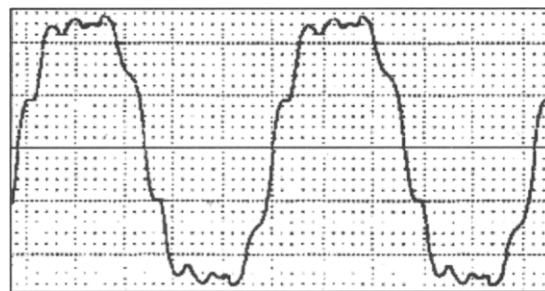


FIGURE E4.5.2 Measured line-to-neutral V_{L-N} voltage wave shape of permanent-magnet generator at load designed for wind-power application [44].

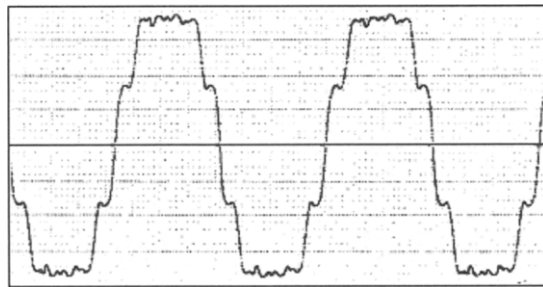


FIGURE E4.5.1 Measured line-to-neutral V_{L-N} voltage wave shape of permanent-magnet generator at no load designed for wind-power application [44].

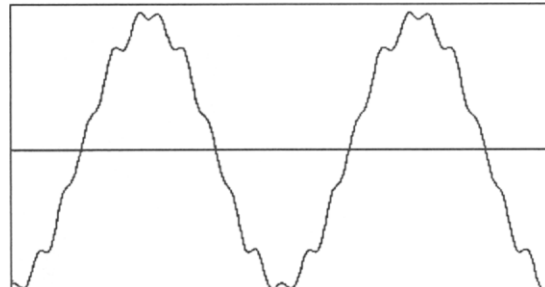


FIGURE E4.5.3 Measured line-to-line V_{L-L} voltage wave shape of permanent-magnet generator at no load designed for wind-power application [44].

TABLE E4.5.1 Harmonic Spectrum of Fig. E4.5.1

Harmonic order	Harmonic magnitude (%)	Harmonic order	Harmonic magnitude (%)
1	100	7	3
2	0	8	0
3	11	9	8
4	0	10	0
5	1	11	7
6	0	12	0

TABLE E4.5.2 Harmonic Spectrum of Fig. E4.5.2

Harmonic order	Harmonic magnitude (%)	Harmonic order	Harmonic magnitude (%)
1	100	7	2
2	0	8	0
3	14	9	7
4	0	10	0
5	1	11	5
6	0	12	0

$V_{(l-n)\text{no-load}} \approx E$ can be used for a permanent-magnet machine if saturation is not dominant. The displacement power factor angle ϕ and the torque angle δ can be determined from an oscilloscope recording and from a stroboscope, respectively. The ohmic resistance R can be measured as a function of the machine temperature. The relationship between these quantities is given by the phasor diagram of Fig. E4.6.1.

From the above phasor diagram one can derive the following relations for the synchronous reactances X_q and X_d .

TABLE E4.5.3 Harmonic Spectrum of Fig. E4.5.3

Harmonic order	Harmonic magnitude (%)	Harmonic order	Harmonic magnitude (%)
1	100	7	3
2	1	8	0
3	0	9	0
4	1	10	0
5	1	11	6
6	0	12	0

TABLE E4.5.4 Harmonic Spectrum of Fig. E4.5.4

Harmonic order	Harmonic magnitude (%)	Harmonic order	Harmonic magnitude (%)
1	100	7	3
2	1	8	0
3	1	9	0
4	0	10	0
5	1	11	6
6	0	12	0

$$X_q = \frac{V_{(l-n)} \sin \delta + RI_{(l-n)} \sin \delta \cos l + RI_{(l-n)} \cos \delta \sin l}{I_{(l-n)} \cos l \cos \delta - I_{(l-n)} \sin l \sin \delta}, \quad (\text{E4.6-1})$$

$$X_d = \frac{E - V_{(l-n)} \cos \delta - RI_{(l-n)} \cos(\delta - l)}{I_{(l-n)} \cos(90^\circ - l - \delta)}. \quad (\text{E4.6-2})$$

An application of these relations is given in [44].

4.2.9 Application Example 4.7: Design of a Low-Speed 20 kW Permanent-Magnet Generator for a Wind-Power Plant

A $P = 20$ kW, $V_{L-L} = 337$ V permanent-magnet generator has the cross sections of Figs. E4.7.1 and E4.7.2. The number of poles is $p = 12$ and its rated speed is $n_{\text{rat}} = n_s = 60$ rpm, where n_s is the synchronous speed. The B-H characteristic of the neodymium–iron–boron (NdFeB) permanent-magnet material is shown in Fig. E4.7.3.

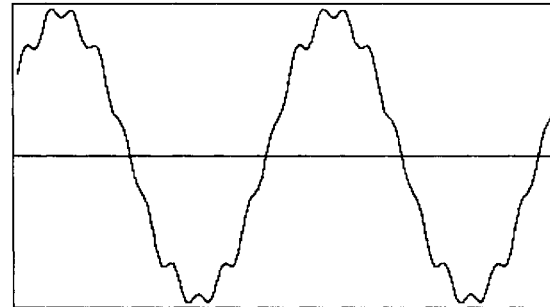


FIGURE E4.5.4 Measured line-to-line V_{L-L} voltage wave shape of permanent-magnet generator at rated load designed for wind-power application [44].

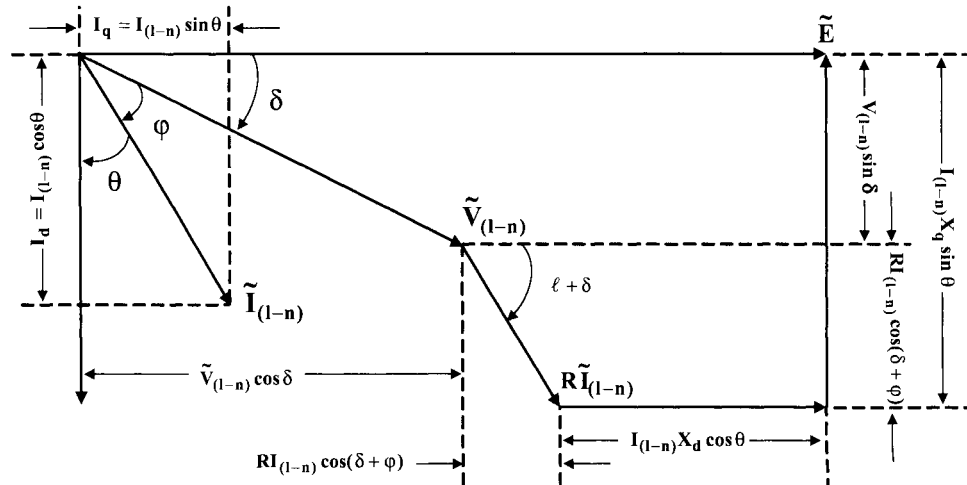


FIGURE E4.6.1 Phasor diagram of synchronous machine with saliency.

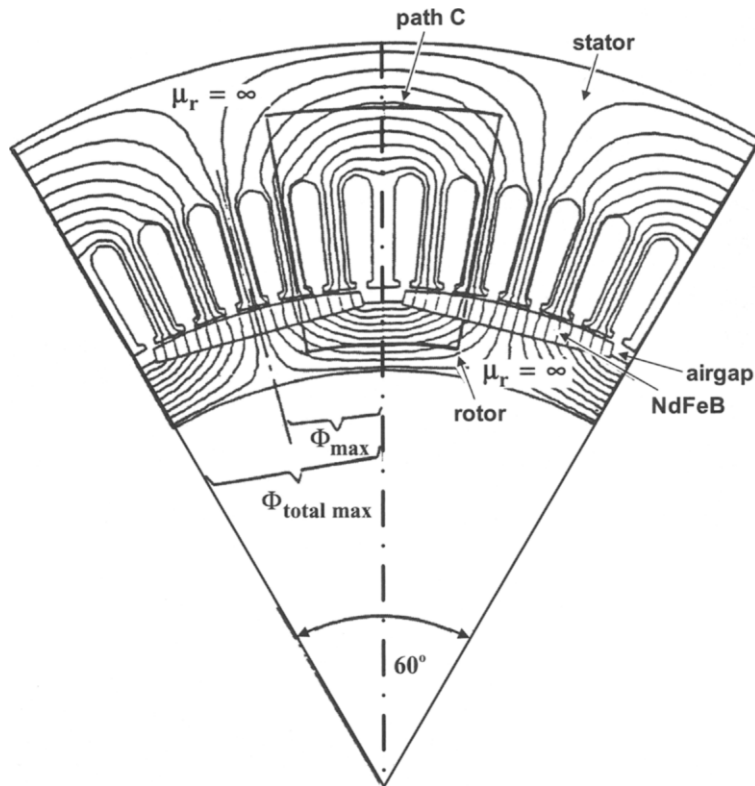


FIGURE E4.7.1 Cross section of one period (two pole pitches) of permanent-magnet machine with no-load field.

- Calculate the frequency f of the stator voltages and currents.
- Apply Ampere's law to path C (shown in Figs. E4.7.1 and E4.7.2) assuming the stator and rotor iron cores are ideal ($\mu_r \rightarrow \infty$).
- Apply the continuity of flux condition for the areas A_m and A_g perpendicular to path C (two times the one-sided magnet (m) length l_m , and two times the one-sided air gap (g) length l_g , respectively). Furthermore $l_m = 7 \text{ mm}$, $l_g = 1 \text{ mm}$, $A_m = 11,668 \text{ mm}^2$, and $A_g = 14,469 \text{ mm}^2$.
- Provided the relative permeability of the stator and rotor cores is $\mu_r \rightarrow \infty$, compute the load line of this machine. Plot the load line in a figure similar to that of Fig. E4.7.3. Is the permanent-magnet material (NdFeB) operated at the point of the maximum energy product?
- What is the recoil permeability μ_R of the NdFeB material?
- Compute the fluxes Φ_{max} and $\Phi_{\text{total max}} = 2\Phi_{\text{max}}$, provided there are $N = 360$ turns per stator phase, the (pitch and distribution) winding factor is $k_w = 0.8$, and the iron-core stacking factor is $k_s = 0.94$.
- Determine the diameter D of stator wire for a copper-fill factor of $k_{cu} = 0.62$ and a stator slot cross section of $A_{\text{st_slot}} = 368 \text{ mm}^2$.

4.2.10 Application Example 4.8: Design of a 10 kW Wind-Power Plant Based on a Synchronous Machine

Design a wind-power plant (Fig. E4.8.1) feeding $P_{\text{out_transformer}} = 10 \text{ kW}$ into the distribution system at a line-to-line voltage of $V_{L-L, \text{system}} = 12.47 \text{ kV} = V_{L-L, \text{secondary of transformer}}$. The wind-power plant consists of a $Y - \Delta$ three-phase (ideal) transformer connected between three-phase PWM inverter and power system, where the Y is the primary and Δ is the secondary of the ideal transformer (Fig. E4.8.2). The input voltage of the PWM inverter (see Chapter 1, Fig. E1.5.1) is $V_{DC} = 600 \text{ V}$, where the inverter delivers an output AC current I_{inverter} at unity displacement power factor $\cos \varphi = 1$ to the primary (Y) of the $Y - \Delta$ transformer, and the inverter output line-to-line voltage is $V_{L-L, \text{inverter}} = 240 \text{ V} = V_{L-L, \text{primary of transformer}}$.

The three-phase rectifier (see Chapter 1, Fig. E1.2.1) with one self-commuted PWM-operated switch (IGBT) is fed by a three-phase synchronous generator. The input line-to-line voltages of the three-phase rectifier is $V_{L-L, \text{rectifier}} = 480 \text{ V} = V_{L-L, \text{generator}}$. Design the mechanical gear between wind turbine and generator (with $p = 2$ poles at $n_S = 3600 \text{ rpm}$, utilization factor $C = 1.3 \text{ kW min/m}^3$,

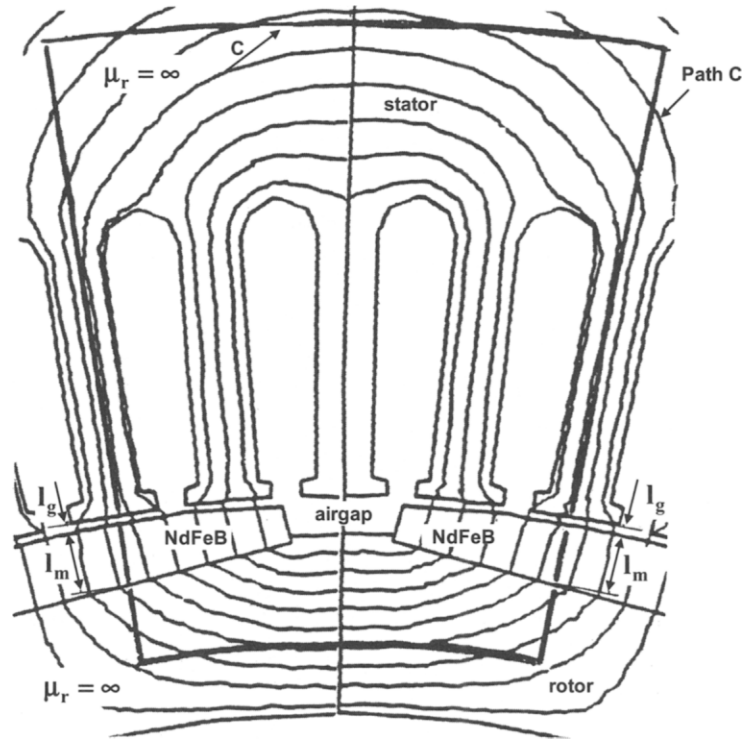


Figure E4.7.2 Magnified cross section of area enclosed by path C of a pole pitch of permanent-magnet machine (see Fig. E4.7.1).

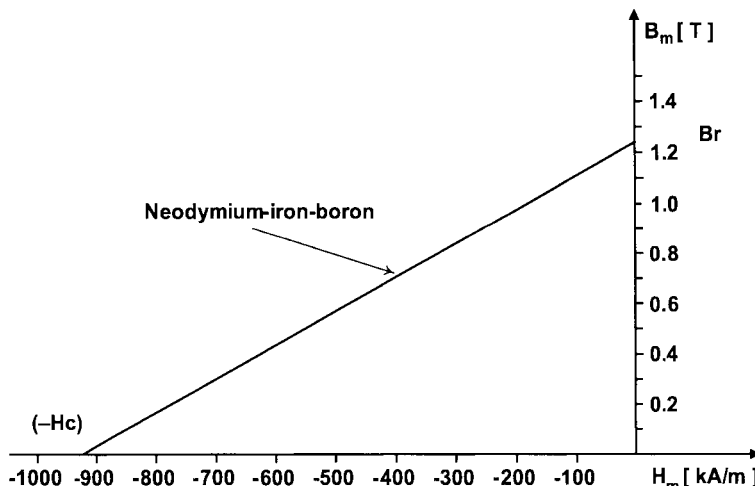


FIGURE E4.7.3 B_m-H_m characteristic of neodymium–iron–boron (NdFeB) permanent-magnet material.

$D_{\text{rotor}} = 0.2 \text{ m}$, the leakage reactance $X_{\text{leakage}} = 2\pi f L_{\text{leakage}}$ is 10% of the synchronous reactance $X_s = 1.5 \text{ pu}$, maximum flux density $B_{\max} = 0.7 \text{ T}$, iron-stacking factor $k_{fe} = 0.95$, stator winding factor $k_s = 0.8$, rotor winding factor $k_r = 0.8$, and torque angle $\delta = 30^\circ$ so that a wind turbine can operate at $n_{\text{turbine}} = 30 \text{ rpm}$. Lastly, the wind turbine – using the famous Lanchester-Betz limit [45] for the

maximum energy efficiency of a wind turbine as a guideline – is to be designed for the rated wind velocity of $v = 10 \text{ m/s}$ at an altitude of 1600 m and a coefficient of performance (actual efficiency) $c_p = 0.3$. You may assume that all components (transformer, inverter, rectifier, generator, mechanical gear) except the wind turbine have each an efficiency of $\eta = 95\%$.

- a) Based on the given transformer output power of $P_{\text{out_transformer}} = 10 \text{ kW}$ compute the output powers of inverter, rectifier, generator, gear, and wind turbine.
- b) For the circuit of Fig. E4.8.1 determine the transformation ratio (N_Y/N_Δ) of the $Y - \Delta$ transformer, where the Y is the primary (inverter side) and Δ the secondary (power system side).
- c) What is the phase shift between $\tilde{V}_{L-L \text{ system}}$ and $\tilde{V}_{L-L \text{ inverter}}$?
- d) What is the phase shift between $\tilde{I}_{L \text{ system}}$ and $\tilde{I}_{L \text{ inverter}}$?
- e) Use sinusoidal PWM to determine for the circuit of Fig. E1.5.1 of Chapter 1 the inverter output current $\tilde{I}_{\text{inverter}}$ which is in phase with $\tilde{V}_{L-N \text{ inverter}} = 138.57 \text{ V}$, that is, a (unity) displacement power factor $\cos \varphi = 1$ at an inverter switching frequency of $f_{sw} = 7.2 \text{ kHz}$. You may assume $R_{\text{system}} = 50 \text{ m}\Omega$, $X_{\text{system}} = 0.1 \Omega$, $R_{\text{inverter}} = 10 \text{ m}\Omega$, and $X_{\text{inverter}} = 0.377 \Omega$ at $f = 60 \text{ Hz}$.
- f) For the circuit of Fig. E1.2.1 of Chapter 1 and a duty cycle of $\delta = 50\%$, compute the input current of the rectifier $I_{\text{rectifier}}$.
- g) Design the synchronous generator for the above given data provided it operates at unity displacement power factor.
- h) Design the mechanical gear.
- i) Determine the radius of the wind turbine blades for the given conditions.

4.2.11 Synchronous Machines Supplying Nonlinear Loads

Frequently synchronous machines or permanent-magnet machines are used together with solid-state converters, that is, either rectifiers as a load [46–49] or inverters feeding the machine. The question arises how much current distortion can be permitted in order to prevent noise and vibrations as well as overheating? It is recommended to limit the total har-

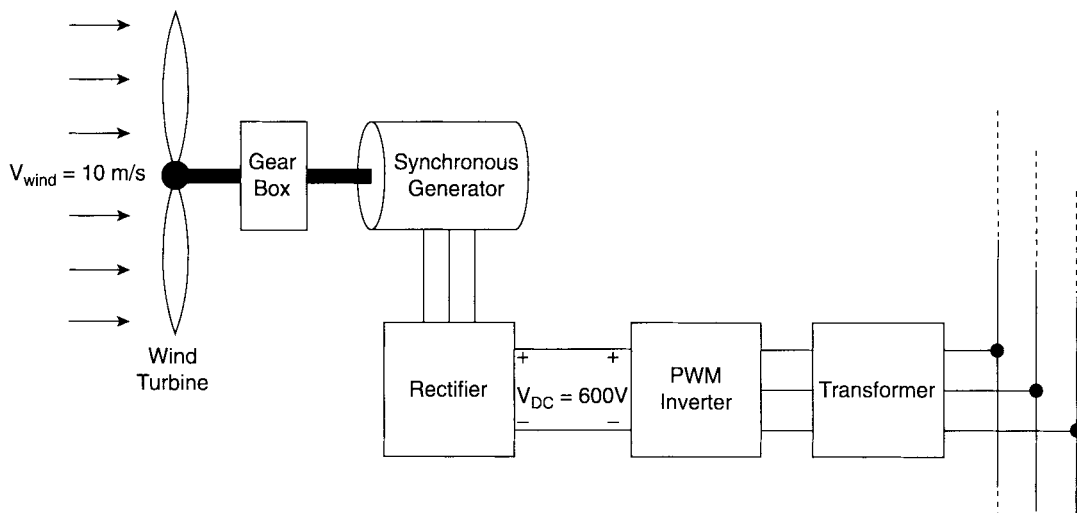


FIGURE E4.8.1 Block diagram of wind-power plant.

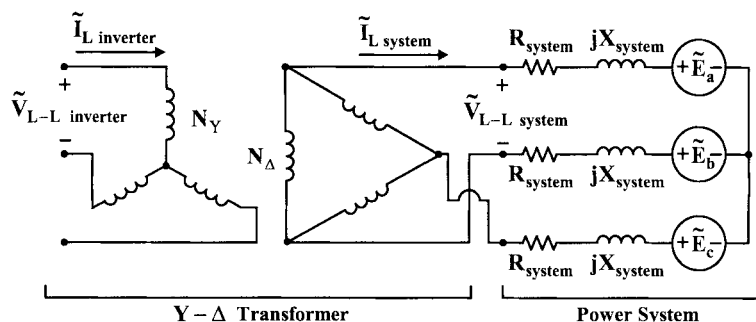


FIGURE E4.8.2 $Y - \Delta$ three-phase transformer connected to power system.

monic current distortion of the phase current to $THD_i \leq 5\text{--}20\%$ as specified by recommendation IEEE-519 (see Chapter 1). The 5% limit is for very large machines and the 20% limit is for small machines. The calculation of the synchronous, transient, and subtransient reactances based on numerical field calculations is addressed in [50]. Synchronous machines up to 5 MW are used in variable-speed drives for wind-power plants. Enercon [51] uses synchronous generators with a large pole number; this enables them to avoid any mechanical gear within the wind-power train. The AC output is rectified and an inverter supplies the wind power to the grid. Hydrogenerators are another example where a large number of poles are used.

4.2.12 Switched-Reluctance Machine

Switched-reluctance machines [52–55] have the advantage of simplicity: such machines consist of a salient pole (solid) rotor member without any winding and the stator member carries concentrated coils that are excited by a solid-state converter. The only disadvantages of such machines are the encoder required to sense the speed of the rotor and the acoustic noise emanating from the salient-pole rotor. The windage losses of such machines can be considerable. Figure 4.19a,b,c,d illustrates how the field of a switched-reluctance machine changes as a function of the rotor position.

4.2.13 Some Design Guidelines for Synchronous Machines

In order for rotating machines to work properly and not to cause power quality problems, limits for maximum flux and current densities must be met so that neither excessive saturation nor heating occurs. These limits are somewhat different for induction (see Chapter 3) and synchronous machines.

4.2.13.1 Maximum Flux Densities

Table 4.1 lists recommended maximum flux densities within the stator and rotor of synchronous machines.

4.2.13.2 Recommended Current Densities

Table 4.2 lists recommended current densities within the stator and rotor windings of synchronous machines. These current densities depend on the cooling methods applied.

4.2.13.3 Relation between Induced E_{phase} and Terminal V_{phase} Voltages

The relationship between induced voltage and terminal voltage is for motor operation approximately $E_{\text{phase}}/V_{\text{phase}} \approx 0.95$ and for generator operation $E_{\text{phase}}/V_{\text{phase}} \approx 1.05$.

4.2.13.4 Iron-Core Stacking Factor and Copper-Fill Factor

The iron-core stacking factor depends on the lamination thicknesses. An approximate value for most commonly used designs is $k_{fe} \approx 0.95$.

The copper-fill factor depends on the winding cross section (e.g., round, square) and the wire diameter. An approximate value for most commonly used designs is $k_{cu} \approx 0.70$.

4.2.14 Winding Forces during Normal Operation and Faults

In power apparatus magnetic forces are often large enough to cause unwanted noise or disabling damage. For instance, in [56] the problem of stator bar vibrations causing mechanical wear in hydrogenerators is addressed. Useful methods for reducing the vibrations, which are caused by magnetic forces, are suggested. Along with the suggestions a force calculation

TABLE 4.1 Guidelines for Maximum Flux Densities (Measured in Teslas) in Synchronous Machines

	Stator teeth, maximum value	Stator teeth, middle of tooth height	Solid rotor	Solid rotor teeth, near winding	Solid rotor teeth, not near winding	Solid rotor back iron, forged iron	Solid rotor back iron, cast iron	
Stator back iron	1–1.4	1.6–1.8	1.35–1.55	1.2–1.5	<2.4	1.4–1.6	1–1.4	0.7

TABLE 4.2 Guidelines for Current Densities (Measured in A/mm²) in Windings of Synchronous Machines

Without forced air cooling	With forced air cooling (e.g., ventilator)	Hydrogen or indirect water cooling	Direct water cooling
1–2	2–4	4–8	8–16

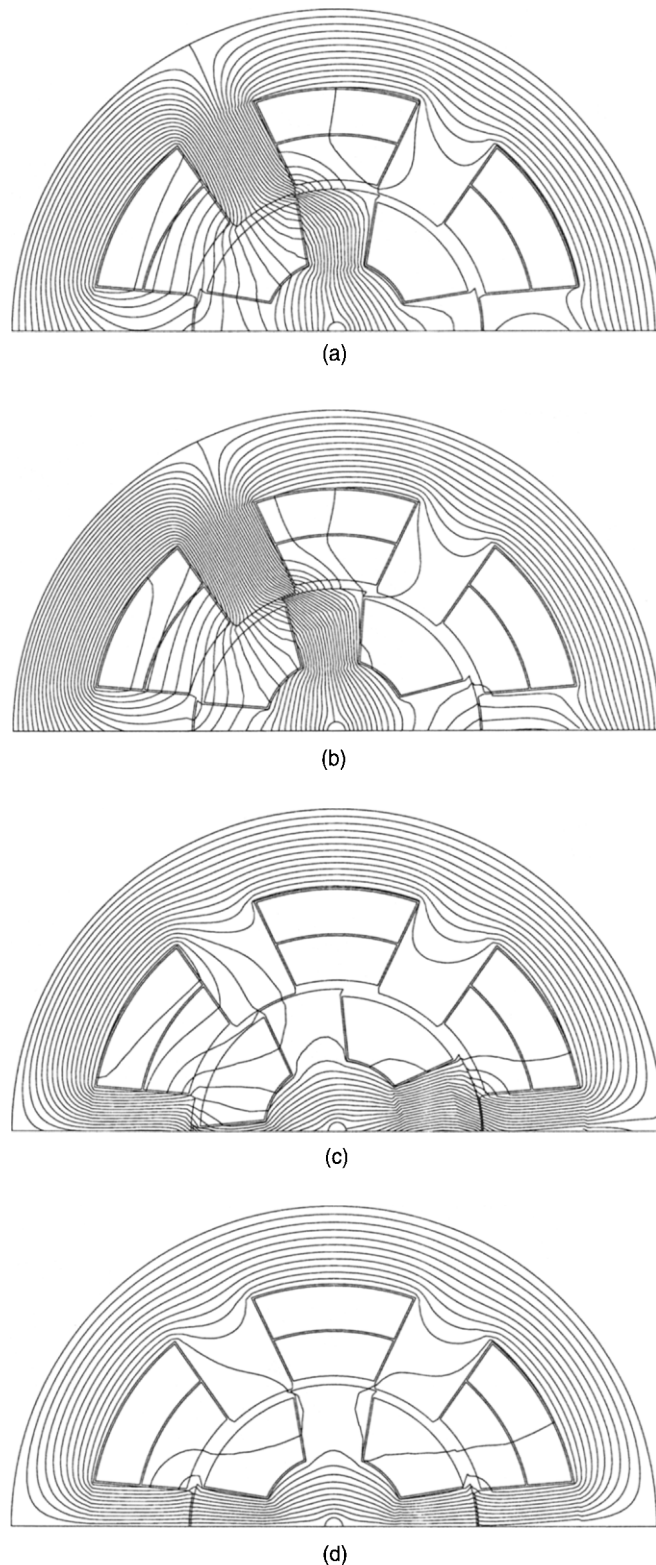


FIGURE 4.19 Field of switched-reluctance machine for (a) rotor position #1 (0 mechanical degrees), rotor position #2 (5 mechanical degrees), (c) rotor position #3 (15 mechanical degrees), and (d) rotor position #4 (30 mechanical degrees).

formula proposed in 1931 is given. The surface integral method recommended in this section is an improvement over such formulas since it uses magnetic field calculation, which accounts for magnetic saturation of the iron cores.

4.2.14.1 Theoretical Basis

Several approaches may be taken to arrive at the expressions necessary for the surface integral force calculations. Using a stress of Maxwell and energy considerations, Stratton [57] formally derives this expression for the total force on a nonferromagnetic body:

$$\bar{F} = \int_{S_1} [\mu \bar{H}(\bar{H} \cdot \vec{n}) - \frac{\mu}{2} H^2 \vec{n}] da. \quad (4-35)$$

In Eq. 4-35 S_1 is an arbitrary surface surrounding the body. Equivalent expressions are given by Carpenter [58]. He begins by assuming that "any distribution of poles or currents, or both, which, when put in place of a piece of magnetized iron, reproduces the magnetic-field condition at all points outside the iron, must experience the same total mechanical force as a part which it replaces." One special distribution consists of poles and currents existing on a surface surrounding the body of interest. The force on the body is thus modeled by the force densities

$$F_t = \mu_o H_n H_t, \quad (4-36a)$$

$$F_n = \frac{1}{2} \mu_o (H_n^2 - H_t^2), \quad (4-36b)$$

in the tangential and normal directions, respectively. Surface integrals of these densities then give the total force on the object.

A third treatment of the subject is made by Reichert [59]. He speaks of a quantity \bar{p} , the surface stress. Integration of stress,

$$\bar{p} = \frac{1}{\mu_o} (\vec{n} \cdot \vec{B}) \bar{B} - \frac{1}{2\mu_o} B^2 \vec{n}, \quad (4-37)$$

is said to give the total force on the body. This force calculation is equivalent to Stratton's and Carpenter's. However, Reichert goes on to adapt the stress to numerical methods.

Required characteristics of the above integration surfaces, which are clarified by Reichert, turn out to limit the possible application of the method. The necessary characteristics are

- Surface must be in air;
- An exception may be made to the above rule by creating an artificial air gap. This may be done if the artificial air gap does not cause a significant change in the magnetic field; and
- Surface may be any that fully encloses the body and follows the above rules.

Especially note that only the total force or torque acting on the body is given by the integration. No information can be obtained about the actual distribution of the force within the body. Figure 4.20 shows forces calculated with the above method.

4.3 HARMONIC MODELING OF A SYNCHRONOUS MACHINE

Detailed nonlinear models of a synchronous machine in the frequency domain have been developed for harmonic analysis [11–13]. These models, however, cannot accurately describe the transient and steady-state unbalanced operation of a synchronous machine under nonsinusoidal voltage and current conditions. A machine model in phase (*abc*) coordinates can naturally reproduce these abnormal operation conditions because it is based on a realistic representation that can take into account the explicit time-varying nature of the stator and the mutual stator–rotor inductances, as well as the spatial (space) harmonic effects. Harmonic modeling of synchronous machines is complicated by the following factors:

- **Frequency-Conversion Process.** Synchronous machines may experience a negative-sequence current in their armature (stator), e.g., under unbalanced three-phase conditions. This current may induce a second-order harmonic of this negative-sequence armature current in the rotor. The rotor harmonic in turn may induce a third-order harmonic of this negative-sequence current in the armature (mirror action), and so on. This frequency conversion causes the machine itself to internally generate harmonics, and therefore complicates the machine's reaction to external harmonics imposed by power sources.

- **Saturation Effects.** Saturation affects the machine's operating point. Saturation effects interact with the frequency-conversion process and cause a cross-coupling between the *d*- and *q*-axes [23].

- **Machine Load Flow (or System) Constraints.** Synchronous machine harmonic models are incorporated into harmonic load flow programs and must satisfy constraints imposed by the load flow program.

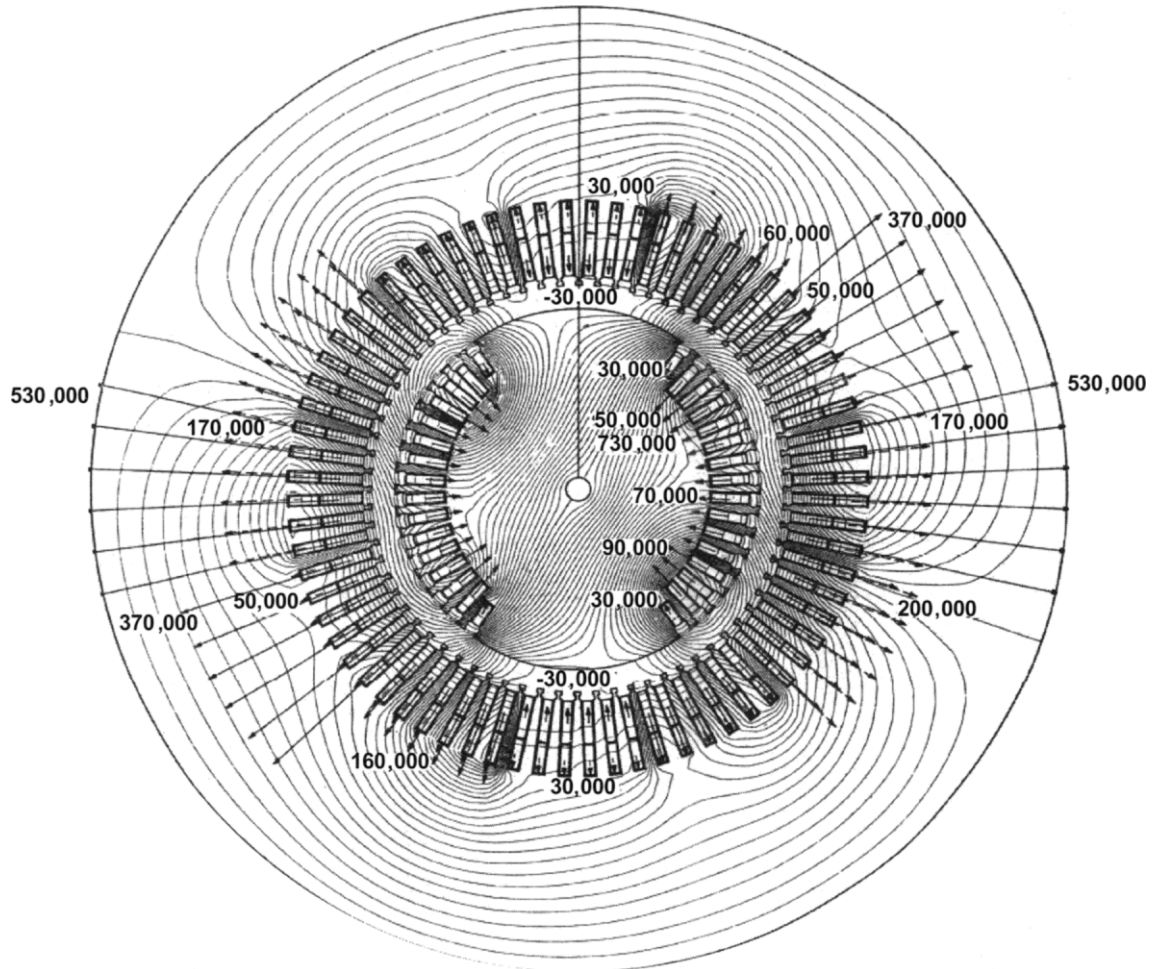


FIGURE 4.20 Flux and force (measured in N/m) distribution in a two-pole turbogenerator during a sudden three-phase short-circuit. The arrows indicate the direction and value (length of arrow) of the winding forces developed due to balanced subtransient, three-phase short-circuit.

- **Inverter-Fed or Rectifier-Loaded Machines.**

Examples are drives employed by the French railroad system, hybrid automobile drives that predominantly are based on brushless DC machines [24, 25], wind-power applications [51], and rotating rectifiers for synchronous generators [49].

In one of the first models in the phase (*abc*) domain, the analysis of [14] discusses the advantages of this synchronous machine representation in *abc* coordinates with respect to the models based on *dq* and $\alpha\beta\theta$ coordinates. A model using *abc* coordinates is employed [15] for the dynamic analysis of a three-phase synchronous generator connected to a static converter for high-voltage DC (HVDC) transmission, where harmonic terms up to the fourth

order are introduced in the stator-inductance matrix. In more recent contributions [16, 17] phase-domain models of the synchronous machine are employed and nonlinear saturation effects are incorporated.

4.3.1 Model of a Synchronous Machine as Applied to Harmonic Power Flow

A well-known harmonic model of a synchronous machine is based on the negative-, positive-, and zero-sequence reactances [60–62]

$$\begin{aligned} X_1(h) &= jhX_1 \\ X_2(h) &= jhX_2, \\ X_o(h) &= jhX_0 \end{aligned} \quad (4-38)$$

where h is the order of harmonics and X_1 , X_2 , X_0 are positive-, negative-, and zero-sequence reactances of the machine at fundamental frequency, respectively.

Losses may be included by adding a resistor, as shown in Fig. 4.21. This model of a synchronous machine is used in harmonic (balanced) power flow analysis.

4.3.1.1 Definition of Positive-, Negative-, and Zero-Sequence Impedances/Reactances

Symmetrical components [10] rely on positive-, negative- and zero-sequence impedances. Figure 4.22 gives a summary for the definition of these compo-

nents [62]. Figure 4.22a represents the three-phase circuit and Fig. 4.22b shows the per-phase equivalent circuit for the positive sequence. Figures 4.22c,d detail the circuits for the negative components, and

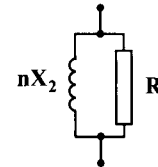


FIGURE 4.21 Harmonic equivalent circuit of synchronous machine based on negative-sequence impedance.

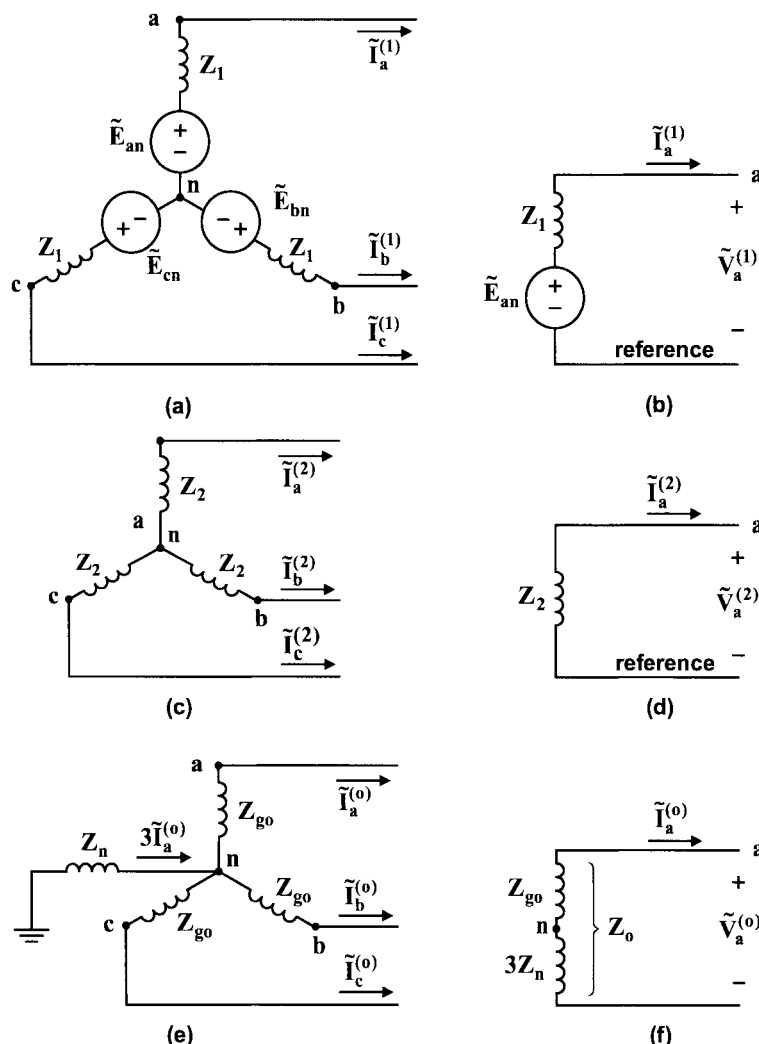


FIGURE 4.22 Definition of symmetrical components: (a) positive-sequence voltages, currents, and impedances; (b) per-phase positive-sequence circuit; (c) negative-sequence voltages, currents, and impedances; (d) per-phase negative-sequence circuit; (e) zero-sequence voltages, currents, and impedances; (f) per-phase zero-sequence circuit.

Figs. 4.22e,f represent the circuits for the zero-sequence components.

4.3.1.2 Relations between Positive-, Negative-, and Zero-Sequence Reactances and the Synchronous, Transient, and Subtransient Reactances

The following relations exist between sequence, transient, and subtransient reactances:

- The positive-sequence reactance X_1 is identical with the synchronous reactance X_s , which is $X_d = X_q$ for an (ideal) round-rotor turbogenerator.
- The negative-sequence reactance X_2 is identical with the subtransient reactance X_d'' .
- The zero-sequence reactance X_0 depends on the stator winding pitch and it varies from 0.1 to 0.7 of X_d'' .

Therefore,

$$\begin{cases} X_1 = X_s (= X_d = X_q, \text{ for an ideal round-rotor turbogenerator}) \\ X_2 = X_d'' \\ X_0 = 0.1X_d'' \text{ to } 0.7X_d'' \end{cases} \quad (4-39)$$

4.3.2 Synchronous Machine Harmonic Model Based on Transient Inductances

The simple model of Fig. 4.21 is inappropriate for harmonic modeling of a synchronous machine when detailed information (e.g., harmonic torque) must be extracted. To improve this model three cases are considered, where the synchronous machine is fed by

- harmonic currents,
- harmonic voltages, and
- combination of current and voltage harmonics (as expected in actual power systems).

Current-Source (Containing Harmonics) Fed Synchronous Machine. The stator voltages that result when balanced harmonic currents of order h are applied to a three-phase synchronous machine are determined. The synchronous machine has a field winding in the d -axis residing on the round rotor and no subtransient properties. In complex exponential notation the applied currents are

$$\begin{aligned} i_a &= i_h \exp j[h\omega t + \angle i_h] \\ i_b &= i_h \exp j[h\omega t + \angle i_h \mp 2\pi/3], \\ i_c &= i_h \exp j[h\omega t + \angle i_h \pm 2\pi/3] \end{aligned} \quad (4-40)$$

where the upper signs in Eq. 4-40 apply to the positive-phase sequence. Expressions for voltage, current, and flux may be obtained by taking the real part of each relevant complex equation. The a -phase stator voltage is according to [60]

$$v_a = i_h j h \omega \left(\frac{L'_d + L'_q}{2} \right) \exp j[h\omega t + \angle i_h] + i_h \left(\frac{L'_d - L'_q}{2} \right) \\ j[(h \mp 2)\omega \exp j(h \mp 2)\omega t + \angle i_h \mp 2\alpha]. \quad (4-41)$$

Using a similar analysis the b -phase voltage is

$$v_b = i_h j h \omega \left(\frac{L'_d + L'_q}{2} \right) \exp j[h\omega t \mp 2\pi/3 + \angle i_h] \\ + i_h j (h \mp 2)\omega \left(\frac{L'_d - L'_q}{2} \right) \exp j[(h \mp 2)\omega t \mp 2\alpha \pm 2\pi/3 + \angle i_h] \quad (4-42)$$

Comparing Eqs. 4-41 and 4-42 it can be noted that the additional harmonic voltage term has the opposite phase sequence than that of the applied current. For example, if the applied current of order $h = 7$ has a positive-phase sequence, then the additional harmonic voltage component has the order 5 with a negative-phase sequence. This is the usual situation for a balanced system. If, however, the applied current of order $h = 7$ has negative-phase sequence, then the additional harmonic voltage component has the order 9 with a positive-phase sequence, that is, not a zero-sequence as is commonly expected. Consequently, the phase voltage set will not be balanced. The analysis is also valid for the application of a negative-sequence current of fundamental frequency; in this case the additional component has the harmonic order 3 and has positive-phase sequence [63].

Voltage-Source (Containing Harmonics) Fed Synchronous Machine. If a balanced set of harmonic voltages is applied to a synchronous machine, an additional harmonic current with harmonic orders $(h \mp 2)$ – based on the results of the prior section – can be expected. The current solution is

$$\begin{aligned} i_a &= i_h \exp j[h\omega t + \angle i_h] + \bar{i}_h \exp j[(h \mp 2)\omega t + \angle \bar{i}_h] \\ i_b &= i_h \exp j[h\omega t + \angle i_h \mp 2\pi/3] + \bar{i}_h \exp j[(h \mp 2)\omega t \\ &\quad + \angle \bar{i}_h \pm 2\pi/3] \\ i_c &= i_h \exp j[h\omega t + \angle i_h \pm 2\pi/3] + \bar{i}_h \exp j[(h \mp 2)\omega t \\ &\quad + \angle \bar{i}_h \pm 2\pi/3] \end{aligned} \quad (4-43)$$

The quantities with a bar ($\bar{\cdot}$) are the current components with the frequency $(h \mp 2)\omega$. The phase sequence of these components is the opposite of that of the applied voltage with frequency $h\omega$. Using the results of the prior section, the a-phase voltage is

$$\begin{aligned} v_a &= i_h j h \omega \left(\frac{L'_d + L'_q}{2} \right) \exp j[h\omega t + \angle i_h] + i_h j (h \mp 2) \\ &\quad \omega \left(\frac{L'_d - L'_q}{2} \right) \exp j[(h \mp 2)\omega t \mp 2\alpha + \angle i_h] \\ &\quad + \bar{i}_h j (h \mp 2) \omega \left(\frac{L'_d + L'_q}{2} \right) \exp j[(h \mp 2)\omega t + \angle \bar{i}_h] \\ &\quad + \bar{i}_h j h \omega \left(\frac{L'_d - L'_q}{2} \right) \exp j[h\omega t \mp 2\alpha - \angle \bar{i}_h] \end{aligned} \quad (4-44)$$

For an applied voltage

$$V_a = V_h \exp j h \omega t. \quad (4-45)$$

Comparing Eqs. 4-44 and 4-45 results in

$$\begin{aligned} v_h &= i_h j h \omega \left(\frac{L'_d + L'_q}{2} \right) + \bar{i}_h j h \omega \left(\frac{L'_d - L'_q}{2} \right) \quad (4-46) \\ \angle i_h &= -\pi/2 \\ 0 &= +i_h (h \mp 2) \omega \left(\frac{L'_d - L'_q}{2} \right) + \bar{i}_h (h \mp 2) \omega \left(\frac{L'_d + L'_q}{2} \right) \end{aligned}$$

$$\angle \bar{i}_h = \mp 2\alpha + \angle i_h. \quad (4-47)$$

Eqs. 4-46 and 4-47 may be rearranged to give

$$v_h = j h \omega i_h \left(\frac{2L'_d L'_q}{L'_d + L'_q} \right). \quad (4-48)$$

Comparing Eqs. 4-42 and 4-48, one notes that the effective inductance at the applied frequency is different for the voltage- and current-source-fed machines.

If harmonic voltages are applied at both frequencies $h\omega$ and $(h \mp 2)\omega$, then Eqs. 4-46 and 4-47 can be modified by the inclusion of V_h and \bar{V}_h . The currents at both frequencies will be affected.

Synchronous Machines Fed by a Combination of Harmonic Voltage and Current Sources. When a synchronous machine is subjected to a harmonic voltage disturbance at frequency $h\omega$, harmonic-current components are drawn at $h\omega$ and at the associated frequency $(h \mp 2)\omega$. The upper sign applies to the positive- and the lower sign to the negative-phase sequence. Current flow at the associated frequency

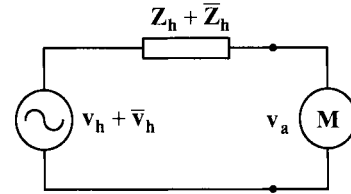


FIGURE 4.23 System in general case: balanced representation.

occurs because the machine is a time-varying electrical system. In a similar manner, a synchronous machine fed by harmonic currents at frequency $h\omega$ develops a voltage across its terminal at both the applied and the associated frequency $(h \mp 2)\omega$. Consequently the machine cannot be modeled by impedances defined by a single harmonic frequency [60].

In the general case, a machine will be subjected to applied voltages v_h and \bar{v}_h via system impedances z_h and \bar{z}_h as shown in Fig. 4.23.

Now a linearized Thevenin model can be employed for the system (left-hand side of Fig. 4.23). The applied harmonic voltages v_h and \bar{v}_h are assumed to have opposite phase sequences: one is of positive and the other of negative sequence. This is the condition that would apply if the distorting load responsible for the harmonic disturbance drew balanced currents. Consequently, a single-phase model may be used. Voltage equations for the general case are obtained by applying a voltage mesh equation at both frequencies $h\omega$ and $(h \mp 2)\omega$. The voltage components applying across the machine are those given by Eq. 4-44 in response to the currents given by Eq. 4-43. Voltage equations suggest the equivalent circuit shown in Fig. 4.24. The interaction between the two sides of the circuit is represented by a mutual inductance, which is a simplification. This mutual inductance is nonreciprocal, and the frequency difference between the two sides is ignored. This model may be used to calculate harmonic current flow.

The results presented here show that a synchronous machine cannot be modeled by one impedance (Fig. 4.21) if voltage sources have voltage components with several frequencies. In the case where one harmonic voltage source is large and the other small then $v_h \approx 0$, and the apparent machine impedance to current flow is linear and time-varying:

$$Z_h = \frac{j h \omega (L'_d + L'_q)}{2} + \frac{(h \mp 2) h \omega^2 \left(\frac{L'_d - L'_q}{2} \right)^2}{\xi_h}. \quad (4-49)$$

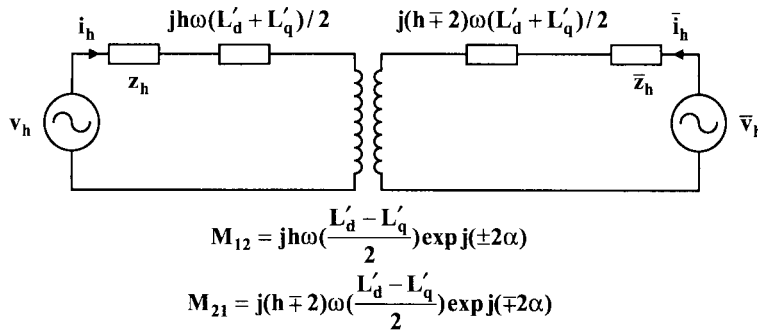


FIGURE 4.24 Harmonic equivalent circuit of synchronous machine based on transient inductances [60].

TABLE E4.9.1 Measured Current Spectrum of a 5 kVA, Four-Pole Synchronous Machine Excited by Positive- and Negative-Sequence 350 Hz Voltages

Positive-phase sequence			Negative-phase sequence		
Frequency (Hz)	Harmonic order	RMS current (mA)	Frequency (Hz)	Harmonic order	RMS current (mA)
50	1	19.7	50	1	26.3
250	5	143.1	250	5	6.6
350	7	324.0	350	7	329.2
450	9	0.8	450	9	141.4
550	11	8.2	550	11	0.1

If several harmonic frequency sources exist, the total current flow can be obtained by the principle of superposition when applied to each harmonic h and its associated harmonics $(h \mp 2)\omega$. Because of the variation of the flux-penetration depth with frequency the governing machine impedances will be a function of frequency.

4.3.2.1 Application Example 4.9: Measured Current Spectrum of a Synchronous Machine

To validate the preceding theory, a series of measurements is recorded for a 5 kVA, 415 V, four-pole synchronous machine [60]. A 350 Hz ($h = 7$) three-phase voltage is applied to the machine and the current spectrum is measured by a spectrum analyzer for both negative- and positive-phase sequence sources (Table E4.9.1). These results are in agreement with the above-outlined theory; that is, for $h = 7$ (positive-sequence voltage excitation) a large current signal is generated at the 5th current harmonic, and for the positive-sequence voltage excitation for $h = 7$ a strong signal occurs at the 9th current harmonic with negative sequence.

In addition, the spectrum shows a frequency range that is associated with the nonsinusoidal inductance variation. The flux waveforms arising from induced damper currents exhibit significant harmonic content, and the frequency range of the spectrum is broader than one would expect based on the nonsinusoidal

inductance variation measured under static conditions.

4.3.3 Synchronous Machine Model with Harmonic Parameters

A synchronous machine model based on modified $dq0$ equations – frequently used in harmonic load flow studies – is presented next [61]. From the physical interpretation of this model one notices that this machine equivalent circuit is asymmetric. This model is then incorporated with the extended “decoupling-compensation” network used in harmonic power flow analysis, and it is now extended to problems including harmonics caused by the asymmetry of transmission lines, asymmetry of loads, and nonlinear elements like static VAr compensators (SVCs). This synchronous machine model has the form

$$\begin{aligned} I_1(h) &= y_{11}(h-1)V_1(h) + \Delta I_1(h) \\ \Delta I_1(h) &= y_{12}(h-1)V_2(h-2) \\ I_2(h) &= y_{22}(h+1)V_2(h) + \Delta I_2(h) \\ \Delta I_2(h) &= y_{21}(h+1)V_1(h+2) \\ I_o(h) &= y_{00}(h)V_0(h) \end{aligned} \quad (4-50)$$

In these equations, the subscripts 1, 2, 0 identify positive-, negative-, and zero-sequence quantities, respectively; $y_{11}(h)$, $y_{12}(h)$, $y_{21}(h)$, $y_{22}(h)$, and $y_{00}(h)$ are harmonic parameters of the machine obtained from the $dq0$ -equation model. In accordance with

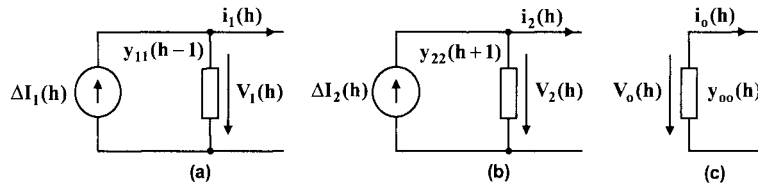


FIGURE 4.25 Synchronous machine equivalent circuits with harmonic parameters; (a) positive sequence, (b) negative sequence, (c) zero sequence.

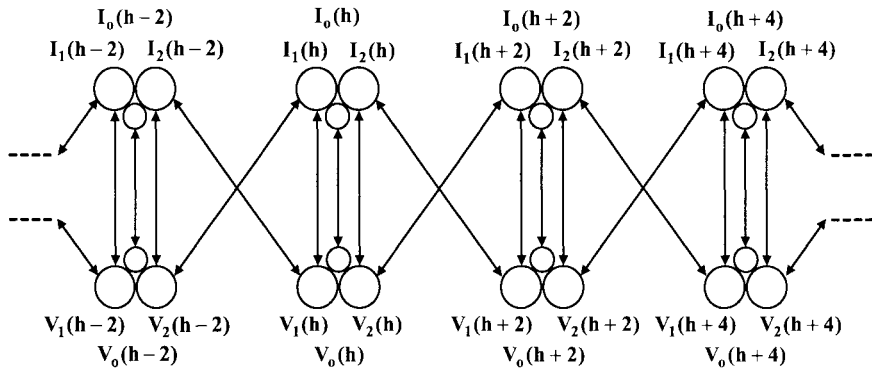


FIGURE 4.26 Derivation of harmonic currents and voltages of synchronous machine in a symmetrical reference frame.

Eq. 4.50 the equivalent circuits of the machine can be assembled based on the different sequence networks as depicted in Fig. 4.25. This is a decoupled harmonic model since $\Delta I_1(h)$ and $\Delta I_2(h)$ are decoupled-harmonic current sources. Equivalent circuits of different sequences and different harmonic orders are decoupled and can be incorporated separately with the corresponding power network models.

The physical interpretation of this harmonic-decoupled model is that

- The h th order positive-sequence current flowing in the machine armature is not entirely caused by the h th order positive-sequence voltage, but will generate in addition a $(h - 2)$ th order negative-sequence voltage at the machine terminal;
- The h th order negative-sequence current flowing in the machine armature is not only caused by the same order negative-sequence voltage, but will also generate a $(h + 2)$ th order positive-sequence voltage at the machine terminal; and
- The zero-sequence harmonic currents are relevant to the same order zero-sequence harmonic voltages only.

Such a phenomenon, stemming from the asymmetry of the machine rotor, is depicted in Fig. 4.26.

The reason why there is always a difference of the order between the positive- and negative-sequence

harmonic current components and their corresponding admittances in Eq. 4.50 is because these admittances are transformed by the $dq0$ equations. The reference frame of the $dq0$ components is attached to the rotor, while the reference frame of symmetrical components remains stationary in space.

This mathematical model of a synchronous machine (Fig. 4.25) can be used in harmonic load flow studies to investigate the impact of a machine's asymmetry and nonlinearity. Moreover, decoupled equivalent circuits of different sequences and harmonics can be incorporated separately with the corresponding power network models.

4.3.3.1 Application Example 4.10: Harmonic Modeling of a 24-Bus Power System with Asymmetry in Transmission Lines

The 24-bus sample system shown in Fig. E4.10.1 is used in this example [61]. Parameters of the system and generators are provided in [61, 64]. Simulation results will be compared for the simple harmonic model (Fig. 4.21, Eq. 4.38) and the model with harmonic parameters (Fig. 4.24, Eq. 4.50).

Two cases are investigated, that is, harmonics caused by the asymmetry of transmission lines (or loads) and by nonlinear SVC devices (see Application Example 4.11). Harmonic admittances of synchronous machines are computed and compared in

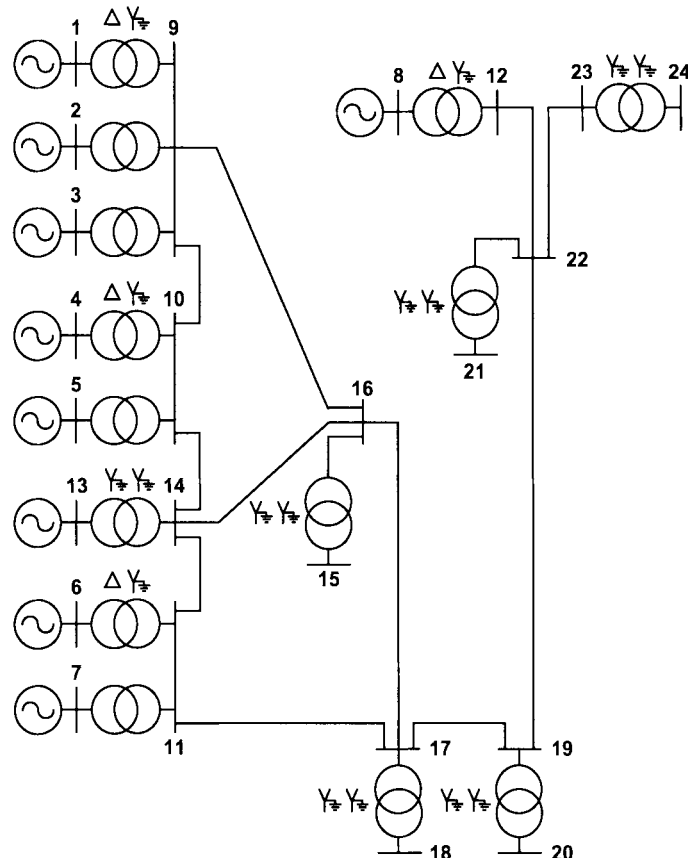


FIGURE E4.10.1 Twenty-four-bus sample system used for harmonic simulation of synchronous machine.

[61]. They remain unchanged with the change of external network conditions. The imaginary components of admittances for the two models are very similar. This may be one of the reasons why the simple model is frequently employed.

All transmission lines (although transposed) are asymmetric, whereas all loads are symmetric. Decoupled positive- and negative-harmonic current sources of the equivalent circuit ($\Delta I_1(h)$ and $\Delta I_2(h)$ in Fig. 4.24 and Eq. 4-50) are computed and listed in [61] for generators 1, 6, and 8. The harmonic frequency voltage components at buses 1, 12, and 16 are also given in the same reference.

4.3.3.2 Application Example 4.11: Harmonic Modeling of a 24-Bus Power System with a Nonlinear Static VAr Compensator (SVC)

All transmission lines and loads in Fig. E4.10.1 are assumed to be symmetric. A static VAr compensator (SVC) device is connected at the additional bus 25 via a step-up transformer placed at bus 14. The

thyristor-controlled reactor (TCR) part of this SVC is a six-pulse thyristor controlled Δ -connected reactor [61] that injects odd harmonics into the system (Table E4.11.1). Harmonic voltages at buses 1, 12, and 14 are given in Table E4.11.2. For comparison, the negative-sequence fifth harmonic voltages (computed with models of Figs. 4.21 and 4.25) are listed in Table E4.11.3. It can be seen that harmonic voltages at those buses near the harmonic source (bus 25) are higher than those of the others.

4.3.4 Synchronous Machine Harmonic Model with Imbalance and Saturation Effects

This section introduces a synchronous machine harmonic model [12] that incorporates both frequency conversions and saturation effects under various machine load-flow constraints (e.g., unbalanced operation). The model resides in the frequency domain and can easily be incorporated into harmonic load-flow programs.

To model these effects and also to maintain an equivalent-circuit representation, a three-phase harmonic Norton equivalent circuit (Fig. 4.27) is developed with the following equations [12]:

$$[I_{km}(h)] = [Y(h)][(V_h(h)] - [V_m(h)] - [E(h)]) + [I_{nl}(h)], \quad (4-51a)$$

$$[E(h)] = 0, \text{ if } h \neq 1$$

$$[I_{km}] = [I_{km-a} \quad I_{km-b} \quad I_{km-c}]^T$$

$$[V_k] = [V_{k-a} \quad V_{k-b} \quad V_{k-c}]^T$$

$$[V_m] = [V_{m-a} \quad V_{m-b} \quad V_{m-c}]^T \quad (4-51b)$$

$$[E] = [E_p \quad a^2 E_p \quad a E_p]^T$$

$$[I_{nl}] = [I_{nl-a} \quad I_{nl-b} \quad I_{nl-c}]^T$$

$$a = \exp(-j2\pi/3)$$

where h is the harmonic order. In the model of Fig. 4.27, nonlinear effects are represented by a harmonic current source ($[I_{nl}(h)]$) that includes the harmonic effects stemming from frequency conversion ($[I_f(h)]$) and those from saturation ($[I_s(h)]$):

$$[I_{nl}(h)] = [I_f(h)] + [I_s(h)]. \quad (4-52)$$

TABLE E4.11.1 Harmonic Current Injections of SVC

h	Positive-sequence voltage magnitude (u)	Negative-sequence voltage magnitude (pu)
5	0	0.9440×10^{-2}
7	0.7897×10^{-2}	0
9	0	0
11	0	0.4288×10^{-2}
13	0.2581×10^{-2}	0

This harmonic model reduces to the conventional, balanced three-phase equivalent circuit of a synchronous machine if $[I_{nl}(h)]$ is zero and $[Y(h)]$ is computed according to reference [65]. Since $[I_{nl}(h)]$ is a known current source (determined from the machine load-flow conditions), the model is linear and decoupled from a harmonic point of view. Therefore, it can be solved with network equations in a way similar to the traditional machine model.

TABLE E4.11.2 Simulation Results for the 24-Bus System (Fig. E4.10.1): Harmonic Voltage Magnitudes at Some Buses

h	Positive-sequence voltage magnitude (pu)			Negative-sequence voltage magnitude (pu)		
	Bus 1	Bus 12	Bus 14	Bus 1	Bus 12	Bus 14
5	0	0	0	0.151×10^{-3}	0.238×10^{-3}	0.302×10^{-3}
7	0.156×10^{-3}	0.312×10^{-3}	0.317×10^{-3}	0	0	0
9	0	0	0	0	0	0
11	0	0	0	0.194×10^{-3}	0.216×10^{-3}	0.334×10^{-3}
13	0.101×10^{-3}	0.330×10^{-4}	0.136×10^{-3}	0	0	0

TABLE E4.11.3 Simulation Results for the 24-Bus System (Fig. E4.10.1): Negative-Sequence Fifth Harmonic Voltages at Different Buses

Bus number	Negative-sequence 5th harmonic voltage magnitude (pu)		Bus number	Negative-sequence 5th harmonic voltage magnitude (pu)	
	Simple model (Fig. 4.21)	New model (Fig. 4.25)		Simple model (Fig. 4.21)	New model (Fig. 4.25)
1	0.161×10^{-3}	0.151×10^{-3}	14	0.302×10^{-3}	0.302×10^{-3}
2	0.161×10^{-3}	0.151×10^{-3}	15	0.247×10^{-3}	0.246×10^{-3}
3	0.161×10^{-3}	0.151×10^{-3}	16	0.292×10^{-3}	0.296×10^{-3}
4	0.184×10^{-3}	0.184×10^{-3}	17	0.279×10^{-3}	0.279×10^{-3}
5	0.184×10^{-3}	0.184×10^{-3}	18	0.265×10^{-3}	0.269×10^{-3}
6	0.185×10^{-3}	0.179×10^{-3}	19	0.276×10^{-3}	0.276×10^{-3}
7	0.185×10^{-3}	0.179×10^{-3}	20	0.224×10^{-3}	0.224×10^{-3}
8	0.141×10^{-3}	0.147×10^{-3}	21	0.200×10^{-3}	0.208×10^{-3}
9	0.259×10^{-3}	0.257×10^{-3}	22	0.237×10^{-3}	0.246×10^{-3}
10	0.269×10^{-3}	0.268×10^{-3}	23	0.233×10^{-3}	0.241×10^{-3}
11	0.281×10^{-3}	0.279×10^{-3}	24	0.194×10^{-3}	0.201×10^{-3}
12	0.229×10^{-3}	0.238×10^{-3}	25	0.119×10^{-3}	0.119×10^{-3}
13	0.268×10^{-3}	0.268×10^{-3}			

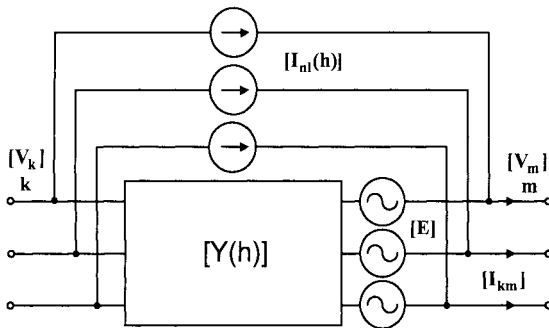


Figure 4.27 Synchronous machine harmonic model with imbalance and saturation effects [12].

To include the usual load-flow conditions, the following constraints are specified at the fundamental frequency ($h = 1$):

- **Slack machine:** The constraints are the magnitude and the phase angle of positive-sequence voltage at the machine terminals:

$$\begin{aligned}[T]([V_k] - [V_m]) &= V_{\text{specified}} \\ [T] &= (1/3)[1 \quad a \quad a^2].\end{aligned}\quad (4-53)$$

- **PV machine:** The constraints are the three-phase real power output and the magnitude of the positive-sequence voltage at machine terminals, where superscript H denotes conjugate transpose:

$$\text{Real}\{-[I_{km}]^H([V_k] - [V_m])\} = P_{\text{specified}}, \quad (4-54)$$

$$|[T]([V_k] - [V_m])| = V_{\text{specified}}. \quad (4-55)$$

- **PQ machine:** The constraints are the three-phase real and the three-phase reactive power outputs:

$$-[I_{km}]^H([V_k] - [V_m]) = (P + jQ)_{\text{specified}}. \quad (4-56)$$

These constraint equations and the machine structure equation (Eq. 4-51a) jointly define a three-phase machine model with nonlinear effects. Combining these equations with other network equations leads to multiphase load flow equations for the entire system [65]. The system is then solved by the Newton-Raphson method for each frequency. Detailed analysis and demonstration of Newton-Raphson based harmonic load flow is presented in Chapter 7.

In the model of Fig. 4.27, $[I_{nl}(h)]$ is not known and will be computed using the following iterative procedure:

- **Step 1. Initialization**

Set the harmonic current source $[I_{nl}(h)]$ to zero.

- **Step 2. Network Load-Flow Solution**

Replace the synchronous machines with their harmonic Norton equivalent circuits (Fig. 4.27) and solve the network equations for the fundamental and harmonic frequencies.

- **Step 3. Harmonic Current-Source Computation**

Use the newly obtained network voltages and currents (from Step 2) to update $[I_{nl}(h)]$ for the machine equivalent circuit.

- **Step 4. Convergence**

If the computed $[I_{nl}(h)]$ values are sufficiently close to the previous ones stop; otherwise, go to Step 2.

The network load-flow solution and the harmonic iteration processes can be performed by any general purpose harmonic load-flow program as explained in Chapter 7 and reference [65]. Therefore, $[I_{nl}(h)]$ needs to be computed (Step 3). This will require the machine harmonic models in the dq0 and abc coordinates.

4.3.4.1 Synchronous Machine Harmonic Model Based on dq0 Coordinates

To incorporate the synchronous machine model (Fig. 4.27) in a general purpose harmonic analysis program, reasonable assumptions and simplifications according to the general guidelines indicated in references [66] and [67] are made. Under these assumptions, the following dq0 transformation is used to transfer the machine quantities from abc coordinates into rotating dq0 coordinates [12]:

$$[v_d \quad v_q \quad v_o]^T = [P]^{-1} [v_a \quad v_b \quad v_c]^T, \quad (4-57)$$

where

$$[P]^{-1} = \sqrt{2/3} \begin{bmatrix} \cos\theta & \cos(\theta - 2\pi/3) & \cos(\theta + 2\pi/3) \\ -\sin\theta & -\sin(\theta - 2\pi/3) & -\sin(\theta + 2\pi/3) \\ \sqrt{1/2} & \sqrt{1/2} & \sqrt{1/2} \end{bmatrix}. \quad (4-58)$$

In this equation $\theta = \omega t + \delta$ and δ is the angle between d -axis and the real axis of the network phasor reference frame. Defining

$$\begin{aligned}[D] &= \begin{bmatrix} 1 & e^{-j2\pi/3} & e^{-j4\pi/3} \\ -j & -je^{-j2\pi/3} & -je^{-j4\pi/3} \\ 0 & 0 & 0 \end{bmatrix} e^{j\delta/\sqrt{6}} \\ [D_o] &= \begin{bmatrix} 0 & 0 & 0 \\ 0 & 0 & 0 \\ \sqrt{1/3} & \sqrt{1/3} & \sqrt{1/3} \end{bmatrix},\end{aligned}\quad (4-59)$$

matrix $[P]^{-1}$ can be simplified as

$$[P]^{-1} = [D]e^{i\omega} + [D]^C e^{-j\omega} + [D_o]. \quad (4-60)$$

Because the $dq0$ transformation is an orthogonal transformation, it follows that

$$[P] = ([P]^{-1})^T = [D]^T e^{i\omega} + [D]^H e^{-j\omega} + [D_o]^T, \quad (4-61)$$

where superscripts T , C , and H represent transpose, conjugate, and conjugate transpose, respectively.

Using these equations for the $dq0$ transformation and the generator reference convention, a synchronous machine is represented in the $dq0$ coordinates as

$$\begin{aligned} [v_{\text{park}}] &= -[R][i_{\text{park}}] - \frac{d}{dt}[\Psi_{\text{park}}] + [F][\Psi_{\text{park}}], \\ [\Psi_{\text{park}}] &= [L][i_{\text{park}}] \end{aligned} \quad (4-62)$$

where

$$[v_{\text{park}}] = [v_d \ v_q \ v_o \ v_f \ v_g \ v_D \ v_Q]^T$$

$$[i_{\text{park}}] = [i_d \ i_q \ i_o \ i_f \ i_g \ i_D \ i_Q]^T,$$

$$[R] = [r_a \ r_a \ r_a \ r_f \ r_g \ r_D \ r_Q]$$

$$[F] = \begin{bmatrix} 0 & -\omega & 0 & 0 & 0 & 0 & 0 \\ \omega & 0 & 0 & 0 & 0 & 0 & 0 \\ 0 & 0 & 0 & 0 & 0 & 0 & 0 \\ 0 & 0 & 0 & 0 & 0 & 0 & 0 \\ 0 & 0 & 0 & 0 & 0 & 0 & 0 \\ 0 & 0 & 0 & 0 & 0 & 0 & 0 \\ 0 & 0 & 0 & 0 & 0 & 0 & 0 \end{bmatrix},$$

$$[L] = \begin{bmatrix} L_d & 0 & 0 & M_{df} & 0 & M_{dD} & 0 \\ 0 & L_q & 0 & 0 & M_{gg} & 0 & M_{gQ} \\ 0 & 0 & L_o & 0 & 0 & 0 & 0 \\ M_{df} & 0 & 0 & L_{ff} & 0 & M_{fp} & 0 \\ 0 & M_{qg} & 0 & 0 & L_{gg} & 0 & M_{gQ} \\ M_{dD} & 0 & 0 & M_{fD} & 0 & L_{DD} & 0 \\ 0 & M_{qQ} & 0 & 0 & M_{gQ} & 0 & L_{QQ} \end{bmatrix}.$$

In these equations, subscripts f and D represent the field and damping windings of the d -axis, and subscripts g and Q indicate the field and damper windings of the q -axis.

Substituting Eq. 4-62 into Eq. 4-61 and defining the differential operator $p = \frac{d}{dt}$:

$$\begin{aligned} [v_{\text{park}}] &= -[R][i_{\text{park}}] - p([L][i_{\text{park}}]) + [F][L][i_{\text{park}}], \\ &= (-[R] - p[L] + [F][L])[i_{\text{park}}] = [Z(p)][i_{\text{park}}] \end{aligned} \quad (4-63)$$

where $[Z(p)] = -[R] - p[L] = [F][L]$ is the operation impedance matrix.

The rotor angular velocity (ω) is constant during steady-state operation; therefore, Eq. 4-63 represents a linear time-invariant system and can be written in the frequency domain for each harmonic $h\omega$, as follows:

$$[V_{\text{park}}(h)] = [Z(h)][I_{\text{park}}(h)]. \quad (4-64)$$

For the harmonic quantities $h \neq 0$ (e.g., excluding DC), the f , g , D , and Q windings are short-circuited; therefore, Eq. 4-64 can be rewritten as

$$\begin{bmatrix} V_d \\ V_q \\ V_o \\ 0 \\ 0 \\ 0 \\ 0 \\ 0 \end{bmatrix} = \begin{bmatrix} Z_{11}(h) & & & & & & I_d \\ & Z_{12}(h) & & & & & I_q \\ & & Z_{21}(h) & & & & I_o \\ & & & Z_{22}(h) & & & I_f \\ & & & & \ddots & & I_g \\ & & & & & \ddots & I_D \\ & & & & & & I_Q \end{bmatrix} \begin{bmatrix} I_d \\ I_q \\ I_o \\ I_f \\ I_g \\ I_D \\ I_Q \end{bmatrix}. \quad (4-65)$$

Solving for the $dq0$ currents as a function of the $dq0$ voltages, we have [12]:

$$\begin{aligned} [I_{dqo}(h)] &= [Z_{11}(h) - Z_{12}(h)Z_{22}^{-1}(h)Z_{21}(h)]^{-1}[V_{dqo}(h)] \\ &= [Y_{dqo}(h)][V_{dqo}(h)], \end{aligned} \quad (4-66)$$

where

$$[Y_{dqo}(h)] = [Z_{11}(h) - Z_{12}(h)Z_{22}^{-1}(h)Z_{21}(h)]^{-1}$$

$$[I_{dqo}(h)] = [I_d \ I_q \ I_o]^T$$

$$[V_{dqo}(h)] = [V_d \ V_q \ V_o]^T$$

Equation 4-66 (consisting of a simple admittance matrix relating the $dq0$ components) defines the harmonic machine model in the $dq0$ coordinates.

For the DC components (e.g., $h = 0$), the voltage of the f -winding is no longer zero. Applying similar procedures, the results will be similar to Eq. 4-66, except that there is an equivalent DC voltage source (which is a function of the DC excitation voltage v_f) in series with the $[Y_{dq0}]$ matrix.

4.3.4.2 Synchronous Machine Harmonic Model Based on abc Coordinates

To interconnect the synchronous machine model of Eq. 4-66 with the rest of the system, the $dq0$ voltages and currents must be converted to the corresponding

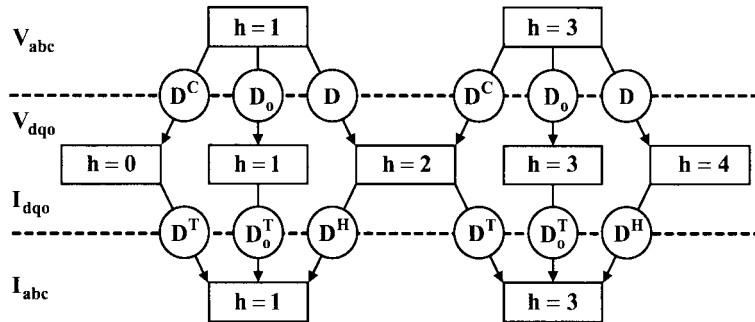


Figure 4.28 Process of frequency conversion (Eq. 4-70) in a synchronous machine [12].

phase (*abc*) quantities using Park's transformation. Assume that the machine voltage [$v_{abc}(t)$] vector consists of a single harmonic component of order h :

$$[v_{abc}(t)] = \text{Real}[\sqrt{2}[V_{abc}(h)]e^{j\omega t}]. \quad (4-67)$$

The corresponding *dq0*-voltage vector is obtained by Park's transformation (Eq. 4-58) as

$$\begin{aligned} [v_{dqo}(t)] &= [P]^{-1}[V_{abc}(t)] = \text{Real}[[P]^{-1}\sqrt{2}[V_{abc}(h)]e^{j\omega t}] \\ &= \sqrt{2}\text{Real}[[D][V_{abc}(h)]e^{j(h+1)\omega t} + [D]^C \\ &\quad [V_{abc}(h)]e^{j(h-1)\omega t} + [D_o][V_{abc}(h)]e^{j\omega t}] \end{aligned} \quad (4-68)$$

Therefore, one harmonic *abc* voltage introduces three harmonics in terms of *dq0* coordinates. The machine's *dq0* model can now be used to obtain the *dq0* currents. From Eq. 4-66:

$$\begin{aligned} [i_{dqo}(t)] &= \sqrt{2}\text{Real}[[Y_{dqo}(h+1)][D][V_{abc}(h)]e^{j(h+1)\omega t} \\ &\quad + [Y_{dqo}(h-1)][D]^C[V_{abc}(h)]e^{j(h-1)\omega t} \\ &\quad + [Y_{dqo}(h)][D_o][V_{abc}(h)]e^{j\omega t}]. \end{aligned} \quad (4-69)$$

Transferring Eq. 4-69 back into the *abc* coordinates (using the inverse Park transformation), and with the condition $[D]^T[D_o] = 0$, we get

$$\begin{aligned} [i_{abc}(t)] &= [P][i_{dqo}(t)] \\ &= \sqrt{2}\text{Real}[[D_o^T Y_{dqo}(h) D_o + D^T Y_{dqo}(h-1) D^C \\ &\quad + D^H Y_{dqo}(h+1) D][V_{abc}(h)]e^{j\omega t} \\ &\quad + [D^H Y_{dqo}(h-1) D^C][V_{abc}(h)]e^{j(h-2)\omega t} \\ &\quad + [D^T Y_{dqo}(h+1) D][V_{abc}(h)]e^{j(h+2)\omega t}]. \end{aligned} \quad (4-70)$$

Based on this equation, the harmonic voltage of order h , $[\mathbf{V}_{abc}(h)]$, can generate harmonic currents of order $(h-2)$ and $(h+2)$ in *abc* coordinates (Fig.

4.28). This is known as frequency conversion. Note that (Fig. 4.28)

- Negative-sequence voltage $[D][\mathbf{V}_{abc}(h)]$ generates harmonic currents of order $(h+2)$ and h .
- Positive-sequence voltage $[D]^C[\mathbf{V}_{abc}(h)]$ generates harmonic currents of order $(h-2)$ and h .
- Zero-sequence voltage $[D_o][\mathbf{V}_{abc}(h)]$ generates only the harmonic current of the same order.
- There are three particular harmonic voltages that can generate harmonic currents of the same order.

All these observations are consistent with the revolving magnetic field theory [68].

4.3.4.3 Computation of Synchronous Machine Injected Harmonic Currents $[I_{nl}(h)]$

The current source $[I_{nl}(h)]$ of the synchronous machine harmonic model (Fig. 4.27) consists of two components: $[I_l(h)]$ due to the frequency-conversion phenomena and $[I_s(h)]$ due to the saturation effects. These currents will be computed separately.

Injected Harmonic Current Due to Frequency Conversion $[I_l(h)]$. As mentioned before, Eq. 4-70 also indicates that there are three particular harmonic voltages that can generate harmonic currents of the same order. Assuming that the voltage vector $[\mathbf{v}_{abc}(t)]$ includes all harmonic components, the harmonic terminal voltages that result in currents of the same harmonic order h can be grouped and described in phasor form as [12]

$$\begin{aligned} [I_{abc}(h)] &= [D^T Y_{dqo}(h-1) D^C + D^H Y_{dqo}(h+1) D \\ &\quad + D^T Y_{dqo}(h) D_o][V_{abc}(h)] \\ &\quad + [D^H Y_{dqo}(h+1) D^C][V_{abc}(h+2)] \\ &\quad + [D^T Y_{dqo}(h-1) D][V_{abc}(h-2)]. \end{aligned} \quad (4-71)$$

If we substitute

$$[Y(h)] = [D^T Y_{dq0}(h-1) D^C + D^H Y_{dq0}(h+1) D + D^T_o Y_{dq0}(h) D_o], \quad (4-72)$$

$$[I_f(h)] = [D^H Y_{dq0}(h+1) D^C] [V_{abc}(h+2)] + [D^T Y_{dq0}(h-1) D] [V_{abc}(h-2)], \quad (4-73)$$

then Eq. 4-71 can be rewritten as

$$[I_{abc}(h)] = [Y(h)] [V_{abc}(h)] + [I_f(h)]. \quad (4-74)$$

This equation defines the machine model shown in Fig. 4.27, where

- $[I_{abc}(h)] = [I_{km}(h)]$.
- $[V_{abc}(h)] = [V_k(h)] - [V_m(h)]$.
- $[Y(h)]$ correlates harmonic voltages to harmonic currents of the same order.
- $[I_f(h)]$ describes the harmonic coupling due to frequency-conversion effects. This current vector is generated from the conversion of voltages of different harmonic orders.

Following a similar approach, the equivalent DC voltage source of the $dq0$ -machine model at harmonic order $h=0$ becomes a set of positive-sequence fundamental frequency voltage sources in abc coordinates. As explained earlier, the values of these voltages are determined in conjunction with load-flow constraints.

Therefore, matrix operations are sufficient to compute the admittance matrix $[Y(h)]$ and the equivalent current source $[I_f(h)]$ needed for the harmonic machine model:

- Compute $[Y(h)]$ according to Eq. 4-72 whenever the machine admittance matrix needs to be added to the network admittance matrix in the frequency scan process; and
- Compute $[I_f(h)]$ according to Eq. 4-73 where $[V_{abc}(h)]$ contains the machine voltages obtained from the load-flow solution of the previous iteration.

Injected Harmonic Currents Due to Saturation

$[I_s(h)]$. Saturation of the stator and rotor cores of a synchronous machine has a significant impact on the machine's operation and the corresponding operating point [68]. Other saturation factors (e.g., cross-coupling between d - and q -axes) are assumed to be negligible and are not considered in the model of Fig. 4.27.

It is shown in [12] that the influence of saturation can be represented as a current source in parallel with the $dq0$ -machine model (Eq. 4-66):

$$[I_{dq0-s}(h)] = [Y_{dq0}(h)] [V_{dq0}(h)] + [I_{dq0-s}(h)], \quad (4-75)$$

where $[I_{dq0-s}(h)]$ is a known current vector representing the effect of saturation. For a given set of machine terminal voltages, vector $[I_{dq0-s}(h)]$ is obtained through a process of subiterations [12].

With saturation effects included in $dq0$ coordinates, Park's transformation can now be applied to obtain the machine's model in abc coordinates. The processing of the first part of Eq. 4-75 has been explained in the previous section. The second part (e.g., $[I_{dq0-s}(h)]$) will be discussed next.

Using Park transformation matrix (Eq. 4-61), the $dq0$ -harmonic currents of order h appear in abc coordinates as

$$\begin{aligned} [i_{abc-s}(t)] &= \text{Real}\{[P]\sqrt{2}[I_{dq0-s}(h)]e^{j\omega t}\} \\ &= \text{Real}\{\sqrt{2}[D^T e^{j(h+1)\omega t} + D^H e^{j(h-1)\omega t} \\ &\quad + D_o e^{jh\omega t}][I_{dq0-s}(h)]\}. \end{aligned} \quad (4-76)$$

It can be seen that the $dq0$ currents $[I_{dq0-s}(h)]$ also introduce three separate harmonic components of order $(h-1)$, h , and $(h+1)$ in the abc coordinates. Assuming that $[I_{dq0-s}(h)]$ includes harmonics of all orders, the particular $dq0$ harmonics that produce harmonic currents of the same order in abc coordinates can be grouped together in phasor form as

$$\begin{aligned} [I_s(h)] &= [D]^T [I_{dq0-s}(h-1)] + [D]^H [I_{dq0-s}(h+1)] \\ &\quad + [D_o] [I_{dq0-s}(h)]. \end{aligned} \quad (4-77)$$

This is the current that is needed to represent the effects of saturation in abc coordinates.

The above equation defines the final machine model used for harmonic load-flow studies. The approach of computing $[I_s(h)]$ can be summarized as follows:

- Compute the saturation current $[I_{dq0-s}(h)]$ using the subiteration process described in reference [12] or any other desired approach; and
- Compute $[I_s(h)]$ according to Eq. 4-77 for all harmonics of interest.

Total Injected Harmonic Current $[I_n(h)]$. The complete machine model with both the frequency-conversion and saturation effects included can now be described by

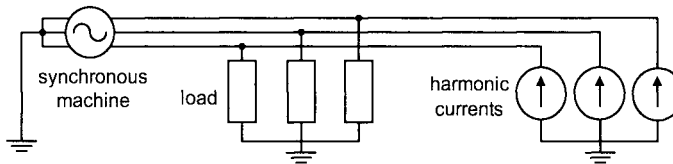
$$[I_{abc}(h)] = [Y(h)] [V_{abc}(h)] + [I_f(h)] + [I_s(h)]. \quad (4-78)$$

TABLE E4.12.1 Values of Negative-Sequence Impedance for Synchronous Machine [12]

Test type	Exact ^a	Harmonic truncation ^b		
		$h = 1$	$h = 1, 3$	$h = 1, 3, 5$
I-definition	$0.0655 + j0.3067$	$0.0857 + j0.2165$	$0.0655 + j0.3066$	$0.0655 + j0.3066$
V-definition	$0.0858 + j0.2165$	$0.0856 + j0.2166$	$0.0859 + j0.2164$	$0.0859 + j0.2164$

^aBased on analytical formulas.

^b $h = 1$: only the fundamental frequency component included; $h = 1, 3$: $h = 1$ modeling plus the third harmonic; $h = 1, 3, 5$: $h = 1, 3$ modeling plus the fifth harmonic.

**Figure E4.13.1** Single machine test system used in application problems [12].

4.3.4.4 Application Example 4.12: Effect of Frequency Conversion on Synchronous Machine Negative-Sequence Impedance

The negative-sequence impedance of a synchronous machine is important for simulation under unbalanced conditions. Its value is different depending on whether negative-sequence currents or negative-sequence voltages are used to determine the impedance [68]. This inconsistency is caused by the frequency conversion process. In this example the harmonic model of Fig. 4.27 (implemented in a multiphase harmonic load flow [65]) is used to run two test conditions that are commonly accepted to define the machine's negative-sequence impedance:

- I-definition: synchronous machine is connected to a negative-sequence current source and the negative-sequence terminal voltage is recorded; and
- V-definition: synchronous machine is connected to a negative-sequence voltage source and the negative-sequence terminal current is recorded.

The impedance resulting from these tests is the ratio of the fundamental frequency voltage to the fundamental frequency current obtained by harmonic analysis. The program was run for three different levels of harmonic truncation (Table E4.12.1).

The following observations can be derived from this table:

- The difference between the machine impedances calculated from the I- and V-definitions is caused by the 3rd harmonic. The contribution of the 5th harmonic is negligible;

- If harmonics are not included, the proposed machine model corresponds to the impedance of V-definition;
- In the general case of unbalanced machine operation, the machine's negative-sequence impedance is neither the one from the V-definition nor the one from the I-definition. The correct machine response can only be fully evaluated with harmonics included. The combination of the load-flow constraints with harmonic solutions is therefore the best approach in such situations; and
- Agreement between simulation and exact results justifies the validity of the synchronous machine harmonic model (Fig. 4.27).

4.3.4.5 Application Example 4.13: Effect of Imbalance on Power Quality of Synchronous Machines

A profile of the harmonic content of the synchronous machine currents and voltages is calculated (using the harmonic model of Fig. 4.27) for two test machines. The voltage and current harmonics in a machine will be influenced by the conditions imposed by the external network. To simplify the interpretation of the results, a straightforward operating condition with grounded Y synchronous machines and unbalanced R , L , and C loads is considered (Fig. E4.13.1 without the harmonic current sources). The loads are adjusted so that the machine's current imbalance at fundamental frequency is around the normal tolerance of 10%. The results (using two synchronous machines with different positive- and negative-sequence currents) are shown in Table E4.13.1 for the voltage harmonics

TABLE E4.13.1 Harmonic Profiles of Two Synchronous Machines (Unbalanced Operating Conditions) [12]

Machine	Item	$h = 1$		$h = 3$		$h = 5$		$h = 7$
		Magnitude	Angle	Magnitude	Angle	Magnitude	Angle	Magnitude
No. 1 NP ^a = 9.35%	V_a	1.103	1.1	0.0148	88.3	0.0002	148.4	0
	V_b	1.025	-121.5	0.0131	-36.5	0.0002	23.8	0
	V_c	1.022	120.2	0.0131	-151.5	0.0002	-90.2	0
	$I_{f,a}$	0.027	167.3	0.0225	-152.5	0.0002	-99.5	0
	$I_{f,b}$	0.027	-72.7	0.0225	87.4	0.0002	140.4	0
	$I_{f,c}$	0.027	47.3	0.0225	-32.4	0.0002	20.4	0
No. 2 NP ^a = 12.41%	V_a	1.080	1.3	0.0345	92.1	0.0011	157.2	0
	V_b	1.041	-121.6	0.0313	-33.0	0.0009	32.4	0
	V_c	1.030	120.3	0.0315	-148.2	0.0010	-82.7	0
	$I_{f,a}$	0.025	155.2	0.0704	-151.3	0.0016	-94.8	0
	$I_{f,b}$	0.025	-84.7	0.0696	88.3	0.0016	145.2	0
	$I_{f,c}$	0.025	35.2	0.0696	-30.9	0.0016	25.2	0

^aNP: ratio of the negative- to positive-sequence current at fundamental frequency.

TABLE E4.14.1 Third Harmonic Currents in Grounded Y- and Δ -Connected Synchronous Generators [12]

		Phase A		Phase B		Phase C	
		Magnitude	Angle	Magnitude	Angle	Magnitude	Angle
V_3	$Y-g$	0.0148	88.3	0.0130	-36.5	0.0131	-151.5
	Δ	0.0091	81.7	0.0071	-40.7	0.0078	-168.4
I_3	$Y-g$	0.0090	48.3	0.0125	-71.7	0.0108	170.1
	Δ	0.0055	41.6	0.0068	-76.0	0.0065	153.3

and for the frequency-conversion-induced equivalent current source $I_f(h)$. Significant harmonics are observed even for cases when the machines are operated within an acceptable range of imbalance. The effects of these harmonics could easily be magnified if voltage resonance takes place. Note that the harmonic magnitudes decrease quickly for higher orders. From the results of Tables E4.12.1 and E4.13.1, it may be concluded that only 3rd and 5th harmonics need to be included in synchronous machine's representation for harmonic studies.

4.3.4.6 Application Example 4.14: Effect of Delta Connection on Power Quality of Synchronous Machines

It is believed that the flow of the third harmonic in lines can be prevented by connecting the three-phase equipment in delta. This assumption is tested here by assuming that the winding of the first synchronous generator (Application Example 4.13) is to be connected in delta. The results of this test (third harmonic currents for the Δ and Y-connected machines) are presented in Table E4.14.1. Even though the third harmonic components are about 40% smaller

in the Δ connection, they do not cancel completely. The reason is

The third harmonic generated by the frequency-conversion process in a synchronous machine is of negative sequence and not of zero sequence, and therefore cannot be eliminated by a Δ connection.

4.3.4.7 Application Example 4.15: Effect of Saturation on Power Quality of Synchronous Machines

In the model of Fig. 4.27, the saturation curve is approximated in a piecewise-linear manner between the data points (MMF, λ) = (0.9, 0.9), (1.5, 1.2), (2.7, 2.8). Table E4.15.1 lists the harmonic profiles of the machine with and without saturation. There are large differences between the cases with and without saturation (the last column of Table E4.15.1). The differences in the phase angles are even more noticeable. These results suggest that

Saturation can have an important influence on harmonic power-flow analysis.

TABLE E4.15.1 Harmonic Profiles of Two Synchronous Machines with and without Saturation (under Unbalanced Operating Conditions) [12]

		<i>h</i> = 1		<i>h</i> = 3		<i>h</i> = 5		Difference (%) ^a
		Magnitude	Phase	Magnitude	Phase	Magnitude	Phase	
NS ^b	<i>V_a</i>	1.103	1.1	0.0148	88.3	0.00020	148.4	
SAT	<i>V_a</i>	1.103	1.1	0.0120	76.3	0.00014	115.8	19.0
NS	<i>V_b</i>	1.025	-121.5	0.0130	-36.5	0.00017	23.8	
SAT	<i>V_b</i>	1.025	-121.5	0.0106	-48.4	0.00012	-8.8	18.6
NS	<i>V_c</i>	1.022	120.2	0.0131	-151.5	0.00017	-90.2	
SAT	<i>V_c</i>	1.022	120.2	0.0106	-163.7	0.00013	-122.9	18.6
NS	<i>I_a</i>	0.0027	167.3	0.0225	-152.5	0.00022	-99.5	
SAT	<i>I_a</i>	0.0022	168.5	0.0182	-164.5	0.00014	-131.3	19.0
NS	<i>I_b</i>	0.0027	-72.7	0.0224	87.4	0.00022	140.4	
SAT	<i>I_b</i>	0.0022	-71.4	0.0182	75.5	0.00014	108.6	18.6
NS	<i>I_c</i>	0.0027	47.3	0.0225	-32.4	0.00022	20.4	
SAT	<i>I_c</i>	0.0022	48.5	0.0182	-44.6	0.00014	-11.3	18.7

^aRelative difference of the 3rd harmonic magnitude.

^bNS: without saturation; SAT: with saturation.

TABLE E4.16.1 Voltages of Machine 1 (Defined in Table E4.13.1) in the Presence of Nonlinear Loads (Fig. E4.13.1) [12]

	Phase A		Phase B		Phase C		Case study
	Magnitude	Phase	Magnitude	Phase	Magnitude	Phase	
<i>h</i> = 1	1.099	0.2	1.023	-120.8	1.028	120.5	1
	1.100	0.3	1.024	-120.9	1.026	120.5	2
	1.000	0.3	1.024	-120.8	1.026	120.5	3
<i>h</i> = 3	0.0607	69.4	0.0304	-171.5	0.0536	-68.4	1
	0.0777	67.3	0.0283	-155.3	0.0572	-82.9	2
	0.724	66.4	0.0295	-156.7	0.0526	-79.7	3
<i>h</i> = 5	0.0336	69.7	0.0450	-59.2	0.0379	-173.5	1
	0.0445	80.1	0.0539	-50.0	0.0458	-173.6	2
	0.0417	76.8	0.0517	-52.9	0.0439	-177.4	3

4.3.4.8 Application Example 4.16: Impact of Nonlinear Loads on Power Quality of Synchronous Machines

The effects of nonlinearities of synchronous machines are further investigated by including nonlinear loads, represented as 3rd and 5th current injections to the generator-load system (Fig. E4.13.1). Three case studies are performed:

- **Case 1:** with no machine nonlinearities,
- **Case 2:** with only frequency conversion, and
- **Case 3:** with both frequency conversion and saturation.

The results (Table E4.16.1) further confirm the need for detailed modeling of machine's nonlinearities.

4.3.5 Static- and Dynamic-Rotor Eccentricities Generating Current and Voltage Harmonics

Most synchronous machines have relatively large radial air-gap lengths, which range from a few milli-

meters to tens of centimeters. This is so because the synchronous reactances (X_d , X_q) must be small enough to guarantee a good dynamic (transient, sub-transient) behavior. Although permanent-magnet machines have a mechanical air gap of less than one millimeter up to a few millimeters, their electrical air gap is always larger than one millimeter because the radial air-gap height (length) of the permanent magnet behaves magnetically like air with the permeability of free space μ_0 because the recoil permeability μ_R of excellent permanent-magnetic material (e.g., NdFeB) is about $\mu_R \approx 1.05\mu_0$. Therefore, an imperfect mechanical mounting – resulting in a static-rotor eccentricity – or a bent shaft – resulting in dynamic-rotor eccentricity – will not significantly alter the magnetic coupling of the stator windings and the rotating magnetic flux will be about circular. Here one should mention that permanent-magnet machines cannot be easily assembled for ratings larger than a few tens of kilowatts because a mounting gear will be required, which maintains a uniform

concentric air gap during the mounting of the rotor.

The modified winding-function approach (MWFA) accounting for all space harmonics has been used for the calculations of machine inductances under rotor eccentricities [69]. Machines can fail due to air-gap eccentricity caused by mechanical problems including the following:

- shaft deflection,
- inaccurate positioning of the rotor with respect to the stator,
- worn bearings,
- stator-core movement, and
- bent rotor shaft.

Electrical asymmetries contribute to harmonic generation such as

- Damper windings (amortisseur) are incomplete, that is, the amortisseur has a different construction between poles as compared with that on the pole d-axis; or
- Eddy currents in the pole faces of salient-pole machines contribute to subtransient response;
- Heating of the rotor due to nonuniform amortisseur and nonuniform eddy-current generation around the rotor circumference may cause shaft bending/deflection; and
- Incomplete shielding of the field winding of a machine fitted with nonuniform amortisseurs and subjected to harmonic disturbance.

Nonsinusoidal air-gap flux wave effects – due to any of the above-listed reasons – can be accounted for by representing the mutual inductances between the field and stator windings, and those between the stator windings, by trigonometric series as a function of the rotor angle θ . It is found that the inclusion of nonsinusoidal inductance variation causes a broad spectrum such that injection of a single-harmonic current results in voltages containing all odd harmonic orders including the fundamental. The extent to which the energy is spread across the spectrum depends on the pole shape, the numbers of stator and rotor slots, and the amortisseur design. The spectral spread is a second-order effect compared to the generation of the associated voltage at frequency ($h \pm 2$). Harmonic behavior is also affected by nonsinusoidal inductance variation with rotor position and by the extent to which induced damper winding currents shield the field winding from the harmonic-gap flux waves. Rotor eccentricity in machines can be of two forms:

- static air gap eccentricity, and
- dynamic air gap eccentricity.

With the static air-gap eccentricity, the position of the minimum radial air-gap length is fixed in space and the center of rotation and that of the rotor are the same. Static eccentricity can be caused by oval stator cores or by the incorrect relative mounting of stator and rotor. In case of dynamic air-gap eccentricity, the center of rotation and that of the rotor are not the same and the minimum air gap rotates with the rotor. Therefore, dynamic eccentricity is both time and space dependent. Dynamic eccentricity can be caused by misalignment of bearings, mechanical resonance at critical speeds, a bent rotor shaft, and wear of bearings [69].

MATLAB/Simulink [70] can be used for the simulation of machine variables. All machine inductances employed for the simulation are expressed in their Fourier series based on the MWFA. Two different cases, namely, a noneccentric and an eccentric rotor case, for this analysis are investigated. In the first case, it is assumed that dynamic air-gap eccentricity is not present, and in the second one 50% dynamic air-gap eccentricity is introduced to investigate the effect of the eccentric rotor on stator-current signatures. To analyze the stator-current signatures of these two cases, FFT (fast Fourier transform) of the current signals are performed for all cases. The stator currents show the existence of the 5th (300 Hz), 7th (420 Hz), 11th (660 Hz), 13th (780 Hz), 17th (1020 Hz), and 19th (1140 Hz) harmonics even when the rotor is not eccentric. Implementing 50% eccentricity will cause the stator and rotor current induced harmonics to increase when compared to those generated without rotor eccentricity as is listed in Table 4.3.

The stator current harmonics exist because the interaction of the magnetic fields caused by both the stator and rotor windings will produce harmonic fluxes that move relative to the stator and they induce corresponding current harmonics in the stationary stator windings. These harmonic fluxes in the air gap will increase as the rotor dynamic eccentricity increases, and consequently the current harmonic content increases too. The 3rd harmonic and its multiples are assumed not to exist in the stator windings because it is a three-phase system with no neutral

TABLE 4.3 Relative Percentage of Stator Harmonics Due to 50% Dynamic Eccentricity

5th	7th	11th	13th	17th	19th
22.8%	12.4%	20.9%	28.4%	47.1%	36.9%

connection. However, third-harmonic components are induced in the rotor-field winding. Because the stator and rotor-current signatures of synchronous machines have changed, either or both signatures can be utilized for detecting dynamic eccentricity. However, it is more practical to implement the stator-current signature analysis for the condition monitoring than the rotor-current signature analysis because some synchronous machines have brushless excitation [49], which will make the rotor current inaccessible. In summary, one can conclude that synchronous machines are not very prone to the effects caused by rotor eccentricity due to their large air gaps.

4.3.6 Shaft Flux and Bearing Currents

The generation of shaft flux [71] due to mechanical and magnetic asymmetries as well as solid-state switching is an important issue for large synchronous generators. Bearing currents are predominantly experienced in PWM AC drives [72–76] due to the high-frequency switching ripples resulting in bearing electroerosion. Techniques for measurement of parameters related to inverter-induced bearing currents are presented in [77].

4.3.7 Conclusions

The most important conclusions of this section are

- Synchronous machines generate harmonics due to
 1. frequency conversion,
 2. saturation, and
 3. unbalanced operation.
- Current harmonics due to nonlinear loads should be limited based on IEEE-519 [78].
- Unbalanced load-flow analysis without taking into account harmonics is not correct due to the ambiguous value of the negative-sequence impedance of synchronous machines. Correct results can only be obtained by including harmonics in a three-phase, load-flow approach.
- Only 3rd and 5th harmonics need to be included for the machine's representation in harmonic analysis. The 3rd harmonic is of the negative-sequence and not of the zero-sequence type. Hence, it cannot be eliminated by Δ transformer connections. The same is true for transformer applications with DC current bias [79].
- Machine saturation can have noticeable effects on the harmonic distribution. These effects are more significant with respect to the harmonic phase angles.

- Rotor eccentricity has a minor influence on harmonic generation due to the large air gap of synchronous machines.
- Shaft fluxes and bearing currents can have detrimental impacts.

4.4 SUMMARY

In the past and at present synchronous generators represent an integral part of a power system. Although the tendency exists to move from a central power station approach to a distributed generation (DG) system with renewable energy sources in the megawatt range, there will be always the requirement of frequency control, which is best performed by a central power station in the gigawatt range that can absorb load-flow fluctuations. Renewable plants will be mostly operated at their maximum power output and therefore cannot provide additional (real or reactive) power if the load increases beyond their assigned output powers. In addition, such plants have an intermittent output, which cannot be controlled by dispatch and control centers. This is to say that also in future power systems the power quality will depend on the reliable operation of synchronous generators.

This chapter starts out with the introduction of the synchronous machine model based on $dq0$ coordinates. To visualize steady-state saturated magnetic fields, numerical solutions are presented for no-load, full-load, and short-circuit conditions. Fields for permanent-magnet machines and switched-reluctance machines are presented as well. Thereafter, the two possible reference systems (e.g., consumer and generator) are addressed. The application examples relate to the calculation of synchronous reactances, the investigation of various fault conditions including reclosing, and the calculation of the amortisseur current for subtransient faults such as line-to-line, line-to-neutral, and balanced three-phase short circuits. The design of synchronous machines and permanent-magnet machines for wind-power and hybrid drive applications, respectively, is discussed. Design guidelines for synchronous machines are presented, and the calculation of magnetic forces – based on the Maxwell stress – is included. The performance of synchronous machines under the influence of harmonics is explained based on models used in application examples. The employment of such models for harmonic power flow analyses is mandatory. Finally, approaches for analyzing static and dynamic eccentricities, shaft fluxes, and bearing currents are outlined.

4.5 PROBLEMS

Problem 4.1: Steady-State Analysis of a Nonsalient-Pole (Round-Rotor) Synchronous Machine Using Phasor Diagrams

A nonsalient-pole synchronous machine has the following data: $X_S = (X_d = X_q) = 1.8 \text{ pu}$, $R_a = 0.01 \text{ pu}$, $I_{\text{phase}} = 1.0 \text{ pu}$ and $V_{L-N} = 1.0 \text{ pu}$.

- Sketch the equivalent circuit using the consumer reference system.
- Draw the phasor diagram (to scale) based on the consumer reference system for a lagging (underexcited) displacement power factor of $\cos \varphi = 0.90$.
- Sketch the equivalent circuit based on the generator reference system.
- Draw the phasor diagram (to scale) employing the generator reference system for a lagging (overexcited) displacement power factor of $\cos \varphi = 0.90$.

Problem 4.2: Steady-State Analysis of a Salient-Pole Synchronous Machine Using Phasor Diagram [7]

A salient-pole synchronous machine has the following data: $X_d = 1.8 \text{ pu}$, $X_q = 1.5 \text{ pu}$, $R_a = 0.01 \text{ pu}$, $I_{\text{phase}} = 1.0 \text{ pu}$, $V_{L-N} = 1.0 \text{ pu}$.

- Sketch the equivalent circuit based on the consumer reference system.
- Draw the phasor diagram (to scale) using the consumer reference system for a lagging (underexcited) displacement power factor of $\cos \varphi = 0.70$.
- Sketch the equivalent circuit based on the generator reference system.
- Draw the phasor diagram (to scale) employing the generator reference system for a lagging (overexcited) displacement power factor of $\cos \varphi = 0.70$.

Problem 4.3: Phasor Diagram of a Synchronous Generator With Two Displaced Stator Windings [80]

Synchronous machines with two by 30° displaced stator windings (winding #1 and winding #2) are used to improve the voltage/current wave shapes so that the output voltages of a generator become more sinusoidal. This is similar to the employment of 12-pulse rectifiers versus 6-pulse rectifiers. To accom-

plish this, stator winding #1 feeds a $Y-Y$ connected transformer and stator winding #2 supplies a $\Delta-\bar{Y}$ connected transformer as illustrated in Fig. P4.3.1. For a $S = 1200 \text{ MVA}$, $V_{L-L} = 24 \text{ kV}$, $f = 60 \text{ Hz}$, $p = 2$ turbogenerator the machine parameters are in per unit (pu): $X_d = 1.05$, $X_{12d} = 0.80$, $X_q = 0.95$, $X_{12q} = 0.73$, $X_{fd} = 2.10$, $k_o = 0.5$, $k_1 = 0.638$, $r = R_a = 0.00146$, $r_f = R_f = 0.0007$.

Draw the phasor diagram (to scale) for rated operation and a displacement power factor of $\cos \varphi = 0.8$ lagging (overexcited, generator reference system).

Problem 4.4: Balanced Three-Phase Short-Circuit Currents of a Synchronous Machine Neglecting Influence of Amortisseur

A three-phase synchronous generator is initially unloaded and has a rated excitation so that $E_f = 1.0 \text{ pu}$. At time $t = 0$, a three-phase short-circuit is applied. The machine parameters are

direct (d) axis: $X_d = 1.2 \text{ pu}$, $X_f = 1.1 \text{ pu}$, $X_m = 1.0 \text{ pu}$, $R_a = 0.005 \text{ pu}$, $R_f = 0.0011 \text{ pu}$;

quadrature (q) axis: $X_q = 0.8 \text{ pu}$, $X_m = 0.6 \text{ pu}$, $R_a = 0.005 \text{ pu}$.

- Plot the first-half cycle of the torque $T_{3\text{phase_short-circuit}}$ due to the three-phase short-circuit neglecting damping and assuming that there is no amortisseur.
- Plot the torque $T_{3\text{phase_short-circuit}}$ as a function of the time angle $\varphi = \omega t$.
- At which angle φ_{\max} (measured in degrees) occurs the maximum torque T_{\max} (measured in per unit)?

Problem 4.5: Torque T_{L-L} and Induced Voltage e_a During the First-Half Cycle of a Line (Line b)-to-Line (Line c) Short-Circuit of a Synchronous Machine Neglecting Influence of Amortisseur

- For the machine parameters of Problem 4.4 calculate and plot the line-to-line torque T_{L-L} for the first half-cycle when phases b and c are short-circuited, and determine at which angle φ_{\max} (measured in degrees) the maximum torque (measured in per unit) occurs.
- Plot the induced open-circuit voltage of phase a, that is, e_a (measured in per unit) as a function of

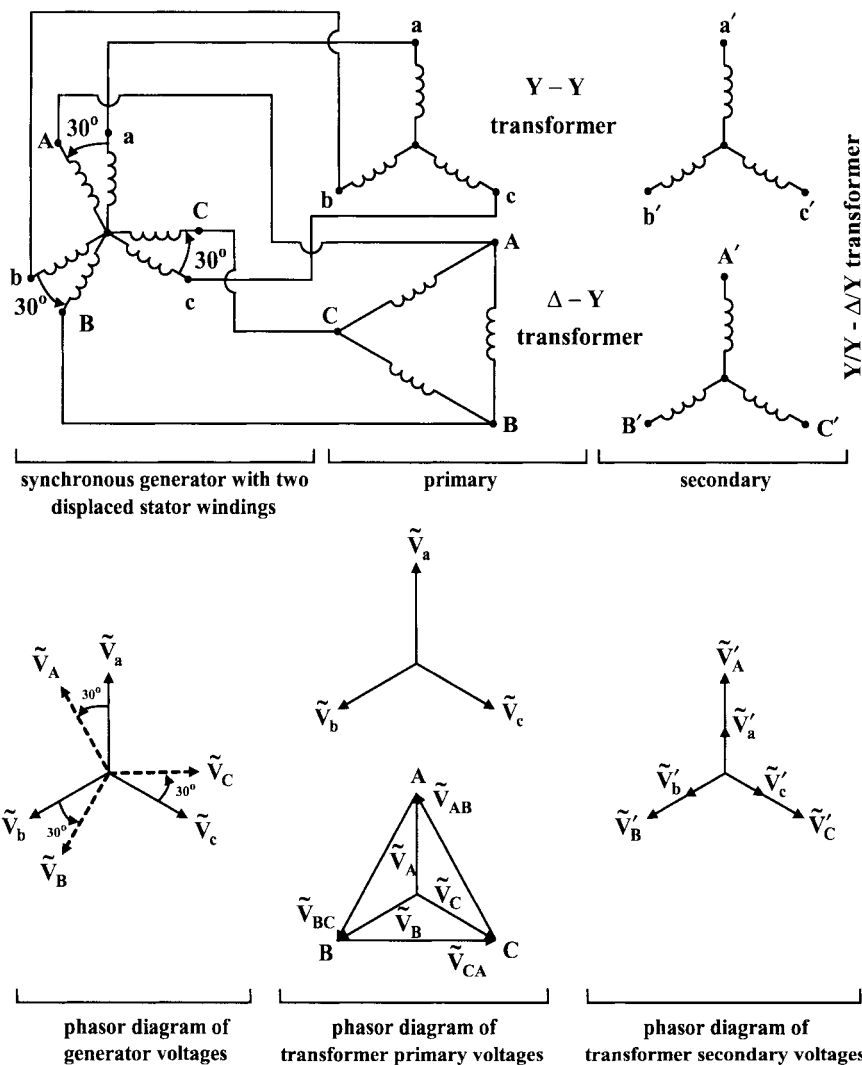


Figure P4.3 Generator-transformer interconnection with two displaced stator windings and a Y/Y- Δ /Y transformer.

the phase angle φ (measured in degrees) for the first half-cycle.

Problem 4.6: Line-to-Neutral Short-Circuit Current of a Synchronous Machine Neglecting Influence of Amortisseur

- For the machine parameters of Problem 4.4 calculate the total (fundamental and harmonics) line-to-neutral short-circuit current i_a for the first half-cycle when phase a and the neutral are short-circuited, and determine at which angle φ_{\max} (measured in degrees) the maximum current $I_{L-N,\max}$ (measured in per unit) occurs.
- Plot the fundamental short-circuit current of phase a i_{a1} (measured in per unit) for the first half-cycle as a function of the phase angle φ (measured in degrees).

Problem 4.7: Out-of-Phase Synchronization Torque of a Synchronous Machine Neglecting Influence of Amortisseur

- For the machine parameters of Problem 4.4 calculate and plot for the first half-cycle the out-of-phase synchronizing torque.
- Determine at which angle φ_{\max} (measured in degrees) the maximum torque (measured in per unit) occurs.

Problem 4.8: Synchronizing and Damping Torques of a Synchronous Machine Neglecting Influence of Amortisseur

For the machine parameters of Problem 4.4 calculate and plot for the first half-cycle the steady-state torque T_0 , the synchronizing torque T_s , and the damping torque T_d . The per-unit transient time

TABLE P4.9 Starting and Accelerating Torque of a Synchronous Machine Developed by Induction-Motor Action as a Function of Slips

s (pu)	1.0	0.9	0.8	0.7	0.6	0.5	0.4	0.3	0.2	0.1	0
$T_{\text{starting}} \text{ (pu)}$	0.0172				0.0685						

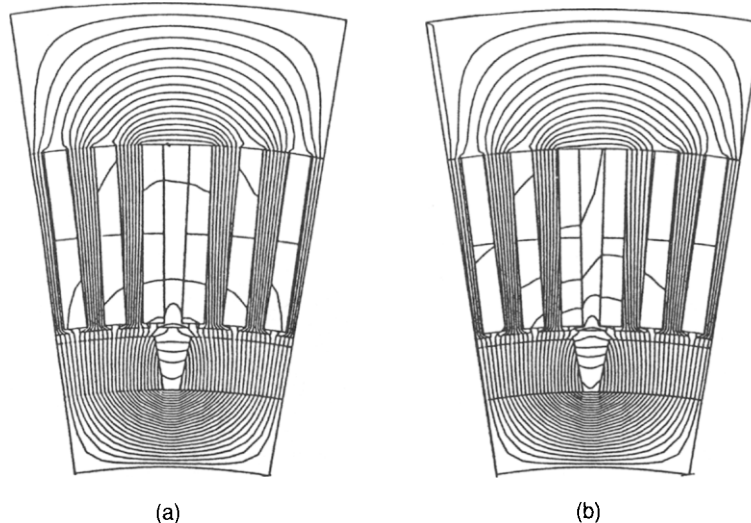


Figure P4.10 No-load (a) and full-load (b) flux patterns of permanent-magnet DC motor where the flux within one tube is $\Delta A = 0.0002 \text{ Wb/m}$.

constant of the d -axis is $T_d = 242 \text{ pu}$ and the per unit voltages $V = V_0 = V_{l,n} = V_{l,n0} = 1.0 \text{ pu}$ may be used.

Problem 4.9: Starting and Accelerating Torque of a Synchronous Machine Developed by Induction Motor Action Neglecting Influence of Amortisseur

The starting of synchronous generators without amortisseur (damper) winding by induction-motor action is not advisable, as will be demonstrated in this problem. Calculate for a synchronous machine with the parameters $X_d = 1.2 \text{ pu}$, $X_q = 0.8 \text{ pu}$, $X_f = 1.1 \text{ pu}$, $X_m = 1.0 \text{ pu}$, $R_a = 0.005 \text{ pu}$, and $R_f = 0.0011 \text{ pu}$ the starting and accelerating torque T_{starting} as a function of the slip s . To do this, start out from the $dq0$ -coordinate system and transform it to the fbo [81] coordinate system. Table P4.9.1 presents some of the results. It is the task of this problem to fill in the missing values of this table.

As can be seen from the few entries of this table, a synchronous machine cannot develop any significant induction motor torque without amortisseur winding. Most large synchronous generators have a very rudimentary amortisseur and must not be started by induction-motor action. Small synchronous machines with ratings of less than 1 MW can be

equipped with a full amortisseur winding and can be started by induction-motor action.

Problem 4.10: Design of a Brushless DC (Permanent-Magnet) Motor Drive [24]

For a hybrid automobile drive a permanent-magnet motor – as a part of a brushless DC machine – is to be analyzed with the following data:

<u>Motor rating</u>	<u>Stator</u>
output power $P = 50 \text{ kW}$	axial length = 300 mm
efficiency $\eta = 0.95$	outer diameter
	$D_{\text{out}} = 244 \text{ mm}$
indirect water cooling	inner diameter
	$D_{\text{in}} = 170.4 \text{ mm}$
$V_{L-L} = 240 \text{ V}, f = 400 \text{ Hz}$	number of slots in stator
	120
$\cos \varphi = 0.9$ lagging (consumer system)	number of poles 20

Rotor

outer diameter $D_{\text{out}} = 169.4 \text{ mm}$
inner diameter $D_{\text{in}} = 140.2 \text{ mm}$

An encoder is used to sense the rotor speed. For your design it will be helpful to rely on the flux patterns and machine cross section of Fig. P4.10a,b. It

is recommended to use as permanent-magnet material NdFeB.

- Design the stator winding.
- What is the rated synchronous speed n_{s_rat} ?
- Compute the (maximum) height (radial one-sided length) of the permanent magnets h_{mag_max} .
- Calculate the maximum flux density of this machine.
- Determine the leakage inductance L_ℓ (from stator phase a to stator phase b) and the winding resistance R_a of one stator phase.
- Determine the current density J_{stator} , provided the stator winding copper fill factor is $k_{cu} = 0.7$, and the average stator-slot width is about the same as the average stator-tooth width.

Problem 4.11: Fourier Analyses of Terminal Currents of a Brushless DC Motor (Permanent-Magnet Motor with Inverter)

Find the Fourier coefficients of the current wave shapes of Fig. P4.11 that represent the input MOSFET current (upper wave shape) and the current of a brushless DC motor (lower wave shape). Select a certain sampling interval, e.g., $\Delta t = 0.025$ ms, perform a Fourier analysis, and show that for a minimum approximation error the Nyquist criterion is satisfied.

Problem 4.12: Steady-State Frequency Variation within an Interconnected Power System as a Result of Two Load Changes [82]

A block diagram of two interconnected areas of a power system (e.g., area #1 and area #2) is shown in

Fig. P4.12. The two areas are connected by a single transmission line. The power flow over the transmission line will appear as a positive load to one area and an equal but negative load to the other, or vice versa, depending on the direction of power flow.

- For steady-state operation show that with $\Delta\omega_1 = \Delta\omega_2 = \Delta\omega$ the change in the angular velocity (which is proportional to the frequency f) is

$$\Delta\omega = \text{function of } (\Delta P_{L1}, \Delta P_{L2}, D_1, D_2, R_1, R_2) \quad (P12-1)$$

and

$$\Delta P_{tie} = \text{function of the same parameters as in Eq. P12-1.} \quad (P12-2)$$

- Determine values for $\Delta\omega$ (Eq. P12-1), ΔP_{tie} (Eq. P12-2), and the new frequency f_{new} , where the nominal (rated) frequency is $f_{rated} = 60$ Hz, for these parameters: $R_1 = 0.05$ pu, $R_2 = 0.1$ pu, $D_1 = 0.8$ pu, $D_2 = 1.0$ pu, $\Delta P_{L1} = 0.2$ pu, $\Delta P_{L2} = -0.3$ pu.
- For a base apparent power $S_{base} = 1000$ MVA compute the power flow across the transmission line.
- How much is the load increase in area #1 (ΔP_{mech1}) and area #2 (ΔP_{mech2}) due to the two load steps?
- How would you change R_1 and R_2 in case R_1 is a wind or solar power plant operating at its maximum power point (and cannot accept any significant load increase due to the two load steps) and R_2 is a coal fired plant that can be overloaded?

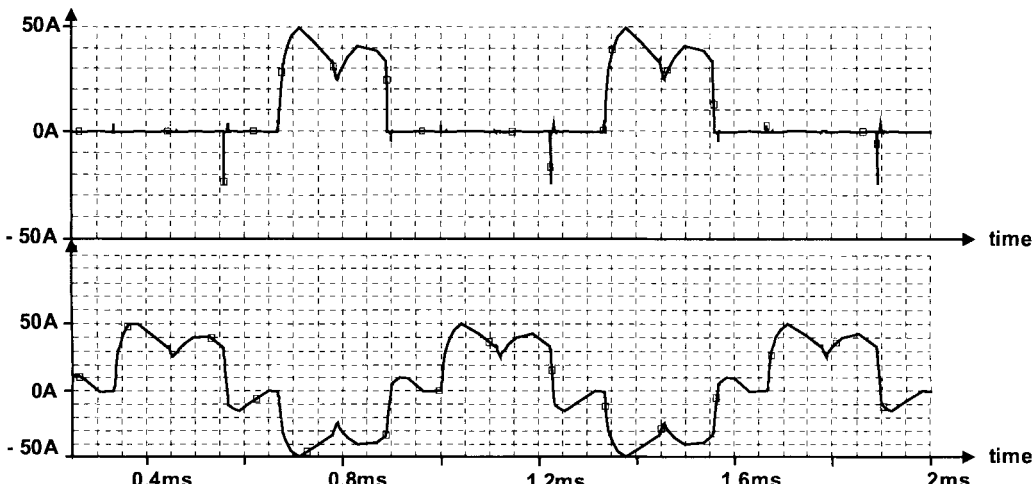


Figure P4.11 Current wave shape of the MOSFET current (upper wave shape), and the input current of a brushless dc-motor (lower wave shape).

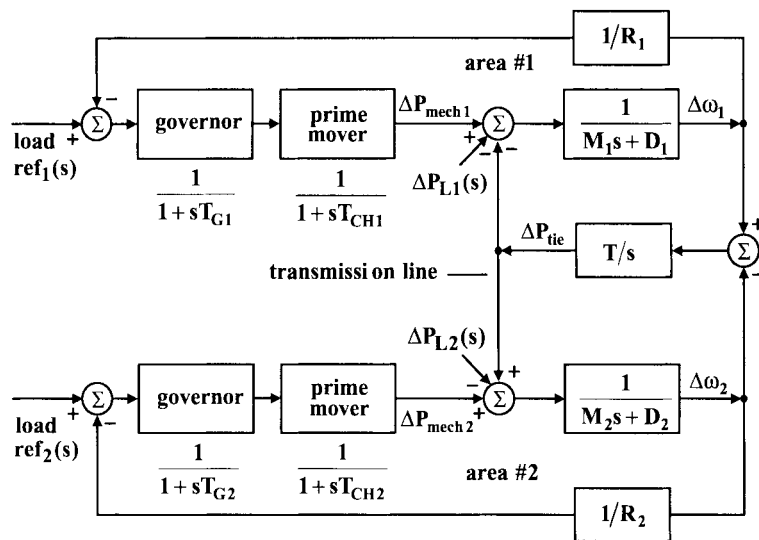


Figure P4.12 Interconnected power system consisting of area #1 and area #2.

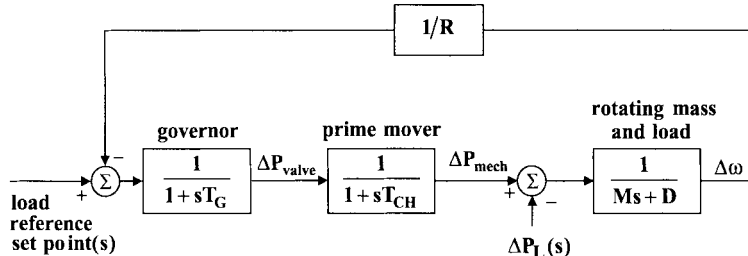


Figure P4.13 Block diagram of governor, prime mover, and rotating mass and load.

Problem 4.13: Frequency Control of an Isolated Power Plant (Islanding Operation)

Figure P4.13 illustrates the block diagram of governor, prime mover (steam turbine), and rotating mass and load of a turbogenerator set. For the frequency change ($\Delta\omega$) per generator output power change (ΔP),

$$R = \frac{\Delta\omega}{\Delta P} \text{ pu} = 0.01 \text{ pu},$$

the load change (ΔP_L) per frequency change

$$D = \frac{\Delta P_L}{\Delta\omega} = 0.8 \text{ pu},$$

$$\text{step load change } \Delta P_L(s) = \frac{\Delta P_L}{s} \text{ pu} = \frac{0.2}{s} \text{ pu},$$

angular momentum of steam turbine and generator set $M = 4.5$,

base apparent power $S_{\text{base}} = 500 \text{ MVA}$,

governor time constant $T_G = 0.01 \text{ s}$,

valve charging time constant $T_{CH} = 1.0 \text{ s}$,

load reference set point = 1.0.

- Derive for Fig. P4.13 $\Delta\omega_{\text{steady state}}$ by applying the final value theorem. You may assume the load reference set point(s) = 0 and $\Delta P_L(s) = \frac{\Delta P_L}{s} \text{ pu} = \frac{0.2}{s} \text{ pu}$, where s is the Laplace operator.
- List the ordinary differential equations and the algebraic equations of the block diagram of Fig. P4.13.
- Use either Mathematica or MATLAB to establish steady-state conditions by imposing a step function for load reference set point (s) = $\frac{1}{s} \text{ pu}$ and run the program with a zero step-load change $\Delta P_L = 0$ for 5 s. After 5 s impose a step load change of $\Delta P_L(s) = \frac{\Delta P_L}{s} \text{ pu} = \frac{0.2}{s} \text{ pu}$ to find the transient response of $\Delta\omega(t)$.
- Use Mathematica or MATLAB to establish steady-state conditions by imposing a step function for load reference set point $\Delta P_L(s) = \frac{\Delta P_L}{s} \text{ pu} = \frac{-0.2}{s} \text{ pu}$ and run the program with a zero

step-load change $\Delta P_L = 0$ for 5 s. After 5 s impose a step load change of $\Delta P_L(s) = \frac{\Delta P_L}{s}$ pu = $\frac{-0.2}{s}$ pu to find the transient response of $\Delta\omega(t)$.

Problem 4.14 Frequency Control of an Interconnected Power System Broken into Two Areas, Each Having One Generator

Figure P4.12 shows the block diagram of two generators interconnected by a tie line (transmission line). Data of generation set (steam turbine and generator) #1:

for frequency change ($\Delta\omega_1$) per generator output power change (ΔP_1): $R_1 = \frac{\Delta\omega_1}{\Delta P_1}$ pu = 0.01 pu,

the load change (ΔP_{L1}) per frequency change ($\Delta\omega_1$): $D_1 = \frac{\Delta P_{L1}}{\Delta\omega_1}$ = 0.08 pu,

step-load change: $\Delta P_{L1}(s) = \frac{\Delta P_{L1}}{s}$ pu = $\frac{0.2}{s}$ pu

angular momentum of steam turbine and generator set: $M_1 = 4.5$,

base apparent power: $S_{\text{base}} = 500$ MVA,

governor time constant: $T_{G1} = 0.01$ s,

valve charging time constant: $T_{CH1} = 1.0$ s,

(load reference set point)₁ = 0.8 pu.

Data of generation set (steam turbine and generator) #2:

for frequency change ($\Delta\omega_2$) per change in generator output power (ΔP_2): $R_2 = \frac{\Delta\omega_2}{\Delta P_2}$ pu = 0.02 pu,

the load change (ΔP_{L2}) per frequency change ($\Delta\omega_2$):

$D_2 = \frac{\Delta P_{L2}}{\Delta\omega_2}$ = 1.0 pu,

step load change: $\Delta P_{L2}(s) = \frac{\Delta P_{L2}}{s}$ pu = $\frac{-0.2}{s}$ pu,

angular momentum of steam turbine and generator set: $M_2 = 6$,

base apparent power: $S_{\text{base}} = 500$ MVA,

governor time constant: $T_{G2} = 0.02$ s,

valve charging time constant: $T_{CH2} = 1.5$ s,

(load reference set point)₂ = 0.8 pu.

Data for tie line:

$$T = \frac{377}{X_{\text{tie}}} \text{ with } X_{\text{tie}} = 0.2 \text{ pu},$$

- a) List the ordinary differential equations and the algebraic equations of the block diagram of Fig. P4.12.

b) Use either Mathematica or MATLAB to establish steady-state conditions by imposing a step function for load reference set point (s_1) = load

$$\text{ref}_1(s) = \frac{0.8}{s} \text{ pu, load reference set point } (s)_2 = \text{load}$$

$$\text{ref}_2(s) = \frac{0.8}{s} \text{ pu and run the program with a zero}$$

step-load changes $\Delta P_{L1} = 0$, $\Delta P_{L2} = 0$ for 10 s.

After additional 5 s impose step-load change $\Delta P_{L1}(s) = \frac{\Delta P_{L1}}{s}$ pu = $\frac{0.2}{s}$ pu, and after additional 2 s impose $\Delta P_{L2}(s) = \frac{\Delta P_{L2}}{s}$ pu = $\frac{-0.2}{s}$ pu to find the

transient responses $\Delta\omega_1(t)$ and $\Delta\omega_2(t)$.

Problem 4.15 Determination of the sequence-component equivalent circuits and matrices $Z^{(1)}_{\text{bus}}$, $Z^{(2)}_{\text{bus}}$, $Z^{(0)}_{\text{bus}}$, line-to-ground (neutral), and line-to-line fault currents at bus 2 of

Fig. P4.15 [83]

Two synchronous generators are connected through three-phase transformers to a transmission line, as shown in Fig. P4.15. The ratings and reactances of the generators and transformers are

1. Generators 1 and 2: 600 MVA, 34.5 kV;

$$X''_d = X_{1,\text{gen}} = X_{2,\text{gen}} = 25\% = 0.25 \text{ pu}$$

$$X_{o,\text{gen}} = 10\% = 0.1 \text{ pu, and}$$

$$X_{n,\text{grounding coil}} = 8\% = 0.08 \text{ pu.}$$

2. Transformer T_1 600 MVA, (34.5 kV connected in Δ)/(345 kV connected in Y);

$X_{\text{transformer leakage}} = 10\% = 0.10 \text{ pu. Note that the } Y$ of transformer T_1 is grounded.

3. Transformer T_2 600 MVA, (34.5 kV connected in Δ)/(345 kV connected in Y);

$X_{\text{transformer leakage}} = 20\% = 0.20 \text{ pu. Note that the } Y$ of transformer T_2 is not grounded.

4. On a chosen base of $S_{\text{base}} = 600$ MVA, $V_{L-L}_{\text{base}} = 345$ kV in the transmission-line circuit, the line reactances are $X_{\text{line}} = X_{2\text{line}} = 10\% = 0.10 \text{ pu}$ and $X_{0\text{line}} = 30\% = 0.30 \text{ pu}$.

- a) Draw each of the three (positive-, negative-, zero-) sequence networks.

- b) Determine the zero-, positive-, and negative-sequence bus impedance (reactance) matrices by means of the Z_{bus} building algorithm, as described in Chapter 8 of [83].

- c) Apply the matrix reduction technique by Kron, as outlined in Chapter 7 of [83].

- d) Determine numerical value (subtransient) for the line-to-ground fault current when the fault occurs at bus 2 of Fig. P4.15.

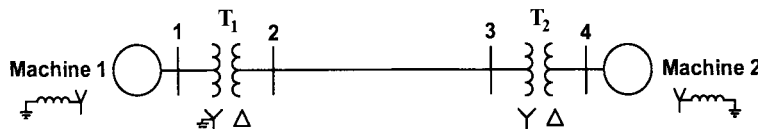


Figure P4.15 Single-line diagram of a two-machine system connected via transformers and transmission line.

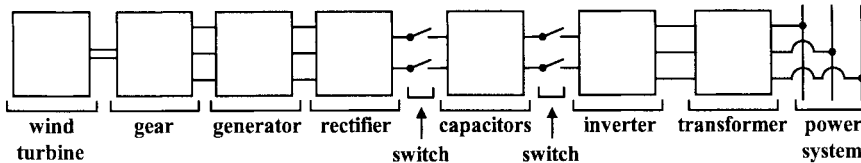


Figure P4.16.1 Block diagram for charging and discharging supercapacitor bank.

- e) Determine numerical value (subtransient) for the line-to-line fault current when the fault occurs at bus 2 of Fig. P4.15.

Problem 4.16 Analysis of a Synchronous Machine Feeding a Rectifier

One of the major problems in using wind and solar energy is energy storage. Wind or solar energy may not be available when it is needed. A report from a wind farm in New Mexico states that the wind farm could lose as much as 60 MW within a minute. For example, there are several scenarios of how the power change of 60 MW per minute can be mitigated through complementary albeit more expensive power sources: one of them is the combination of a compressed-air power plant with a supercapacitor plant for bridging the time from when the wind power plant output decreases (60 MW per minute) to when the compressed-air energy storage (CAES) plant can take over. A CAES plant requires a start-up time of about 6 minutes. To bridge this 6 minute start-up time required for a 100 MW compressed-air power plant, supercapacitors or ultracapacitors are proposed to provide up to 100 MW during a 6 minute interval amounting to a required energy storage of 10 MWh. Inverters fed from supercapacitors can deliver power within milliseconds to the power system replacing the lost power of 60 MW per minute almost instantaneously. This combination of compressed-air power plant and supercapacitors or ultracapacitors as bridging energy sources can be employed for peak-power operation as well as for improving power quality by preventing short brown-outs or blackouts.

Figure P4.16.1 depicts the block diagram of such a supercapacitor plant consisting of wind turbine, mechanical gear, synchronous generator, three-phase rectifier, supercapacitor bank, three-phase inverter, transformer, and power system.

- a) Design a controlled three-phase rectifier in the tens of kilowatts range. Figure P4.16.2 shows the three-phase rectifier of Fig. P4.16.1 with six diodes and one self-commutated switch, an insulated-gate bipolar transistor (IGBT). The nominal phase voltages of the generator can be assumed to be $v_{an} = 1200 \text{ V} \sin \omega t$, $v_{bn} = 1200 \text{ V} \sin(\omega t - 120^\circ)$, and $v_{cn} = 1200 \text{ V} \sin(\omega t - 240^\circ)$. The IGBT is gated with a switching frequency of 3 kHz and you may assume a duty cycle of $\delta = 50\%$. $C_{fl} = 200 \mu\text{F}$, $L_{fl} = 90 \text{ mH}$, $C_{f2} = 50 \mu\text{F}$, ideal diodes D_1 to D_6 and D_f , $v_{gs} = 40 \text{ V}$ magnitude, $R_{sd} = R_{ss} = 10 \Omega$, $C_{sd} = C_{ss} = 0.1 \mu\text{F}$, $C_f = 1000 \mu\text{F}$, $L_f = 1 \text{ mH}$, and $R_{load} = 10 \Omega$.

- 1) Perform a PSpice analysis and plot output voltage $v_{load}(t)$, generator phase current i_{aphase} , and the generator line-to-line voltage v_{ab} .
- 2) Subject the generator phase current to a Fourier analysis.
- 3) Determine the displacement power factor of the generator.
- 4) Determine the power factor of the generator.

- b) Design PWM (pulse-width-modulated) three-phase current controlled voltage-source inverter feeding power into the utility system via $Y_{grounded}/\Delta$ transformer in the tens of kilowatts range. The inverter circuit of Fig. P4.16.3 is to be analyzed with PSpice where the DC voltage is $V_{dc} = 600 \text{ V}$, AC output voltage of the inverter is $V_{acL-L} = 360 \text{ V}$, and the switching frequency of the IGBTs is $f_{switch} = 7.2 \text{ kHz}$. $C_{filter} = 1000 \mu\text{F}$, $L_w = 1 \text{ mH}$, $R_w = 10 \text{ m}\Omega$, $L_f = 45 \mu\text{H}$, $C_f = 10.3 \mu\text{F}$, $R_f = 10 \text{ m}\Omega$, $L_{syst} = 265 \mu\text{H}$, $R_{syst} = 50 \text{ m}\Omega$. The power system phase voltages are $v_{agrid}(t) = 7200 \text{ V} \sin \omega t$, $v_{bgrid}(t) = 7200 \text{ V} \sin(\omega t - 120^\circ)$, and $v_{cgrid}(t) = 7200 \text{ V} \sin(\omega t - 240^\circ)$. Note the voltages $v_{asyst}(t)$,

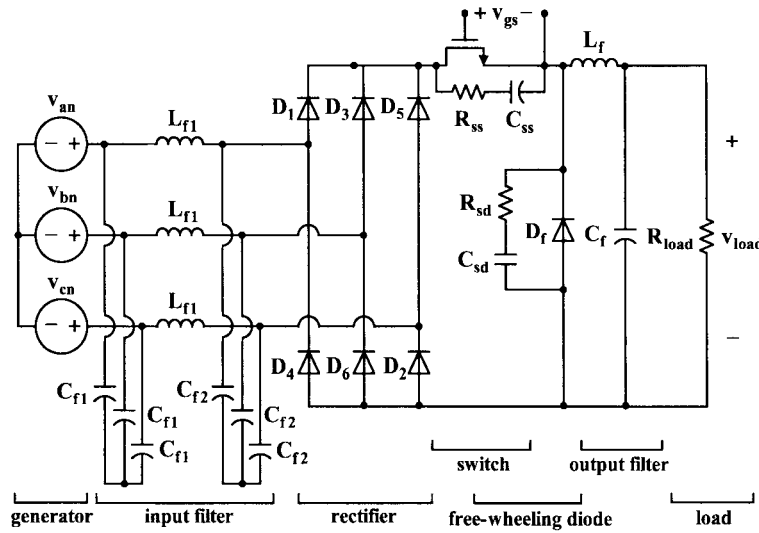


Figure P4.16.2 Controlled three-phase rectifier.

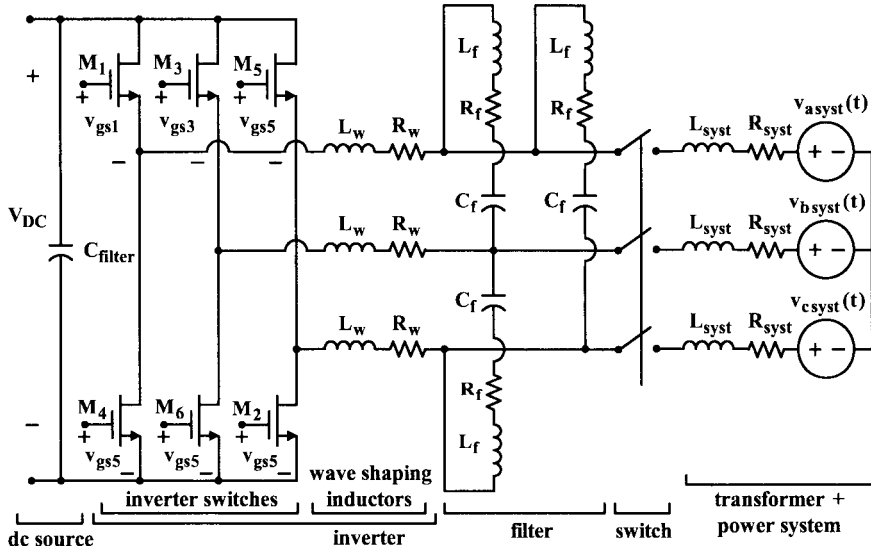


Figure P4.16.3 PWM (pulse-width-modulated) three-phase current controlled voltage-source inverter.

$v_{bsyst}(t)$, and $v_{csyst}(t)$ are the power system voltages $v_{agrid}(t)$, $v_{bgrid}(t)$, and $v_{cgrid}(t)$ referred to the Y- or inverter side of the Y/Δ transformer.

- 1) Determine the transformation ratio of the Y/Δ transformer between inverter and power system; you may assume ideal transformer conditions.
- 2) Using PSpice calculate and plot input and output voltages and currents of the inverter, provided the output voltage is a sinusoid as given by the power system.
- 3) Subject the output current of the inverter to a Fourier analysis.

- 4) Determine the overall costs of this power plant if a specific cost of \$4000/kW installed capacity is assumed. Note that a coal-fired plant has a specific cost of \$2000/kW installed capacity.

Problem 4.17 Voltage Stress in a Synchronous Motor Winding Fed Through a Cable Of 10 m Length by a PWM Current-Source Inverter

Voltage and current ripples due to PWM current-source inverters cause voltage stress in windings of machines. The configuration of Fig. E3.14.1 represents the first two turns of the winding of an induction motor, which is assumed to be identical to the

winding of a synchronous motor. Each turn can be represented by four segments having an inductance L_i , a resistance R_i , a capacitance to ground (frame) C_i , and some interturn capacitances C_{ij} and inductances L_{ij} . Figure E.3.14.2 represents a detailed equivalent circuit for the configuration of Fig. E3.14.1.

To simplify the analysis neglect the capacitances C_{ij} and the inductances L_{ij} . This leads to the circuit Fig. E3.14.3, where the winding is fed by a PWM current source. One obtains the 15 differential equations as listed below.

$$\frac{dv_1}{dt} = \frac{i_s}{C_1} - \frac{G_1}{C_1} v_1 - \frac{i_2}{C_1},$$

$$\frac{di_2}{dt} = -\frac{R_2}{L_2} i_2 - \frac{v_2}{L_2} + \frac{v_1}{L_2},$$

$$\frac{dv_2}{dt} = \frac{i_2}{C_2} - \frac{G_2}{C_2} v_2 - \frac{i_3}{C_2},$$

$$\frac{di_3}{dt} = -\frac{R_3}{L_3} i_3 - \frac{v_3}{L_3} + \frac{v_2}{L_3},$$

$$\frac{dv_3}{dt} = \frac{i_3}{C_3} - \frac{G_3}{C_3} v_3 - \frac{i_4}{C_3},$$

$$\frac{di_4}{dt} = -\frac{R_4}{L_4} i_4 - \frac{v_4}{L_4} + \frac{v_3}{L_4},$$

$$\frac{dv_4}{dt} = \frac{i_4}{C_4} - \frac{G_4}{C_4} v_4 - \frac{i_5}{C_4},$$

$$\frac{di_5}{dt} = -\frac{R_5}{L_5} i_5 - \frac{v_5}{L_5} + \frac{v_4}{L_5},$$

$$\frac{dv_5}{dt} = \frac{i_5}{C_5} - \frac{G_5}{C_5} v_5 - \frac{i_6}{C_5},$$

$$\frac{di_6}{dt} = -\frac{R_6}{L_6} i_6 - \frac{v_6}{L_6} + \frac{v_5}{L_6},$$

$$\frac{dv_6}{dt} = \frac{i_6}{C_6} - \frac{G_6}{C_6} v_6 - \frac{i_7}{C_6},$$

$$\frac{di_7}{dt} = -\frac{R_7}{L_7} i_7 - \frac{v_7}{L_7} + \frac{v_6}{L_7},$$

$$\frac{dv_7}{dt} = \frac{i_7}{C_7} - \frac{G_7}{C_7} v_7 - \frac{i_8}{C_7},$$

$$\frac{di_8}{dt} = -\frac{R_8}{L_8} i_8 - \frac{v_8}{L_8} + \frac{v_7}{L_8},$$

$$\frac{dv_8}{dt} = \frac{i_8}{C_8} - v_8 \left(\frac{1}{Z C_8} + \frac{G_8}{C_8} \right).$$

The parameters are

$R_1 = R_2 = R_3 = R_4 = R_5 = R_6 = R_7 = R_8 = 25 \mu\Omega$;
 $L_1 = L_3 = L_5 = L_7 = 1 \text{ mH}$, and $L_2 = L_4 = L_6 = L_8 = 10 \text{ mH}$;
 $C_1 = 0.2 \mu F$ for the cable of 10 m
length; $C_3 = C_5 = C_7 = 0.7 \text{ pF}$, $C_2 = C_4 = C_6 = C_8 = 7 \text{ pF}$, $C_{15} = C_{37} = 0.35 \text{ pF}$, $C_{26} = C_{48} = 3.5 \text{ pF}$;
 $G_1 = G_3 = G_5 = G_7 = 1/(5000 \Omega)$, $G_2 = G_4 = G_6 = G_8 = 1/(500 \Omega)$; and $L_{15} = L_{37} = 0.005 \text{ mH}$, $L_{26} = L_{48} = 0.01 \text{ mH}$. Z is either 1 $\mu\Omega$ (short-circuit) or 1 $M\Omega$ (open circuit).

Assume a PWM triangular current-step function $i_s(t)$, as indicated in Fig. E3.14.4. Using Mathematica or MATLAB compute all state variables for the time period from $t = 0$ to 2 ms. Plot the voltages $(v_1 - v_5)$, $(v_2 - v_6)$, $(v_3 - v_7)$, and $(v_4 - v_8)$.

4.6 REFERENCES

- 1) Blondel, A.; "Application de la methode des deux reactions a l'etude de phenomenes oscillatoires des alternateurs couples," *Rev. Gen. Electr.*, vol. 13, pp. 235, 275, 331, 387, 515, 1923.
- 2) Doherty, R.E.; and Nickle, C.A.; "Synchronous machines I and II, an extension of Blondel's two-reaction theory," *Trans. AIEE*, vol. 45, pp. 912–927, 1926.
- 3) Doherty, R.E.; and Nickle, C.A.; "Synchronous machines III," *Trans. AIEE*, vol. 46, p. 1, 1927.
- 4) Park, R.H.; "Two-reaction theory of synchronous machines, generalized method of analysis, part I," *Trans. AIEE*, vol. 48, pp. 716–730, 1929.
- 5) Park, R.H.; "Two-reaction theory of synchronous machines II," *Trans. AIEE*, vol. 52, pp. 352–355, 1933.
- 6) Kilgore, L.A.; "Effects of saturation on machine reactances," *Trans. AIEE*, vol. 54, pp. 545–550, 1930.
- 7) Concordia, C.; *Synchronous Machines Theory and Performance*, John Wiley & Sons, Inc., New York, 1951.
- 8) Lyon, W.V.; *Transient Analysis of Alternating Current Machinery*, John Wiley & Sons, Inc., New York, 1954.
- 9) <http://www.fes-muenchen.de/rund/herbst.99/walchsee.htm>
- 10) Clarke, E.; "Circuit analysis of AC power systems," vol. II, John Wiley & Sons, 1950.
- 11) Roark, J.D.; and Fross, C.A.; "Unbalanced synchronous machine analysis using frequency domain methods," *Proceeding IEEE Power Engineering Society Summer Meeting*, Los Angeles, CA, 1978, paper 78SM S24-1.
- 12) Xu, W.W.; Dommel, H.W.; and Marti, J.R.; "A synchronous machine model for three-phase harmonic analysis and EMTP initialization," *IEEE Transactions on Power Systems*, 1991, 6, (4), pp. 1530–1538.
- 13) Medina, A.; Arrillaga, J.; and Eggleston, J.F.; "A synchronous machine model in the harmonic domain," *Proceeding International Conference on Electrical Machines*, Manchester, UK, September 1992, pp. 647–651.
- 14) Subramaniam, P.; and Malik, P.P.; "Digital simulation of a synchronous generator in direct-phase coordinates," *Proc. Inst. Electr. Eng.*, 1971, 118(1), pp. 153–166.
- 15) Arrillaga, J.; Campos-Barros, J.G.; and Al-Kashali, H.J.; "Dynamic modeling of single generators connected to HVDC converters," *IEEE Transactions on Power Apparatus and Systems*, 1978, 97(4), pp. 1018–1029.
- 16) Marti, J.R.; and Louie, K.W.; "A phase-domain synchronous generator model including saturation effects," *IEEE Transactions on Power Apparatus and Systems*, 1997, 12(1), pp. 222–229.
- 17) Rodriguez, O.; and Medina, A.; "Fast periodic steady-state solution of a synchronous machine model incorporating the effects of magnetic saturation and hysteresis," *Presented at IEEE PES Winter Meeting*, vol. 3, pp. 1431–1436, 28 January–1 February, Columbus, OH, 2001.
- 18) Fuchs, E.F.; and McNaughton, G.A.; "Comparison of first-order finite difference and finite element algorithms for the analysis of magnetic fields, part I: theoretical analysis," *IEEE Transactions on Power Apparatus and Systems*, May 1982, vol. PAS-101, no. 5, pp. 1170–1180, and "Comparison of first-order finite difference and finite element algorithms for the analysis of magnetic fields, part II: numerical results," *IEEE Transactions on Power Apparatus and Systems*, May 1982, vol. PAS-101, no. 5, pp. 1181–1201.
- 19) Erdelyi, E.A.; and Fuchs, E.F.; "Non-linear electrical generator study final report on phase "B", part II non-linear synchronous alternators," Contract No. N00014-67-A-405-0003, Project No. 097-374/5-19-70, Code 473, University of Colorado, July 1972.
- 20) Fuchs, E.F.; and Erdelyi, E.A.; "Nonlinear theory of turbogenerators, part I: magnetic fields at no-load and balanced loads," *IEEE Transactions on Power Apparatus and Systems*, March/April 1973, vol. PAS-92, no. 2, pp. 583–591, and "Nonlinear theory of turbogenerators, part II: load-dependent synchronous reactances," *IEEE Transactions on Power Apparatus and Systems*, March/April 1973, vol. PAS-92, no. 2, pp. 592–599.
- 21) Fuchs, E.F.; and Senske, K.; "Comparison of iterative solutions of the finite difference method with measurements as applied to Poisson's and the diffusion equations," *IEEE Transactions on Power Apparatus and Systems*, August 1981, vol. PAS-100, no. 8, pp. 3983–3992.
- 22) Fuchs, E.F.; "Lastabhangige transiente Reaktanzen von gesättigten Turbogeneratorn," *Archiv für Elektrotechnik*, vol. 55, 1973, pp. 263–273.
- 23) El-Serafi, A.M.; Abdallah, A.S.; El-Sherbiny, M.K.; and Badawy, E.H.; "Experimental study of the saturation and the cross-magnetizing phenomenon in saturated synchronous machines," *IEEE Transactions on Energy Conversion*, vol. 3, issue 4, Dec. 1988, pp. 815–823.
- 24) Fuchs, E.F.; and Fardoun, A.A.; "Simulation of Controller-Motor drive System Using PSpice," Final Report prepared for Unique Mobility, Inc., 3700 S.

- Jason Street, Englewood, Colorado, 80110, University of Colorado, January 1991.
- 25) Fardoun, A.A.; Fuchs, E.F.; and Huang, H.; "Modeling and simulation of an electronically commutated permanent-magnet machine drive system using SPICE," *IEEE Transactions on Industry Applications*, vol. 30, no. 4, July/August 1994, pp. 927-937.
- 26) Muljadi, E.; and Green J.; "Cogging torque reduction in a permanent magnet wind turbine generator, *Proceedings of the 21st American Society of Mechanical Engineers Wind Energy Symposium*, Reno, Nevada, January 14-17, 2002.
- 27) Fuchs, E.F.; and Pohl, G.; "Computer generated polycentric grid design and a novel dynamic acceleration of convergence for the iterative solution of magnetic fields based on the finite difference method," *IEEE Transactions on Power Apparatus and Systems*, August 1981, vol. PAS-100, no. 8, pp. 3911-3920.
- 28) Dubey, G.K.; *Power Semiconductor Controlled Drives*, Prentice Hall, Englewood Cliffs, New Jersey, 1989.
- 29) Yildirim, D.; "Commissioning of a 30 kVA variable-speed, direct-drive wind power plant," Ph.D. Thesis, University of Colorado, Boulder, Colorado, 1999.
- 30) Yildirim, D.; Fuchs, E.F.; and Batan, T.; "Test results of a 20 kW, direct-drive, variable-speed wind power plant," *Proceedings of the International Conference on Electrical Machines*, Istanbul, Turkey, September 2-4, 1998, pp. 2039-2044.
- 31) Palmer, H.; EE 673, "Advanced synchronous machinery," Class Notes, University of Colorado, 1967.
- 32) Fuchs, E.F.; "Parallelschalteinrichtungen," Diplomarbeit, Technical University of Stuttgart, Germany, 1967.
- 33) Fuchs, E.F.; "Automatic paralleling of power systems," *Proceedings of the 1969 Midwest power Symposium*, University of Minnesota, October 1969.
- 34) Fuchs, E.F., "Automatic paralleling of power systems," *Proceedings of the Third Pan American Congress of Mechanical, Electrical, and Allied Engineering Branches*, San Juan, Puerto Rico, September 6-13, 1969, Paper 30.
- 35) Joyce, J.S.; Kulig, T.; and Lambrecht, D.; "Torsional fatigue of turbine-generator shafts caused by different electrical system faults and switching operations," *IEEE Trans. on Power Apparatus and Systems*, vol. PAS-97, 1978, pp. 1965-1977.
- 36) Joyce, J.S.; Kulig, T.; and Lambrecht, D.; "The impact of high-speed reclosure of single and multiphase system faults on turbine-generator shaft torsional fatigue," *IEEE Transactions on Power Apparatus and Systems*, vol. PAS-99, 1980, pp. 1764-1779.
- 37) El-Serafi, A.M.; and Faried, S.O.; "Effect of sequential reclosure of multi-phase system faults on turbine-generator shaft torsional torques," *IEEE Transactions on Power Systems*, vol. 6, issue 4, Nov. 1991, pp. 1380-1388.
- 38) Hammons, T.J.; and Lim, C.K.; "Probability assessment of turbine-generator shaft torque following severe disturbances on the system supply," *IEEE Transactions on Energy Conversion*, vol. 14, issue 4, Dec. 1999, pp. 1115-1123.
- 39) Ledesma, P.; and Usaola, J.; "Minimum voltage protections in variable speed wind farms," *2001 IEEE Porto Power Tech Proceedings*, vol. 4, 10-13 Sept. 2001, 6 pp.
- 40) Fuchs, E.F.; "Industrial experience with the relaxation solutions of the quasi-Poissonian differential equation," *Proceedings of International Conference on Electrical Machines*, Vienna, Austria, September 1315, 1976, pp. D20-1 to 10.
- 41) Kulig, T.S.; Buckley, G.W.; Lambrecht, D.; and Liese, M.; "A new approach to determine transient generator winding and damper currents in case of internal and external faults and abnormal operation, part 1: fundamentals," *Paper presented at IEEE Winter Meeting*, New Orleans, 1986.
- 42) Kulig, T.S.; Buckley, G.W.; Lambrecht, D.; and Liese, M.; "A new approach to determine transient generator winding and damper currents in case of internal and external faults and abnormal operation, part 2: analysis," *Paper presented at IEEE Winter Meeting*, New Orleans, 1986.
- 43) Kulig, T.S.; Buckley, G.W.; Lambrecht, D.; and Liese, M.; "A new approach to determine transient generator winding and damper currents in case of internal and external faults and abnormal operation, part 3: results," *IEEE Transactions on Energy Conversion*, vol. 5, issue 1, March 1990, pp. 70-78.
- 44) Fingersh, L.J.; "The testing of a low-speed, permanent-magnet generator for wind power applications," M.S. Thesis, University of Colorado, Boulder, 1995.
- 45) Bergey, K.H.; "The Lanchester-Betz limit," *J. Energy*, vol. 3, no. 6, Nov.-Dec. 1979, pp. 382-384.
- 46) Franklin, P.W.; "Theory of the three-phase, salient-pole type generator with bridge rectified output, parts I and II," *IEEE Transactions on Power Apparatus and Systems*, vol. PAS-91, Sept./Oct. 1972, pp. 1960-1975.
- 47) Jatskevich, J.; Pekarek, S.D.; and Davoudi, A.; "Parametric average-value model of synchronous machine-rectifier systems," *IEEE Transactions on*

- Energy Conversion*, vol. 21, issue 1, March 2006, pp. 9–18.
- 48) Jadric, I.; Borojevic, D.; and Jadric, M.; "Modeling and control of a synchronous generator with an active DC load," *IEEE Transactions on Power Electronics*, vol. 15, issue 2, March 2000, pp. 303–311.
- 49) Abolins, A.; Achenbach, H.; and Lambrecht, D.; "Design and performance of large four-pole turbogenerators with semiconductor excitation for nuclear power stations," *Cigre-Report*, 1972 Session, August 28–September, Paper No 11-04.
- 50) Fuchs, E.F.; "Numerical determination of synchronous, transient, and subtransient reactances of a synchronous machine," Ph.D. Thesis, University of Colorado, Boulder, Colorado, 1970.
- 51) http://www.enercon.de/en/_home.htm
- 52) Batan, T.; "Real-time monitoring and calculation of the derating of single-phase transformers under non-sinusoidal operation," Ph.D. Thesis, University of Colorado, Boulder, 1999.
- 53) Gallegos-Lopez, G.; Kjaer, P.C.; and Miller, T.J.E.; "A new sensorless method for switched reluctance motor drives," *IEEE Transactions on Industry Applications*, vol. 34, issue 4, July–Aug. 1998, pp. 832–840.
- 54) Staton, D.A.; Soong, W.L.; and Miller, T.J.E.; "Unified theory of torque production in switched reluctance and synchronous reluctance motors," *IEEE Transactions on Industry Applications*, vol. 31, issue 2, March–April 1995, pp. 329–337.
- 55) Miller, T.J.E.; "Faults and unbalance forces in the switched reluctance machine," *IEEE Transactions on Industry Applications*, vol. 31, issue 2, March–April 1995, pp. 319–328.
- 56) Forster, J.A.; and Klataske, L.F.; "IEEE Working group report of problems with hydrogenerator thermoset stator windings," *IEEE Transactions on Power Apparatus and Systems*, vol. PAS-100, no. 7, July 1981, pp. 3292–3300.
- 57) Stratton, J.A.; *Electromagnetic Theory*, McGraw-Hill Book Company, Inc., New York and London, pp. 153–155, 1941.
- 58) Carpenter, C.J.; "Surface-integral methods of calculating forces on magnetized iron parts," *Proc. IEE*, 106C, 1960, pp. 19–28.
- 59) Reichert, K.; Freundl, H.; and Vogt, W.; "The calculation of forces and torques within numerical magnetic field calculation methods," *Proceedings of Compumag Conference*, London, 1976.
- 60) Hart, P.M.; and Bonwick, W.J.; "Harmonic modeling of synchronous machine," *IEE Proceedings on Electric Power Applications*, vol. 135, Proceedings B, no. 2, pp. 5258, March 1988.
- 61) Chen, H.; Long, Y.; and Zhang, X.P.; "More sophisticated synchronous machine model and the relevant harmonic power flow study," *IEE Proceedings, Transactions on ac Distribution*, vol. 146, no. 3, May 1999.
- 62) Grainger, J.J.; and Stevenson, W.D.; *Power System Analysis*, McGraw-Hill, Inc., New York, 1994.
- 63) Kimbark, E.W.; *Direct Current Transmission*, vol. 1, Wiley-Interscience, New York, 1971.
- 64) Zhang, X.-P.; and Chen, H.; "Asymmetrical three-phase load-flow study based on symmetrical component theory," *IEEE Proc. C*, 1994, 141, (3), pp. 248–252.
- 65) Xu, W.; Marti J.R.; and Dommel, H.W.; "A multiphase harmonic load flow solution technique," *IEEE Transactions on Power Systems*, vol. 6, issue 1, Feb. 1991, pp. 174–182.
- 66) CIGRE-Working Group 36-05, "Harmonics, characteristic parameters, methods of study, estimates of existing values in the network," *Electra*, no. 77, pp. 35–54, July 1981.
- 67) Dommel, H.W.; *Electromagnetic transients program reference manual (EMTP theory book)*, Prepared for Bonneville Power Administration by the Dept. of Electrical Engineering, University of British Columbia, Canada, Aug. 1986.
- 68) Smith, R.T.; *Analysis of Electrical Machines*, New York, Pergamon Press, 1982.
- 69) Al-Nuaim, N.A.; and Toliyat, H.A.; "A novel method for modeling dynamic air-gap eccentricity in synchronous machines based on modified winding function theory," *IEEE Transactions on Energy Conversion*, vol. 13, pp. 156–162, June 1998.
- 70) MATLAB, Version 4.2c.1, and Simulink, Version 1.3c, Mathematical packages by the MathWorks, Inc., Natick, MA.
- 71) Ammann, C.; Reichert, K.; Joho, R.; and Posedel, Z.; "Shaft voltages in generators with static excitation systems – problems and solution," *IEEE Transactions on Energy Conversion*, vol. 3, issue 2, June 1988, pp. 409–419.
- 72) Busse, D.; Erdman, J.; Kerkman, R.J.; Schlegel, D.; and Skibinski, G.; "System electrical parameters and their effects on bearing currents," *IEEE Transactions on Industry Applications*, vol. 33, issue 2, March–April 1997, pp. 577–584.
- 73) Muetze, A.; and Binder, A.; "Calculation of circulating bearing currents in machines of inverter-based drive systems," *Conference Record of the 2004 IEEE Industry Applications Conference, 2004, 39th IAS Annual Meeting*, vol. 2, 3–7 Oct. 2004, pp. 720–726.
- 74) Maki-Ontto, P.; and Luomi, J.; "Bearing current prevention of converter-fed ac machines with a

- conductive shielding in stator slots," *Proceedings of the IEEE International Electric Machines and Drives Conference*, 2003, vol. 1, 1–4 June 2003, pp. 274–278.
- 75) Busse, D.; Erdman, J.; Kerkman, R.J.; Schlegel, D.; and Skibinski, G.; "Bearing currents and their relationship to PWM drives," *IEEE Transactions on Power Electronics*, vol. 12, issue 2, March 1997, pp. 243–252.
- 76) Hyypio, D.; "Mitigation of bearing electro-erosion of inverter-fed motors through passive common-mode voltage suppression," *IEEE Transactions on Industry Applications*, vol. 41, issue 2, March–April 2005, pp. 576–583.
- 77) Muetze, A.; and Binder, A.; "Techniques for measurement of parameters related to inverter-induced bearing currents," *Industry Applications Conference, 2005, 40th IAS Annual Meeting, Conference Record of the 2005*, vol. 2, 2–6 Oct. 2005, pp. 1390–1397.
- 78) *IEEE Standard 519*, "IEEE recommended practices and requirements for harmonic control in electric power systems," IEEE-519, 1992.
- 79) Fuchs, E.F.; You, Y.; and Roesler, D.J.; "Modeling, simulation and their validation of three-phase transformers with three legs under DC bias," *IEEE Transactions on Power Delivery*, vol. 14, no. 2, April 1999, pp. 443–449.
- 80) Fuchs, E.F.; and Rosenberg, L.T.; "Analysis of an alternator with two displaced stator windings," *IEEE Transactions on Power Apparatus and Systems*, November/December 1974, vol. PAS-93, no. 6, pp. 1776–1786.
- 81) White D.C.; and Woodson, H.H.; *Electrical Energy Conversion*, John Wiley & Sons, Inc., New York, 1959.
- 82) Wood, A. J.; and Wollenberg, B.F.; *Power Generation Operation and Control*, John Wiley & Sons, Inc., 1984.
- 83) Grainger, J.J.; and Stevenson, Jr., W.D.; *Power System Analysis*, McGraw-Hill, Inc. 1994.
-
- ## 4.7 ADDITIONAL BIBLIOGRAPHY
- 84) Sarma, M.S.; *Electric Machines – Steady-State and Dynamic Performance*, 2nd edition, West Publishing Company, Minneapolis/St. Paul, 1994.
- 85) Fuchs, E.F.; and Fardoun, A.A.; "Architecture of a variable-speed, direct-transmission wind power plant of wind-farm size," Invention Disclosure, University of Colorado, Boulder, February 1994.
- 86) Fuchs, E.F.; and Gregory, B.; "Control of a wind power plant with variable displacement (or power factor) angle and waveshape of AC current fed into the power system," Invention Disclosure, University of Colorado, Boulder, February 1994.
- 87) Fuchs, E.F.; and Yildirim, D.; "Transverse electric flux machines with phase numbers higher than two," Invention Disclosure, University of Colorado, Boulder, January 1995.
- 88) Fuchs, E.F.; and Yildirim, D.; "Permanent-magnet reluctance machine for high torques at low rated speeds and low weight based on alternating magnetic field theory," Invention Disclosure, University of Colorado, Boulder, April 1997.
- 89) Fuchs, E.F.; and Yildirim, D.; "Pulse-width-modulated (PWM) current-controlled inverter with reduced switching and filtering losses," Invention Disclosure, University of Colorado, Boulder, July 1999.